RETROGRADE TRANSPORT OF RADIOIODINATED NERVE GROWTH FACTOR VIA TROPOMYOSIN RECEPTOR KINASE A

RETROGRADE TRANSPORT OF RADIOIODINATED NERVE GROWTH FACTOR VIA TROPOMYOSIN RECEPTOR KINASE A

By Rojin Falah, PharmD

A Thesis Submitted to the School of Graduate Studies In Partial Fulfillment of the Requirements for the Degree Master of Science

McMaster University MASTER OF SCIENCE (2024) Hamilton, Ontario (Chemical Biology)

TITLE: Retrograde Transport of Radioiodinated Nerve Growth Factor via Tropomyosin Receptor Kinase A

AUTHOR: Rojin Falah, PharmD (Azad University of Pharmaceutical Science)

SUPERVISOR: Dr. Sam Sadeghi and Dr. Margaret Fahnestock

PAGES: xii, 86

Abstract

Clinical symptoms of Alzheimer's disease (AD), like memory loss and cognitive decline, are rooted in neuronal loss and synaptic disruptions. Basal forebrain cholinergic neurons (BFCNs), crucial for learning and memory, deteriorate early in aging and AD. Cognitive decline in aging and AD correlates with reduced levels of tropomyosin receptor kinase A (TrkA), the nerve growth factor (NGF) receptor, in the cholinergic neurons, and impaired NGF axonal transport. Currently, TrkA levels can only be measured post-mortem. We proposed developing a TrkA-positron emission tomography (PET) tracer for in vivo measurement, potentially serving as an early diagnostic biomarker for aging and AD-associated cognitive decline. As part of our optimization efforts, we initially assessed the transport of iodinated NGF in mice. The primarily aim was to synthesize and characterize radioiodinated NGF and evaluate its uptake and retrograde transport from hippocampus to basal forebrain via BFCNs. The approach taken to track the radiotracer in the mouse brain involved the intracranial administration of ^{125}I-NGF. Several optimization and preliminary steps were taken to establish a consistent method and coordinates to target the site of injection, hippocampal dentate gyrus (DG).

NGF was radiolabeled with the isotope Iodine-125 (^{125}I) using the direct labeling method with a radiochemical yield of 91.08 ± 1.20% and purified to a radiochemical purity of 99.17 ± 0.18%. Characterization methods such as iTLC and HPLC were employed to evaluate the purity of ^{125}I-NGF. Additionally, stability tests were conducted to ensure the compound's stability before further use for *in vitro* and *in vivo* purposes. The specificity of ^{125}I-NGF and its biological activity was validated by assaying *in vitro* receptor binding to TrkA-overexpressing PC12nnrB5 cells compared to TrkA-knockout PC12nnr cells.

Stereotaxic intracranial administration of 1 µL (1.5-2 µCi) of ^{125}I-NGF was conducted on young C57Bl/6 mice. After survival time of two and six hours post injection, mice were euthanized, and the brains were removed. Specific brain regions were sub-dissected including hippocampus, basal forebrain, cortex, midbrain, and cerebellum. Radioactivity of each brain region was measured by a gamma counter. Autoradiography was performed to analyze the localization of the radioligand in the brain. Consistency in delivering ^{125}I-NGF into the hippocampus was confirmed through gamma measurements in mice euthanized prior to the injection. Comparison of the injected dose per gram of tissue (%ID/g) of basal forebrain from two-hour (mean: 3.190 ± 0.884) and six-hour (mean: 16.80 ± 2.683) intervals exhibited slight transportation to basal forebrain. Additionally, qualitative observation of autoradiography analysis revealed that the majority of the activity was found to remain in the site of injection in pre-euthanized mice and 2 hours post injection. Extended time points may be worth evaluating in the future to determine if they increase transport.

The utilization of a healthy mouse model to demonstrate successful transport of ^{125}I-NGF will facilitate future investigations into retrograde transport in aging and AD mouse models. These studies will allow for comparisons with healthy mice, shedding light on whether the absence of NGF transport, due to TrkA loss, contributes to memory loss and neurodegeneration in aging and neurodegenerative disorders.

Acknowledgements

First and foremost, I extend my deepest gratitude to my supervisors, Dr. Sam Sadeghi and Dr. Margaret Fahnestock, for their unwavering guidance throughout my academic journey. They have continuously challenged me to grow and excel in my research endeavors. I am also profoundly thankful to the members of the McMaster Radiochemistry Group, past and present, for their invaluable support in the laboratory and their friendship.

Special appreciation goes to Yusra for not only being my ride or die but for the most genuine friendship and having my back in all the needing moments and good times and being my confidante to alleviating the burdens of immigration. I am grateful to Mohamed and Afaf for their incredible assistance not only in research but also in personal growth. Rafael's assistance in all animal studies and thesis writing has been a source of immense relief during stressful times. Rowan's dignified presence and kindness, coupled with Shirley's delightful snacks, have served as steadfast pillars of support, providing comfort and joy to me. Sama, your friendship, and collaboration have enriched my journey with laughter and fond memories. Stefano, thank you for always correcting me and teaching me English. Kevin, thank you for all your help with my project.

Lastly, thanks to my friends and family who have stood by me through the rollercoaster of the last two years. Shayan, thank you for being the best friend and brother I could ever ask for. Your unwavering support and guidance have been invaluable in both my personal and professional life. Mojgan and Shadi, your positivity, support and listening ears have been a source of comfort during stressful times. Agnius, your vibrant presence has added color to my life, especially during the toughest moments of my academic journey. Finally, to my parents, who have believed in me since day one and encouraged me to pursue my dreams, I owe an immense debt of gratitude. Your support and encouragement have been the driving force behind my accomplishments.

Dedication

I would like to dedicate this thesis to my family and all my friends who have supported me in every possible way over the past 2 years. I would not have made it through without your kindness and support. Your presence during challenging times has been invaluable, and I am forever grateful for always having the purest souls beside me.

Table of contents

Abstract ..... **i**
Acknowledgements ..... **iii**
Dedication ..... **iv**
List of Figures ..... **x**
List of Tables ..... **xii**
List of Schemes ..... **xii**
Chapter 1 – Introduction **1**
1.1 Aging and Alzheimer's Disease **1**
1.2 Predominant Presence of proNGF **4**
1.3 *In vitro* proNGF Retrograde Transport **5**
1.4 Molecular Imaging **8**
1.5 Nuclear imaging **9**
1.5.1 SPECT and PET imaging **9**
1.6 Radiopharmaceutical Chemistry of the Radioisotopes of Iodine **11**
1.7 Research overview **12**
Chapter 2 – In vitro Assessment of Association of ^{125}I-NGF with PC12 Cells **16**
2.1 Abstract **16**
2.2 Introduction **17**
2.3 Experimental **20**
2.3.1 Materials and Instruments 20
2.3.2 PC12 nnr5B5 and nnr5 Western Blot Analysis 22
2.3.3 Synthesis and Characterization of ^{125}I-NGF 24
2.3.4 *In Vitro* Binding Assay 29
2.3.5 Optimized *In Vitro* Binding Assay: Minimizing Non-Specific Binding 32
2.4 Conclusion **35**
Chapter 3- Preliminary In Vivo Tracking of ^{125}I-NGF Transportation Following Intrahippocampal Injection **37**
3.1 Abstract **37**
3.2 Introduction **38**
3.3 Experimental **39**
3.3.1 Materials and Instruments 39
3.3.2 Animal Studies General 40
3.3.3 *In-vivo* Study of ^{125}I-NGF Transport in C57BL/6 Mice 40
3.4 Results and Discussion **44**
3.4.1 *In vivo* Distribution Results 44
3.4.2 Autoradiography analysis 47
3.5 Conclusion **49**
Chapter 4 – Conclusion and Future Work **51**
4.1 Summary **51**
4.2 Future Directions **52**
4.2.1 *In Vitro* Binding Assay Improvement 52
4.2.2 Retrograde Transport of ^{125}I-NGF in Adult Mice 54
4.2.3 Assessing TrkA Levels and NGF Transport in Rodent Models of Aging and Disease with a PET Tracer 54

4.2.4 Therapeutic Approaches for reversing aging and neurodegenerative Disorders 56
Appendix I **.....58**
Chapter 2 – Supplementary Information **.....58**
A-1 Materials and Methods 58
A-2 PC12 Cells Priming and Neurite Outgrowth 59
A-3 Western Blot Analysis of PC12 and nnr5 Cells 60
A-4 ^{125}I-NGF Characterization 65
A-5 Gel Electrophoresis 69
A-6 Liquid Chromatography Mass Spectroscopy 72
A-7 *In Vitro* Saturation Binding Study 75
A-8 *In Vitro* Competition Binding Assay 79
References **.....82**

List of Abbreviations

%ID/g	Percentage Injected Dose per Gram
Aβ	Beta Amyloid
Ab	Antibody
AD	Alzheimer Disease
ACN	Acetonitrile
ATP	Adenosine Triphosphate
AP	Anteroposterior
BB	Blocking Buffer
BBB	Blood Brain Barrier
BCA	Bicinchoninic Acid
BDNF	Brain derived Neurotrophic Factor
BFCN	Basal Forebrain Cholinergic Neurons
BSA	Bovine Serum Albumin
CBF	Cholinergic Basal Forebrain
CNS	Central Nervous System
CT	Computed Tomography
CT	Chamber Temperature
DC	Detergent Compatible
DG	Dentate Gyrus
DIV	Day *In Vitro*
DV	Dorsoventral
ET	Emission Tomography
ERK	Extracellular signal-Regulated Kinase
FBS	Fetal Bovine Serum
FI	Fluorescent Imaging
GAPDH	Glyceraldehyde 3-Phosphate Dehydrogenase
HPLC	High Performance Liquid Chromatography
^{124}I	Iodine-124
^{125}I	Iodine-125
^{131}I	Iodine-131
IC	Intracranial
ICL	Iodine Monochloride
iTLC	Instant Thin Layer Chromatography
Kd	Dissociation Constant
Ki	Inhibition Constant
KI	Potassium Iodide
LB	Loading Buffer

LC-ESI-MS	Liquid Chromatography Electrospray Ionization Mass Spectroscopy
mAb	Monoclonal Antibody
MI	Molecular Imaging
ML	Mediolateral
MRI	Magnetic Resonance Imaging
MW	Molecular Weight
NGF	Nerve Growth Factor
NHS	N-Hydroxysuccinimidyl
O.C.T	Optimum Cutting Temperature
OI	Optical Imaging
OT	Specimen Temperature
PAI	Photoacoustic Imaging
PBS	Phosphate Buffered Saline
PC12	Pheochromocytoma Cell 12
PD	Postnatal Day
PET	Positron Emissions Tomography
pH	Power of Hydrogen
PI3K	Phosphatidylinositol-3-Kinase
PLCγ	Phospholipase C γ
PLL	Poly L Lysine
pPC12	Primed Pheochromocytoma Cell 12
ProNGF	Nerve Growth Factor Precursor
P/S	Penicillin/Streptomycin
PTP1B	Protein Tyrosine Phosphatase 1B
PVDF	Polyvinylidene Fluoride
$p75^{NTR}$	p75 Neurotrophin Receptor
QD	Quantum Dot
RAS/MAPK	Ras/Mitogen Activated Protein Kinase
ROS	Region of Interest
RP	Reverse Phase
RT	Retention Time
RT	Room Temperature
SDS-PAGE	Sodium Dodecyl Sulfate–Polyacrylamide Gel Electrophoresis
SEM	Standard Error of Mean
SMG	Submandibular Gland
SPECT	Single Photon Emissions Computed Tomography
TBS	Tris-Buffered Saline

TFA	Trifluoroacetic Acid
TrkA	Tropomyosin Receptor Kinase A
TrkB	Tropomyosin Receptor Kinase B
TrkC	Tropomyosin Receptor Kinase C
UV	Ultraviolet

List of Figures

Figure 1. AD neuropathology in a postmortem aged human brain.....1
Figure 2. Retrograde axonal transport of NGF via TrkA from cortical and hippocampal area to the cell bodies of BFCN's cell body in basal forebrain.....3
Figure 3. Comigration of NGF-immunoreactive bands observed in mouse, rat, and human brain samples with proNGF from mouse submandibular gland (SMG) though western blot analysis....5
Figure 4. Representative proNGF uptake in BFCNs is depicted, highlighting the effective retrograde transportation of QD-proNGF from axon to neuron cell body.....6
Figure 5. QD-proNGF uptake and transport in BFCNs. Images were captured one hour after addition of 50 pM QD-proNGF to the axon terminal side of the microfluidic chambers.....7
Figure 6. Reduced TrkA immunoreactivity was observed in *in-vitro*-aged BFCNs 7
Figure 7. Immunoreactivity of $p75^{NTR}$ remained stable during *in-vitro* aging.....8
Figure 8. The two opposing 511 keV ϒ-rays produced by positron decay and positron-electron annihilation are detectable via an annihilation coincidence circuit 10
Figure 9. Schematic illustrating a standard gamma camera for SPECT imaging, highlighting the role of the collimator, scintillation crystals, photomultiplier tubes, and computer in capturing and processing patient images.....11
Figure 10. Radioiodination of peptides using of pre-labeled prosthetic agents containing an active ester……..……12
Figure 11. Schematic representation of the NGF metabolic pathway under physiological conditions and its deregulation in the Alzheimer's pathology, explaining the "trophic disconnect" of NGF-dependent cholinergic neurons of the basal forebrain 13
Figure 12. Morphological features of PC12 cells 17
Figure 13. Illustration depicting the intricate network of pathways activated by TrkA and $p75^{NTR}$ 19
Figure 14. TrkA Western blot result in nnr5B5, PC12, nnr5, and HEK293 cells 23
Figure 15. Western blot quantification normalization of TrkA to GAPDH expression levels among nnr5B5, PC12, nnr5, and HEK293 (Negative control) cells.....24
Figure 16. iTLC analyses illustrating the proportion of NGF labeled with ^{125}I relative to unlabeled ^{125}I 27
Figure 17. iTLC analyses demonstrating the stability of ^{125}I-NGF in cell media after 1 hour of incubation at 37°C (left), and in PBS pH 7.4 after 24 hours (right) 28
Figure 18. HPLC traces: (A) Blank PBS pH 7.4), (B) BSA 0.5 mg/mL dissolved in PBS pH 7.4, (C) Blank run following the BSA run. (D) Co-injection of 1 µL cold NGF (0.1 µg/ µL) + 10 µL ^{125}I-NGF.....28
Figure 19. Binding and uptake of ^{125}I-NGF by PC12nnr5B5 and nnr5.....30
Figure 20. Evaluating 125I-NGF stickiness after BSA coating and Tween 80 addition 31
Figure 21. Binding and uptake of ^{125}I-NGF by PC12nnr5B5 and nnr5 under optimized assay conditions 33
Figure 22. Non-linear regression and Scatchard analysis of ^{125}I-NGF binding to TrkA in nnr5B5 cells 33
Figure 23. Binding and uptake of 28 nM ^{125}I-NGF by nnr5B5 and nnr5 cells.....34
Figure 24. Topography of the injection site (cortex) and retrograde transport of 125I-NGF to regions where BFCNs have projections, observed 24 hours post-injection.....39
Figure 25. Pilot injection practice is used to optimize the coordinates for the injection site 43

Figure 26. Coronal brain slice (1.94 mm anterior to the bregma) indicating the target coordinates (ML: -1.3 mm, AP: -2 mm, DV: -1.9 mm) highlighted by the red dot.....43
Figure 27. Bar graphs depicting the distribution of ^{125}I-NGF across distinct brain regions 44
Figure 28. Comparison between uptake and distribution of ^{125}I-NGF: pre-euthanized, 2-, and 6-hours post-injection in various brain sections 45
Figure 29. Percent ratio of ^{125}I activity in basal forebrain to activity detected in total brain.....45
Figure 30. Autoradiography of brain slices 48
Figure 31. Assessment of Pixel Saturation and Resolution. A controlled volume of ^{125}I-NGF with varying activity was exposed for seven days to evaluate pixel saturation at a resolution of 25 µm 48
Figure 32. Mouse brain half-profile view: the white bracket indicates the minimal distance between the hippocampus and basal forebrain.....50
Figure S2-1. Microscopy images capturing the progression of cell growth and neurite outgrowth over 5 days treat period with NGF.....59
Figure S2-2. Scanned membrane depicting the order of samples loaded in each lane 62
Figure S2-3. Scanned membrane after stripping and reintubation with GAPDH and total-TrkA antibodies.....63
Figure S2-4. Western blot analysis comparing levels of downstream proteins, AKT, ERK44 and 42, and TrkA among pPC12, PC12, and nnr5.....64
Figure S2-5. Radio-iTLC of crude ^{125}I-NGF (A), fraction 1 (B), fraction 2 (C).....67
Figure S2-6. Maximum UV wavelength absorbance of NGF, measured using the TECAN microplate reader 67
Figure S2-7. HPLC trace for blank (top), "test" tube (bottom, left) and "control" tube (bottom, right) at 245nm (black) and 280nm (red), and gamma trace (orange).....68
Figure S2-8. HPLC trace for blank (top), fraction 2 non-filtered (bottom, left) and fraction 2 filtered through 0.22µm filter (bottom, right) at 245nm (black), 280nm (red) and gamma trace (orange) 68
Figure S2-9. Gel electrophoresis result after staining with QC colloidal Coomassie Blue and destaining with Water.....70
Figure S2-10. Autoradiography obtained by phosphor plate scanning with Amersham Typhoon imaging machine.....71
Figure S2-11. A: UV-HPLC chromatogram using a Jupitor analytical RP C4 column. B: LC-ESI-MS analysis.....73
Figure S2-12. Saturation binding assay with pPC12 and nnr5 cells, indicating CPM versus concentration of ^{125}I-NGF 76
Figure S2-13. Morphological assessment of nnr5 cells exposed to 4 nM NGF for 5 days.....77
Figure S2-14. Saturation binding assay with pPC12 and PC12 cells, indicating CPM versus concentration of ^{125}I-NGF 78
Figure S2-15. Competition assay performed with PC12 (top) and pPC12 (bottom), illustrating CPM versus concentration of K252a 79

List of Tables

Table 1. Selected iodine radioisotopes of interest for molecular imaging and targeted radiotherapy 11
Table S2-1. Concentration of samples obtained from DC protein assay, and the corresponding amount of protein loaded per lane in a 10 well SDS PAGE 60
Table S2-2. The table indicates the expected MW and the channel for observing the protein bands for each protein 61
Table S2-3. Gel electrophoresis loaded wells specifications.....70

List of Schemes

Scheme 1. Synthesis of the highly reactive mixed halogen species (ICl), using Iodogen and ^{125}I……..25
Scheme S2-1. Sample preparation for characterization analysis of unlabelled NGF and ^{125}I-NGF……...66

Chapter 1 - Introduction

1.1 Aging and Alzheimer's Disease

Alzheimer's disease (AD) is a debilitating and irreversible neurodegenerative disorder that commonly presents itself with cognitive impairment and adverse short-term memory. Depending on the disease severity, AD can also impair expressive speech, visuospatial processing, and mental agility.[1] AD stands as a contributor to morbidity and fatality and is the most common cause of dementia [2], which is expected to increase from 50 million people in 2010 to 113 million people by 2050 worldwide.[1]

Under microscopic observation, AD pathophysiology is defined by β-amyloid (Aβ) containing extracellular plaques and tau-containing intracellular neurofibrillary tangles (Fig. 1).[2] Additionally, AD can entail the loss of synaptic homeostasis, neurons, or neuronal network integrity. Despite extensive research to better understand the mechanisms that result in synaptic and neuronal loss, which are the likely causes of cognitive impairment, the origin of the disease remains ambiguous.[1]

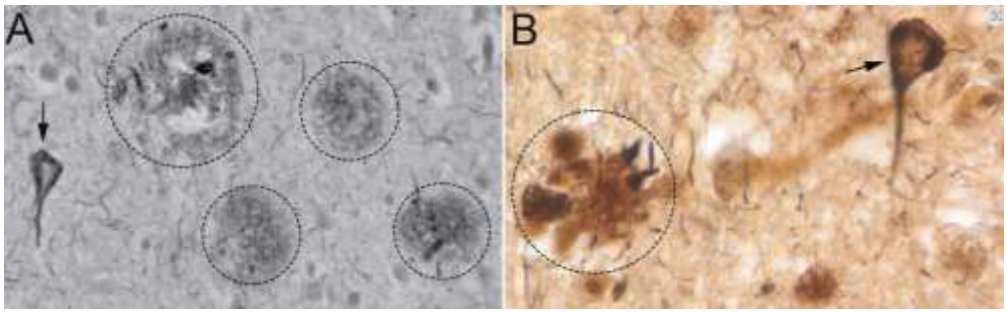

Figure 1. AD neuropathology in a postmortem aged human brain. A and B, Amyloid plaques (dashed circle) and neurofibrillary tangle (arrow).[2]

The central nervous system's (CNS) primary cholinergic innervation source, the basal forebrain, is crucial for learning, memory, attention and controlling cortical blood flow.[3] Basal forebrain cholinergic neurons (BFCNs) represent the earliest and most severely affected neurons

in aging and many neurodegenerative diseases due to their extensive projections and intricate connectivity throughout the brain.[4] These neurons depend on essential neurotrophins such as brain derived neurotrophic factor (BDNF) and nerve growth factor (NGF) for their survival and synaptic connectivity.[5] However, BFCNs do not make their neurotrophins, instead they rely on the uptake and retrograde axonal transport of the neurotrophins from the hippocampal and cortical targets across their long axons (Fig. 2).[3,5] NGF promotes the survival and differentiation of these neurons by engaging with two vital cell surface receptors: the high-affinity tropomyosin-related kinase A (TrkA) and low-affinity p75 neurotrophin receptor ($p75^{NTR}$).[6] These receptors are synthesized within cholinergic neurons in the basal forebrain and transport along their axons to reach the cortex mantle and hippocampus.[7] It has been proposed that both receptors are necessary for NGF to achieve high-affinity binding, however TrkA alone seems adequate for transmitting NGF neurotrophic effects.[6,7] After binding to TrkA, the ligand-receptor complex undergoes internalization into an endosome and retrogradely transported to the cell bodies of the cholinergic basal forebrain (CBF) neurons. Tyrosine kinase autophosphorylation also occurs following neurotrophin binding at the axon terminals, initiating signaling transduction along the axon, which sustains synaptic plasticity and axon integrity, and regulates gene expression.[8] The retrograde transport of NGF has been demonstrated *in vivo* by injecting radiolabeled NGF into the cortex or hippocampus of adult rats, leading to its transport to CBF areas.[43-45]

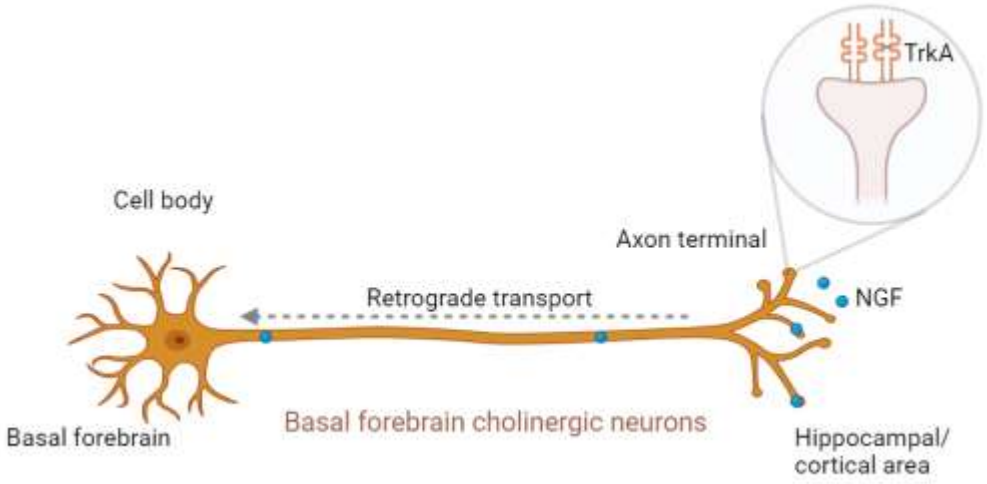

Figure 2. Retrograde axonal transport of NGF via TrkA from cortical and hippocampal area to the cell bodies of BFCN's cell body in basal forebrain.

Patients with AD and other age-related neurodegenerative disorders show signs of basal forebrain dysfunction which arises from its degeneration.[3] Synaptic loss in BFCNs correlates strongly with dementia severity in AD.[5]

Post-mortem stereological analysis is the current method for measuring TrkA expression *in vivo* for individuals with varying degrees of AD. This method of analysis suggested a causal relationship between alterations in TrkA levels within BFCN terminals in the hippocampus and cortex and the degeneration of the basal forebrain.[7] Key observations showed that while NGF mRNA remained unchanged, the level of NGF increased in the cortex of AD patients compared to the aged match controls.[9] Similarly, NGF immunoreactivity was reduced in specific neurons of the CBF in AD patients.[9] However, the expression of $p75^{NTR}$ within CBF neurons is either unaffected or increased in AD brains.[9] The ratio of TrkA to $p75^{NTR}$ plays a crucial role in determining whether NGF signals cell survival or apoptosis. When TrkA is absent, the signaling pathway tends to favor apoptosis as NGF binds to $p75^{NTR}$, thereby signaling the initiation of apoptosis.[10] Despite the unaffected NGF synthesis in the AD cortex, the protein

accumulates [9], hypothetically due to a defect in the retrograde transport of NGF to CBF neurons.[7] The loss of transport is potentially linked to receptor impairment or loss, contributing to neurotrophin transport deficits in AD pathogenesis.[7,9] Further findings from the post-mortem analysis revealed that the levels of TrkA were reduced in the cortical regions of individuals diagnosed with moderate AD compared to those with mild or no cognitive impairment.[11] This reduction in cortical TrkA expression persisted lower in severe AD cases, consisting with earlier research findings.[11] In addition to post-mortem analysis, the mouse model of Down's syndrome exhibited decreases in both size and number of BFCNs, along with regressive changes in their hippocampal terminal regions. These changes were observed to correlate with a marked impairment in the retrograde transport of NGF from the hippocampus to the basal forebrain, attributable to diminished levels of TrkA.[12] Overall, these studies highlight the importance of TrkA expression and its role in the effective retrograde transport of NGF and its function.

1.2 Predominant Presence of proNGF

The precursor of NGF (proNGF) can undergo a posttranslational process into NGF. Fahnestock et al. demonstrated that proNGF is the only form existing in the in healthy and AD brains.[13]

NGF and proNGF immunoreactive forms have been identified in the cortex of mice, postmortem humans, and rat, using Western blot analysis with three distinct antibodies.[13] These antibodies have a specific affinity towards the murine 2.5S NGF or, the first 20 amino acids of the N-terminus of the human NGF. A single band at 32 kilodalton (kDa), previously associated with proNGF, was identified in all tissue samples from mice, postmortem humans, and rat cortex. However, the mouse and rat cortex detected a very faint band aligning with the control, purified

mouse NGF monomer (13 kDa) (Fig. 3). Therefore, this study indicated that proNGF is the only form found in distinct brain areas, with the mature forms likely resulting from cleavage during the Western blotting process.

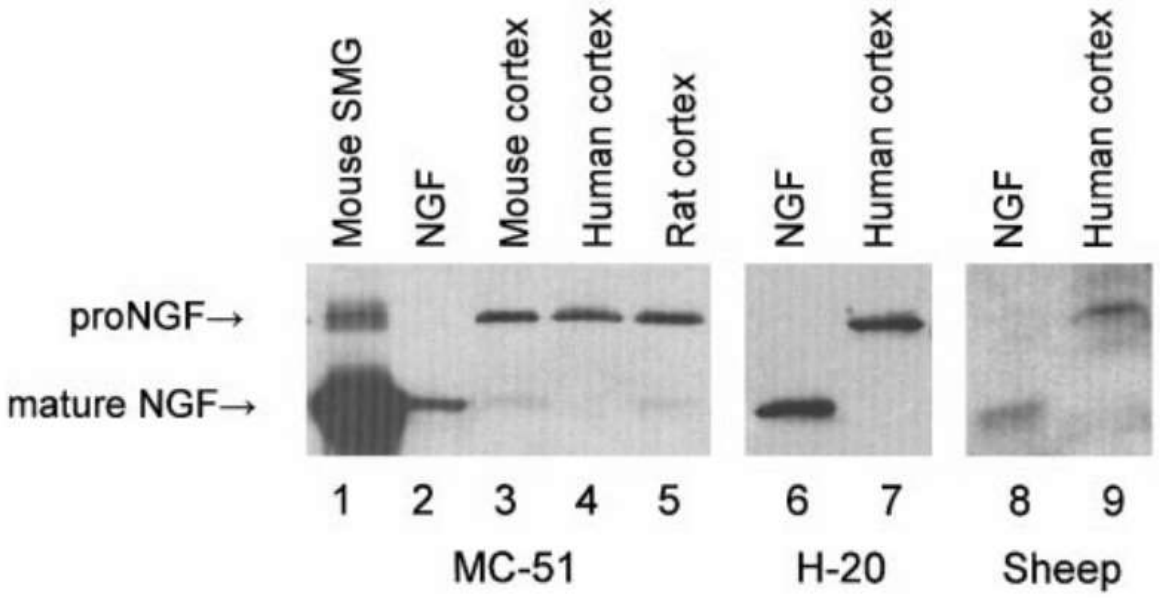

Figure 3. Comigration of NGF-immunoreactive bands observed in mouse, rat, and human brain samples with proNGF from mouse submandibular gland (SMG) by western blot analysis. NGF is also included as a control, showing a distinct band at 13 kDa. Detection of bands was achieved using three primary antibodies: MC-51, H-20, and Sheep.[13]

1.3 *In vitro* proNGF Retrograde Transport

After synthesis at the neuronal sites of production, proNGF binds to TrkA receptors at axon terminals followed by receptor endocytosis into signalling endosomes and its long-distance retrograde transport to CBF.[14]

To better understand the effect of age on BFCN axonal retrograde transport of proNGF *in vitro*, a combination of fluorescent imaging (FI) and immunostaining was executed by Fahnestock et al.[15] FI detecting Quantum Dot (QD) emissions that visualized QD-proNGF transport in

neurons, post neurotrophins starvation, indicated a reduction in proNGF transport in aged BFCNs (Fig. 4A and B & 5A-D).

Additionally, immunostaining neurons for TrkA and $p75^{NTR}$ in microfluidics chambers demonstrated a decreased mean intracellular fluorescence intensity for TrkA in aged BFCNs cells (day *in vitro* (DIV) 18) relative to young BFCNs (DIV 10) (Fig. 6A-C), while $p75^{NTR}$ immunoreactivity was not significantly different (Fig. 7A-C). While this and other *in vitro* investigations continue to provide an understanding of the proNGF transport process, they highlight the susceptibility of BFCNs to age-related changes, resulting in downregulation of TrkA and deficits in proNGF retrograde transport.[15,16] A technique for imaging this process *in vivo* has yet to be developed.

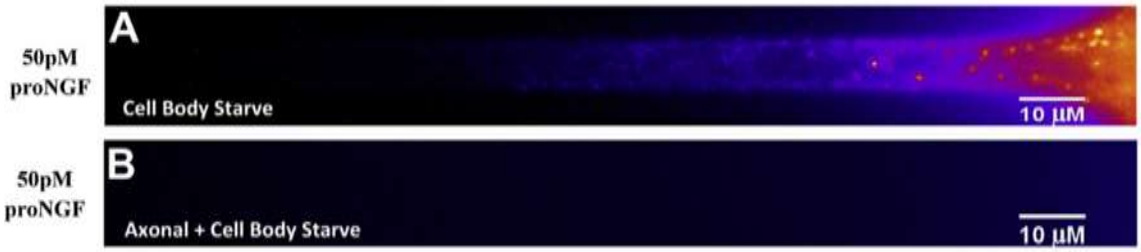

Figure 4. Representative proNGF uptake in BFCNs is depicted, highlighting the effective retrograde transport of QD-proNGF from axon to neuron cell body. Images of QD-proNGF were taken 15 minutes after the starvation of cell bodies only, followed by immediate QD-proNGF addition.[15]

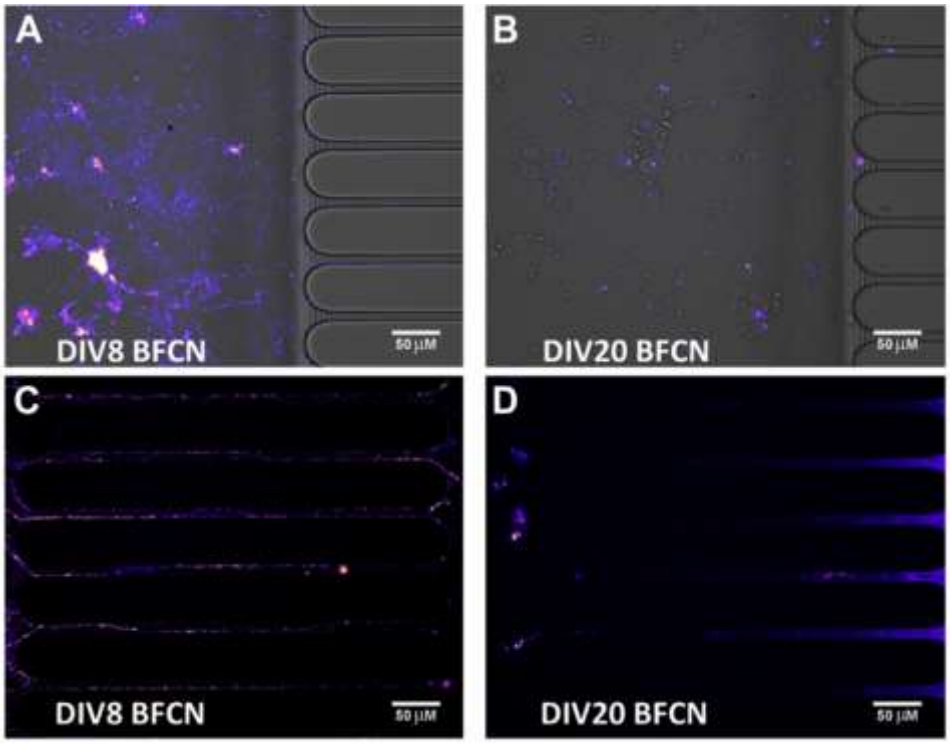

Figure 5. QD-proNGF uptake and transport in BFCNs. Images were captured one hour after addition of 50 pM QD-proNGF to the axon terminal side of the microfluidic chambers. A and B depict cell bodies, while C and D show microgrooves (axons).[15]

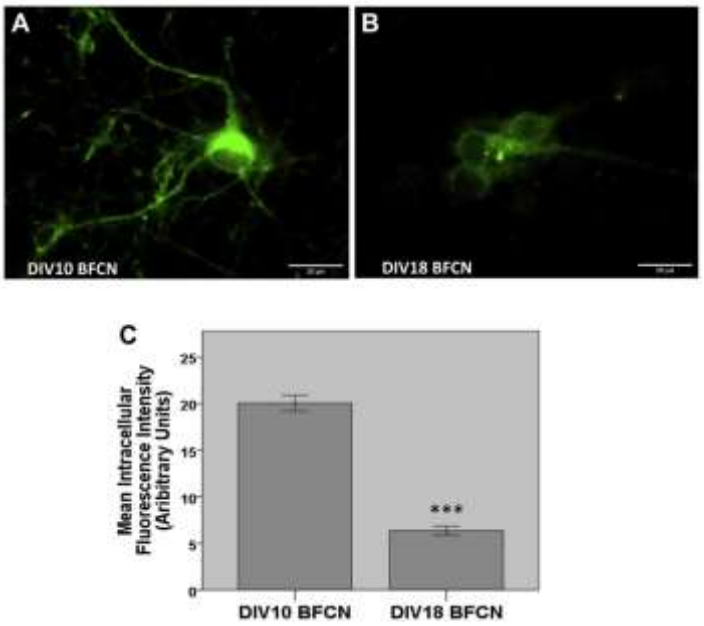

Figure 6. Reduced TrkA immunoreactivity was observed in *in-vitro*-aged BFCNs. At DIV18 (panel B), the cell bodies of BFCNs exhibited significantly lower TrkA immunoreactivity in comparison to DIV10 (panel A) The quantification of these differences is presented in panel C.[15]

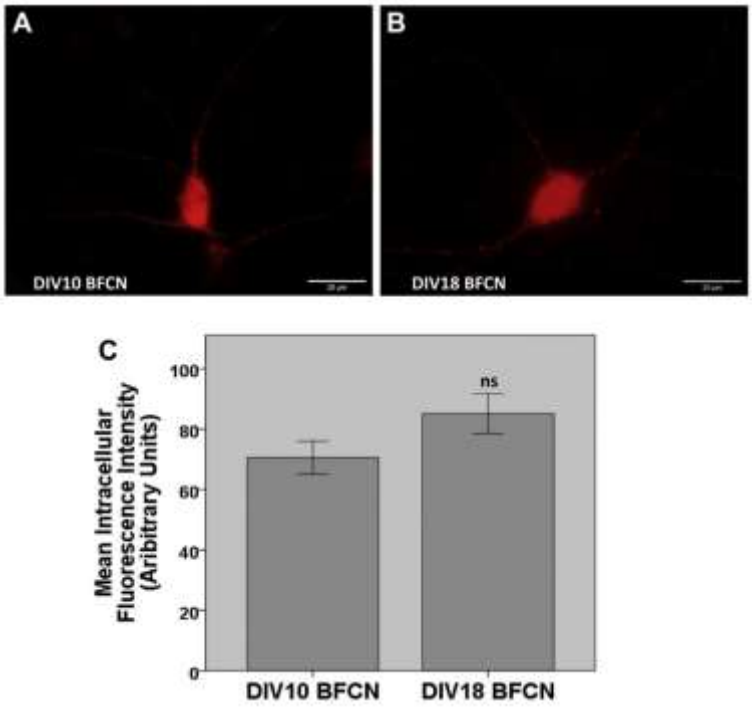

Figure 7. Immunoreactivity of $p75^{NTR}$ remained stable during *in-vitro* aging (A and B). Quantification analysis revealed no significant change in $p75^{NTR}$ immunoreactivity between DIV10 and DIV18 in BFCNs (C).[15]

1.4 Molecular Imaging

In vivo, molecular imaging (MI) techniques integrate the examination of biochemical and physiological alterations occurring within living organisms on a molecular level. Several techniques, including fluorescence, luminescence, single photon emission computed tomography (SPECT), positron emission tomography (PET), computed tomography (CT), and magnetic resonance imaging (MRI) have been developed to capture detailed images of these processes. Innovative imaging probes have been developed and characterized to enhance our understanding of diseases and biological processes, such as cancer therapy or dementia appraisal, in preclinical and clinical studies.[17-19]

1.5 Nuclear Imaging

The application of radiolabeled compounds in medical practices and research gained prominence after the advent of “radioactivity” in 1897, intravenous injections of radioactive radium in 1913, and PET/MRI scanning installation in 2008. The properties of radioactive elements (radionuclides) including half-life, decay mode, and particle or electromagnetic radiation emission, determine their application in either nuclear imaging (PET and SPECT) or nuclear radiotherapy. Thus, researchers can leverage the radiation properties of radioisotopes through radiopharmaceuticals, enabling the monitoring of pathological processes or molecular biochemistry of diseases *in vivo*. The significant contrasts in signal between healthy tissues and targeted tissues provide sensitivity and resolution for imaging or facilitate the effective delivery of therapeutic radiation to target tissues.[19] According to the 'tracer principle', radiopharmaceuticals can be administered at low molar masses to avoid perturbing biological systems while still achieving high imaging contrast, thus enabling effective visualization of target structures.[19,20]

1.5.1 SPECT and PET Imaging

Emission tomography (ET) comprises PET and SPECT imaging modalities, utilizing radioactive substances to visualize the body’s physiological processes.[21] The primary distinction between PET and SPECT lies in the type of radioisotope integrated into the radiotracer. In SPECT, a radiopharmaceutical is labelled with a single-photon emitter. This radioisotope emits a solitary gamma-ray photon during each radioactive decay event, while in PET, a ligand is labelled with a positron emitter.[21] When undergoing decay, the nucleus of a positron-emitting isotope expels a positron, and the annihilation of the positron and an electron result in the emission of two colinear 511 keV ϒ-rays (180° apart) (Fig. 8).[18,20] The ionizing radiation emitted from

radiopharmaceuticals following their radioactive decay, such as X-rays, ϒ-rays, and β-particles, can be detected using a gamma-ray detector (Fig. 9) or PET scanner.[19]

Over the years, there have been advancements in developing targeted radiotracers with high specificity and selectivity toward their biomarkers. Various vectors such as small molecules, peptides, proteins, or nanoparticles can target molecular biomarkers. Peptides and small proteins are advantageous in receptor imaging and radiotherapy due to their small size, facilitating rapid diffusion within target tissues and quick clearance from non-target organs.[22]

Proteins are good candidates for radiolabeling due to their diverse structures and functionalities, allowing for specific targeting and interaction with biological systems. They can be engineered to include specific binding motifs or targeting sequences, making them ideal for various imaging and therapeutic applications.[19,23] When radiolabelling proteins, several factors such as stability, specificity, and biological compatibility are essential to consider.[24] The compound's lipophilicity is another critical factor for specific targeting, with moderate lipophilicity suitable for most applications but higher lipophilicity required to cross the blood-brain barrier (BBB) when targeting neurological diseases such as AD.[25]

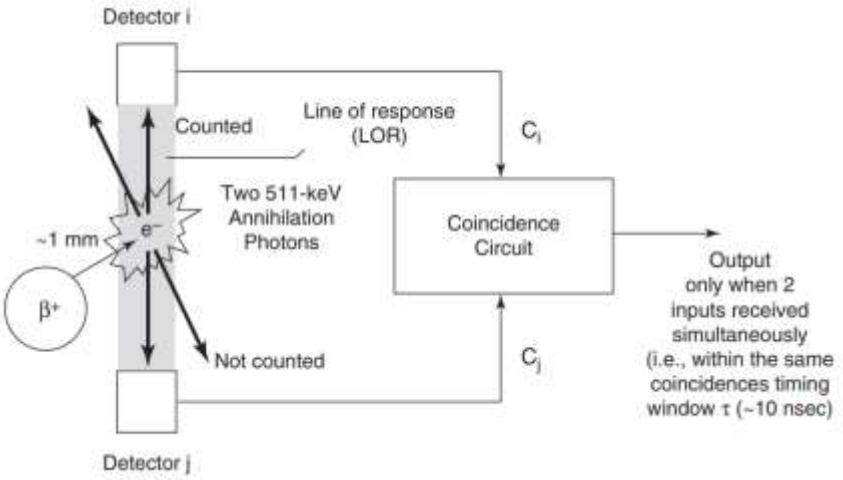

Figure 8. The two opposing 511 keV ϒ-rays produced by positron decay and positron-electron annihilation are detectable via an annihilation coincidence circuit.[19]

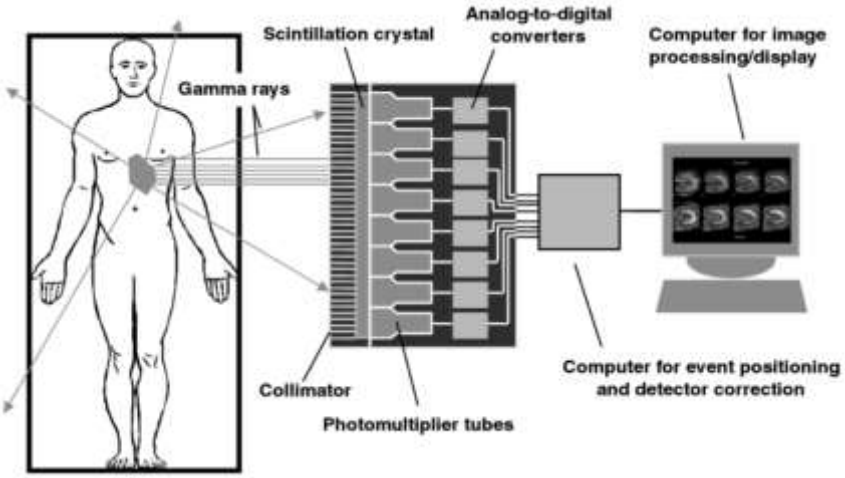

Figure 9. Schematic illustrating a standard gamma camera for SPECT imaging, highlighting the role of the collimator, scintillation crystals, photomultiplier tubes, and computer in capturing and processing patient images.[19]

1.6 Radiopharmaceutical Chemistry of the Radioisotopes of Iodine

Iodine has more than 30 known radioisotopes, each with a unique physical half-life and nuclear decay route, making it an excellent choice for radiolabeling molecules (Table 1). Proteins and peptides can be labelled directly, or through conjugation reactions using prosthetic groups without perturbing their biological activity.[19] Due to its cost effectiveness, wide availability, minor shielding difficulties, and long half-life (60-days), Iodine-125 (^{125}I) has become the cornerstone for radiochemistry, cell culture, and animal model research for the development of radioiodine-based radiopharmaceuticals. Other isotopes of iodine, such as Iodine-123 (^{123}I) emit radiation with the ideal energy for SPECT imaging, while others such as Iodine-124 (^{124}I) have potential for PET imaging.[19]

Radioisotope	Half-life	Type of decay	Energy (keV)	Imaging application	Therapeutic application
^{123}I	13.2 h	Gamma EC/Auger	159 <5	SPECT	Auger electrons
^{124}I	4.2 days	Positron Annihilation radiation	687 + 975 β$^+$(mean) 511γ	PET	
^{125}I	60.1 days	Gamma EC/Auger	35.5 <5	Preclinical SPECT	Auger electrons
^{131}I	8.0 days	Gamma β-particle	364 192 (mean)	SPECT	β-particles

Table 1. Selected iodine radioisotopes of interest for molecular imaging and targeted radiotherapy.[16]

Protein iodination, unlike peptides, needs to be done in aqueous buffers, ideally at physiological pH. Although direct electrophilic radioiodination is the most widely used technique for radioiodinating proteins, directly iodinated proteins can demonstrate limited stability in an *in vivo* setting, leading to dehalogenases and sequestration of radioiodine in the thyroid. In addition, the oxidizing agents required for radioiodination can oxidize aromatic amino acids such as tryptophan, reducing binding affinity. Indirect labelling methods can offer milder radiolabeling conditions despite the two-step process. This method uses activated ester chemistry to attach pre-labelled prosthetic agents with ^{125}I to the protein via biochemical conjugation (Fig. 10). The resulting conjugates typically exhibit excellent *in vivo* stability without the risk of oxidizing amino acids.[19]

Figure 10. Radioiodination of peptides using of pre-labeled prosthetic agents containing an active ester, such as N-hydroxysuccinimidyl (NHS).[19]

1.7 Research Overview

Although proNGF is recognized as the prevalent form in the brain [13], research in this thesis utilizes NGF due to its stability and limited access to micrograms of stable proNGF that does not undergo cleavage.

In AD and other neurodegenerative disorders, elevated levels of proNGF in the hippocampal and cortical regions are hypothesized by different research groups to be either due to TrkA loss or result from dysregulation in the protease cascade controlling proNGF conversion and NGF degradation.[26] The conversion of proNGF to NGF is primarily mediated by the serine protease plasmin.[27] NGF then exists transiently in the extracellular space, where it either binds to its receptors (TrkA and $p75^{NTR}$) for retrograde transport to cholinergic neuron cell bodies or undergoes degradation, facilitated by matrix metalloprotease 9 (MMP-9) in the healthy brain (Fig. 11).[28] This degradation process is inhibited in AD.[26,28] Overall, the two hypotheses provide different perspectives on the molecular mechanisms underlying AD and neurodegeneration, highlighting the complex interplay between neurotrophic factor signaling, protease activity, and neuronal function. Further research is needed to elucidate the relative contributions of TrkA loss and protease dysregulation to disease pathogenesis.

In this study we aim to investigate the mechanisms underlying the accumulation of proNGF in the hippocampus and cortex due to TrkA loss, leading to the lack of binding and uptake of this neurotrophin.

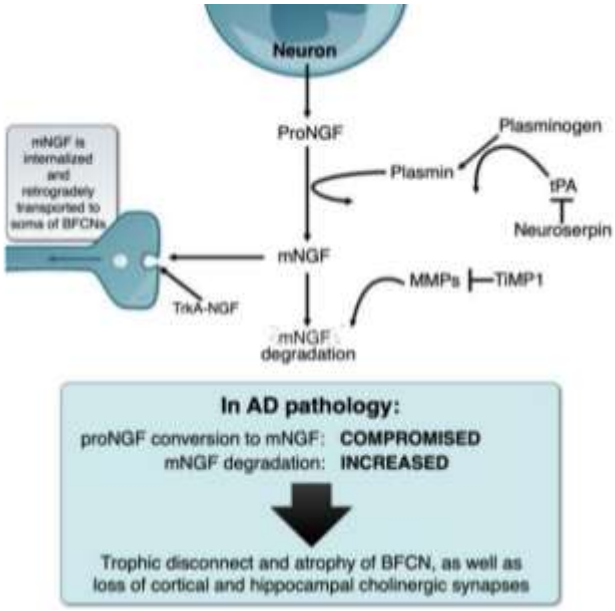

Figure 11. Schematic representation of the NGF metabolic pathway under physiological conditions and its deregulation in the Alzheimer's pathology, explaining the "trophic disconnect" of NGF-dependent cholinergic neurons of the basal forebrain.[29]

The ultimate objective of this study would be to develop a TrkA-PET tracer capable of quantifying TrkA loss *in vivo* and detecting BFCN neurodegeneration. Currently available PET radiotracers are flawed due to their various limitations, including lack of specificity for individual members of the Trk receptor family, low brain uptake, limited BBB penetration, and applicability only in cases of high Trk receptor expression. Therefore, there is a critical need for a specific TrkA-targeting PET tracer and validation of its ability to measure TrkA levels and the retrograde transport of NGF in real time. Being able to quantify TrkA in vivo will facilitate the comparison of the amount and speed of TrkA retrograde transport in real-time between healthy and diseased mice.

Prior to synthesizing the TrkA-PET tracer for live imaging in rodent models of aging and AD, the initial step involves synthesizing and demonstrating the retrograde transport of radioiodinated NGF (^{125}I-NGF) in healthy adult mice. Despite the extensive research conducted on rats [43-45], it is notable that a retrograde transport distribution study of this nature is yet to be done on mice. The choice of mice for this study is driven by the access to two crucial mouse models: 3xTg-AD mice which are considered the most applicable mouse models of AD, and TrkA-R685A knock-in mice which carry a mutation in the TrkA gene leading to reduced TrkA levels, thereby mimicking the age-related loss of TrkA. The utilization of ^{125}I-NGF will facilitate the validation of the newly developed PET tracer's specificity for TrkA in *in vitro* receptor binding studies. Furthermore, a comparative analysis can be conducted between PET imaging results obtained with the PET tracer and the autoradiography pattern of ^{125}I-NGF. This comparative analysis will furnish insights into the accuracy and reliability of the PET tracer in real-time for

detecting known TrkA expression regions in cholinergic areas and the striatum.[30] Such validation is crucial for comprehending the dynamics of NGF transport and receptor binding *in vivo*, as well as for delineating its potential clinical applications.

Therefore, in short-term the research aims to include the radiochemical synthesis, purification, and characterization of an NGF-based TrkA imaging tracer (^{125}I-NGF). Following validation of ^{125}I-NGF binding to TrkA, the tracer will be used for *in vivo* brain uptake and retrograde transport distribution via intracranial (IC) injections in mice. Examining the molecular mechanism of memory loss in aging and AD facilitates future *in vivo* testing and monitoring of therapeutics for age-related cognitive decline, and restoration of TrkA and NGF transport.

Before conducting in-vivo studies, it is necessary to perform *in vitro* tests to predict the *in vivo* characteristics of a newly developed radiopharmaceutical. Diverse *in vitro* tests can be implemented to assess the specificity of the radioligand for its target.[31] The specificity and selectivity of ^{125}I-NGF for TrkA are evaluated in this thesis to set the stage for advancing to *in vivo* studies. The following chapters elaborate on preliminary IC injections of ^{125}I-NGF in mice, which confirmed the localization and delivery of the radioligand in the region of interest, the hippocampal dentate gyrus (DG).

Chapter 2 – *In vitro* Assessment of Binding of ^{125}I-NGF to PC12 Cells

2.1 Abstract

This chapter focuses on investigating the specific binding of ^{125}I-NGF to its receptor by *in vitro* radio-binding assays. *In vitro* binding assays provide insight into radiolabelled compounds' binding kinetics, receptor interactions, and binding characteristics within a controlled environment.

The utilization of pheochromocytoma cell line 12 (PC12) nnr5B5 cells, which overexpress TrkA, provided a good *in vitro* model for studying the binding affinity of radiolabeled NGF to TrkA. The aim of this study was to characterize the receptor binding kinetics, dissociation constant (Kd), and maximum binding capacity (Bmax) values of ^{125}I-NGF. Additionally, we aimed to prove that ^{125}I-NGF maintains its binding capacity without compromising protein's ability to bind the receptor. It is important to observe labeling conditions that might affect binding capacity such as harsh conditions or excessive random binding of ^{125}I to tyrosine residues. This chapter outlines the experimental approach, including iodination of NGF, associated characterization, stability tests, and *in vitro* binding assays.

This section describes the radioiodination process of NGF through electrophilic substitution with ^{125}I, achieving a radiochemical purity of 99.17 ± 0.18%. The purity of the compound was validated by instant thin-layer chromatography (iTLC) and high-performance liquid chromatography (HPLC). The stability of the radioiodinated NGF in cell media and over various days was verified by iTLC. The expression levels of TrkA were assessed in PC12nnr5B5 and nnr5 (TrkA knockout) cells via western blot. Subsequently, the specific binding of ^{125}I-NFG to TrkA was demonstrated with an *in vitro* binding assay.

2.2 Introduction

The mature form of NGF (2.5S NGF) was initially isolated and purified from the submandibular glands of mice.[32] 7S NGF comprises a protein complex with a molecular weight (MW) of 140 kDa, composed of three subunits known as α, β and ϒ. Among these subunits, the β-subunit, which has monomer MW of 13 kDa, is found as dimer of 26.5 kDa, and is commonly referred to as 2.5S NGF, possesses the ability to promote neurite outgrowth.[32]

A secondary cell line, PC12, derived from a rat pheochromocytoma, is a valuable model for studying the mechanisms of NGF function *in vitro*. PC12 cells can adopt characteristics resembling those of normal sympathetic neurons when treated with NGF (Fig. 13), making them suitable for investigating NGF-related processes.[33] When exposed to nanogram levels of NGF in the culture medium, PC12 cells undergo significant changes including ceasing cell division, extending neurites, becoming electrically excitable, and exhibiting increased chemosensitivity to acetylcholine. These effects are reversible; the withdrawal of NGF leads to neurite disintegration and the resumption of mitotic activity. These findings suggested that, under NGF treatment, PC12 cells adopt characteristics resembling those of normal sympathetic neurons (Fig. 12).[33]

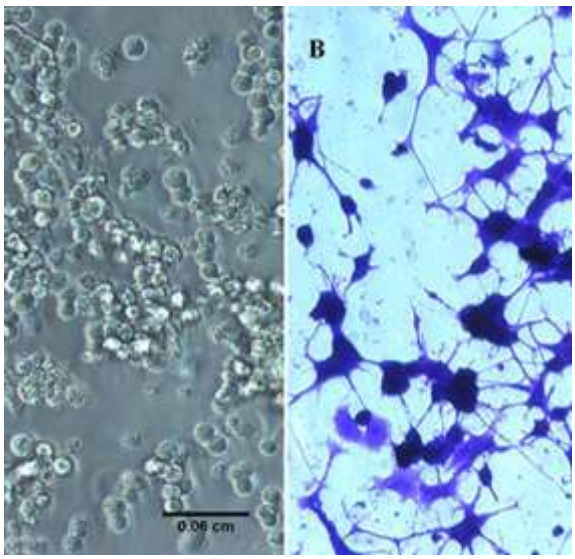

Figure 12. Morphological features of PC12 cells. Undifferentiated cells grow as round aggregates (A) in the medium (unstained). NGF exposed cells (B) develop extensive growth of neurites (stained with crystal violet dye) with intercellular junctions.[34]

PC12 cells do not depend on NGF for survival. As a result, their receptors can be examined and compared both before and after different durations of NGF exposure.[35] Activation of the neurotrophin receptor TrkA by its ligand NGF initiates a cascade of signaling events, promoting neuronal survival and differentiation *in vitro*.[36,37] Upon NGF binding, TrkA receptors undergo rapid phosphorylation on tyrosine residues, activating their tyrosine kinase domain. Phosphorylated tyrosine residues in the TrkA cytoplasmic domain act as binding sites for downstream signalling molecules, connecting TrkA to various intracellular pathways including the Ras/mitogen activated protein kinase (RAS/MAPK) and phosphatidylinositol-3-kinase (PI3K/AKT) pathway (Fig. 13).[5] The activation of MAPK, also known as extracellular signal-regulated kinases (ERKs), subsequently triggers the activation of transcription factors and the induction of immediate-early genes. The induction of these genes suggests a feedback mechanism that allow NGF to modify its own signaling pathway by influencing the expression of its receptors.[36]

The effects of NGF on TrkA were found to be time-dependent.[36] After seven days of NGF treatment, cells demonstrated a modest increase in binding to $gp140^{TrkA}$, the protein product of the proto-oncogene TrkA, and enhanced signaling through this receptor. Moreover, previous *in vitro* binding studies of PC12 cells pre-treated with NGF for several days show a higher binding and uptake of ^{125}I-NGF compared to non-NGF-treated cells.[34] These findings highlighted the gradual up-regulation of TrkA in response to NGF exposure, providing evidence of NGF's influence on surface receptor levels and its multi-stage regulation of TrkA.[34,37]

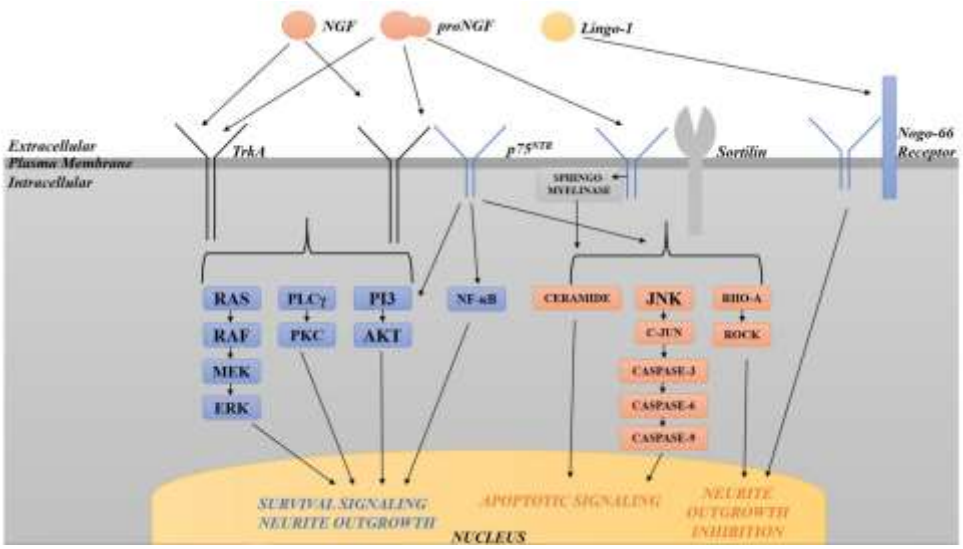

Figure 13. Illustration depicting the intricate network of pathways activated by TrkA and $p75^{NTR}$. TrkA triggers pro-survival pathways, including the RAS/MAPK, Phospholipase C γ (PLCγ), and PI3K/Akt pathways.[5]

PC12nnr5 and PC12nnr5B5 have been genetically modified to alter TrkA expression.[38] Specifically, TrkA expression was eliminated in nnr5 cells, whereas it was enhanced in nnr5B5 cells. Ioannou and Fahnestock demonstrated minimal TrkA protein levels in PC12 nnr5 cells, in contrast to the high TrkA expression observed in PC12nnr5B5 cells via western blot.[38] While NGF still interacts with its low-affinity binding site ($p75^{NTR}$) in PC12nnr5 cells, there is no TrkA expressed for binding and subsequent internalization through its conventional pathway.[39]

Previous *in vitro* studies have investigated the association of ^{125}I-NGF with both PC12 and PC12 nnr5 cells under varied conditions.[37,39] The purpose of these studies was to distinguish between low ($p75^{NTR}$) and high-affinity (TrkA) binding sites, evaluate ^{125}I-NGF surface binding versus internalization, and identify the receptor responsible for internalization during incubation with ^{125}I-NGF. Results indicated that PC12 cells' uptake of NGF occurs by high-affinity receptors via receptor-mediated endocytosis, not involving low-affinity receptors. Therefore, nnr5B5 and

nnr5 cell lines can serve as representative models of TrkA-positive and TrkA-negative expression for in vitro studies. Nnr5B5 cells exhibit enhanced TrkA expression, while nnr5 cells only possess low-affinity p75NTR receptors and do not uptake NGF.

2.3 Experimental

2.3.1 Materials and Instruments

Chemicals and reagents were purchased from Thermo Fisher Scientific (chloroglycoluril available as IODO-GEN® (Pierce)) and Alomone Labs (native mouse NGF 2.5S protein, 99% (Cat. N-240)) and used without further purification unless otherwise stated. HPLC was performed on a Waters 1525 Binary HPLC system connected to a BioScan g-detector and a Waters 2998 Photodiode Array Detector monitoring at 220 and 280 nm. Analytical reverse phase (RP) HPLC separation was performed with a Waters XBridge BEH C4 column 300Å, 3.5 µm, 10K – 500K, 1/pkg. Column dimension: 2.1mm × 250 mm using methods A: 0.1% Trifluoroacetic Acid (TFA) in 100% HPLC grade water, B: 0.075% TFA in 71% acetonitrile (ACN)/28.6% HPLC grade water. Gradient: 28% B to 100% B in 25 minutes, curve 6. Flow rate: 0.20 mL/min. Temperature: RT, loop size: 20 µL. Agilent, Amicon Ultra-4 (Ultracel-3k) was purchased form Millipore Sigma (Cat. UFC800324) and used for product purification. Radioactivity was measured with a dose calibrator (Capintec, Remsey, NJ, USA) or a Perkin Elmer Wizard 1470 Automatic Gamma Counter. ^{125}I was produced by the McMaster Nuclear Reactor and provided as a solution of NaOH 0.010 Ci in 0.100 mL (pH: 10.6). Radio-TLC was performed using a Bioscan AR-2000 imaging scanner on iTLC-SG glass microfiber chromatography paper (SGI0001, Agilent Technologies) and eluted with 0.1 M citrate buffer (pH 5.5).

PC12 cells were purchased from ATCC (CRL-1721). Components of the complete growth media, including RPMI 1640 (Cat. A1049101), 10% Fetal Bovine Serum (FBS) (Cat. FB12999102), 5% HI Horse serum (Cat. 26050-088), and 1% Penicillin/Streptomycin (P/S) (Cat. 15140-122), were purchased from Thermo Fisher Scientific. T75 flasks (Cat. 83.3911.592) and 96-well plates (Cat. 821581200) were acquired from SARSTEDT. RIPA lysis buffer (1M Tris pH 7.5), 4M NaCl, 0.5 EDTA from Thermo Scientifc (Cat. 1860851), 10% SDS, 10% Nonidet p-40, 10% Sodium Deoxycholate, Halt protease and Phosphate Inhibitor were aquired from Thermo Scientific (Cat. 87785); Roche PhosStop was aquired from Roche (Cat. 04906837001); and ddH2O) was prepared in-house. A detergent compatible (DC) protein assay kit was purchased from BioRad: Reagent A (Cat. 5000113), Reagent S (Cat. 500-0115), and Reagent B (Cat. 5000114). Samples were mixed with Laemmeli-loading buffer (LB) from BioRad (Cat. 1610747) and β-mercaptoethanol from Sigma (Cat. M6250) before being loaded into 10% precast Polyacrylamide gel from BioRad (Cat. 4561034) for western blotting. For transfer, blotting paper from BioRad (Cat. 1703956) and Polyvinylidene Fluoride (PVDF) membrane from Sigma Aldrich (Cat. IPFL00010) were utilized. All buffers used for western blot were prepared in-house unless otherwise stated. The standard protein ladder used for western blot was purchased from FroggaBio (Cat. PM0080500F). The blocking buffer (BB) from LI-COR (Cat. 92780001) was employed to block the PVDF membrane. Primary antibodies (Abs) used were as follows: Anti-TrkA Rabbit Ab (1:800, Sigma, Cat. 06-574). Glyceraldehyde 3-phosphate dehydrogenase (GAPDH) (D4C6R) mouse monoclonal antibody (mAb) (1:10,000, Cat. 97166S), and β-Actin (13E5) rabbit mAb (1:10,000, Cat. 4970S). Secondary Antibodies used: IRDye 680 Goat Anti Rabbit (1:10,000 in BB/PBS-T (phophate buffered saline-Tween 20) Licor BioSciences 926-32221), and IRDye 800

Goat-Anti-Mouse (1:10,000 in BB/PBS-T, Licor Bioscinces 926-32210). Detection was performed using an Odyssey Infrared Imager (Li-COR Bioscience).

2.3.2 PC12 nnr5B5 and nnr5 Western Blot Analysis

As stated in the Appendix for Chapter 2, western blot analysis was conducted to visualize TrkA expression in both primed PC12 (pPC12), which were pre-treated with NGF to induce overexpression of TrkA, and PC12 cells. However, a difference in expression levels was not visualized. Therefore, the study proceeded with mutagenized PC12 nnr5B5 and nnr5 cells as positive and negative controls, with TrkA overexpressed and knocked out, respectively.

Both PC12 nnr5B5 and nnr5 cells were cultured in T75 flasks containing complete media (RPMI 1640, 10% horse serum, 5% FBS, and 1% P/S). Following culturing, the cells were washed with PBS, and lysed using RIPA buffer. The lysates were then incubated on ice for 15 minutes, sonicated, and spun down at 4°C for 10 minutes at 13,000 rpm. The supernatant was stored at -20°C. Total protein concentration of the cell lysates was assessed using DC protein assay. Samples with various dilutions were loaded in triplicate into each well of a 96-well plate. After the addition of Reagents S:A (1:50) and 200 µL Reagent B to each sample, the plate was incubated for 20 minutes at room temprature (RT). The concentration of proteins was determined by measuring the absorbance at 750 nm using a microplate reader. The maximum amount of protein loaded per lane was determined based on the volume that could fit into individual wells of a 10% polyacrylamide gel. Different masses of protein were loaded for nnr5B5 and PC12 cells due to the higher amount of protein obtained from their cell lysates (Fig. 15). The gel was run at 90 V for the first 20 minutes and then increased to 118 V for the remaining hour and more, totaling one and a half hours of electrophoresis. The proteins were transferred to a PVDF membrane at 4°C for 1.5 hours at 250

mA. Following membrane transfer, the membrane was washed with Tris-Buffered Saline (TBS) and then incubated with blocking buffer (2.5 mL protein-free BB and 2.5 mL TBS) for 1 hour at room temperature (RT). Subsequently, the membrane was incubated overnight at 4°C with a solution containing 5 mL TBS/BB, 12 µL 0.05% Tween-20, and primary antibody anti-TrkA (1:800). Housekeeping antibodies, GAPDH (D4C6R) (1:10,000) and β-Actin (13E5) (1:10,000), in a 1:1 ratio of BB to TBS, and 0.05% Tween-20 were used as reference, and were incubated for 1 hour at RT.

The membrane was washed and then incubated with secondary antibodies (IRDye 680 goat anti-rabbit and IRDye 800CW goat anti-mouse) (1:10,000) in 5 mL BB/TBS-T (0.05% Tween-20) for 1 hour at RT. Finally, the membrane was scanned using an Odyssey Infrared Imager with an 84 µm resolution (Fig. 14).

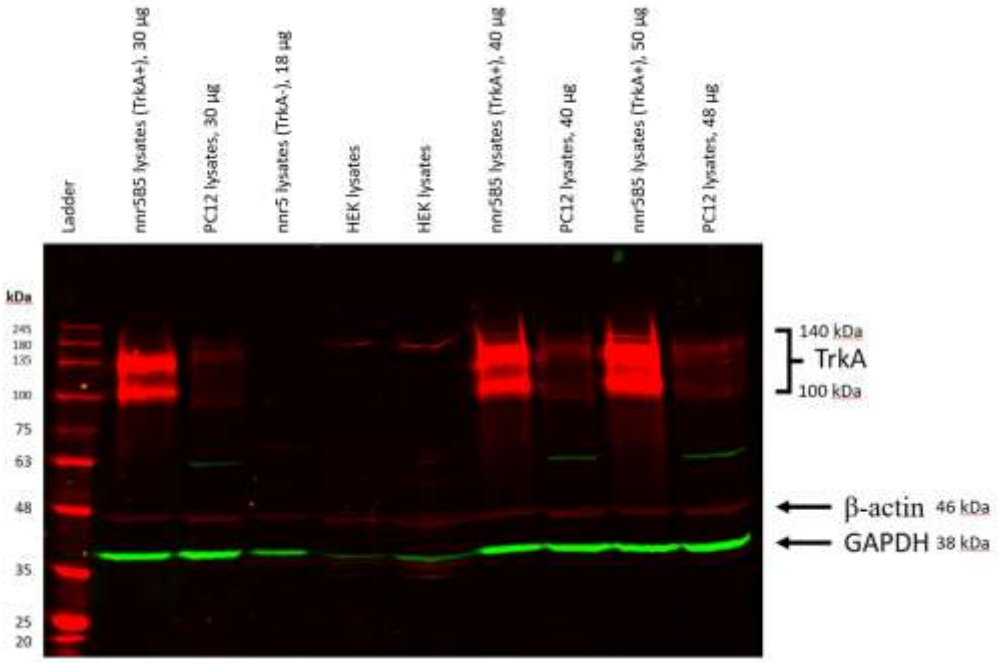

Figure 14. TrkA Western blot result in nnr5B5, PC12, nnr5, and HEK293 cells. nnr5B5 cells, which overexpress TrkA, PC12 cells, which moderately express TrkA, and nnr5 cells, which are TrkA knockout, were loaded to observe high, moderate, and absent levels of TrkA expression, respectively. HEK cells were incorporated as a negative control since they do not express TrkA.

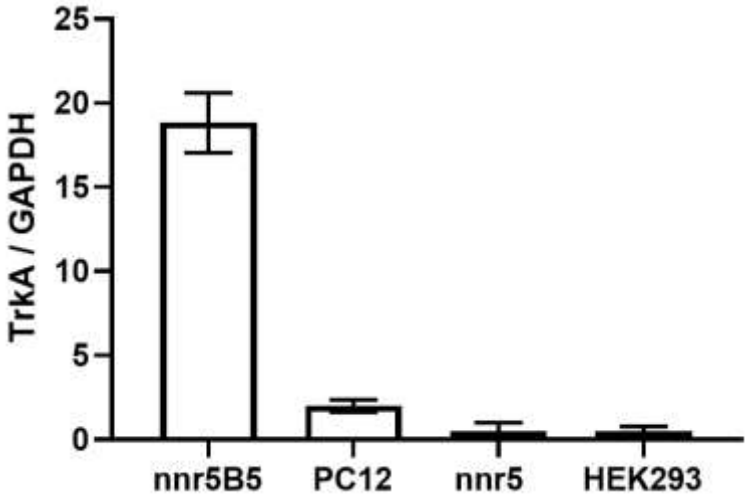

Figure 15. Western blot quantification normalization of TrkA to GAPDH expression levels among nnr5B5, PC12, nnr5, and HEK293 (Negative control) cells.

The quantitative analysis of the western blot involved dividing the signal for TrkA by the signal for GAPDH for each cell line (Fig. 15). As expected, the normalized TrkA expression at 140 kDa is higher in the overexpressing nnr5B5 cells (mean: 18.83) than in regular PC12 (mean: 2). A lower mean of 0.5 was observed for both nnr5 and HEK293 cells, indicating negligible TrkA expression compared to the nnr5B5 and PC12 cells.

2.3.3 Synthesis and Characterization of ^{125}I-NGF

Direct method of radioiodination using Iodogen was employed to radiolabel NGF with ^{125}I. Since Iodogen is insoluble in aqueous solutions, it functions as a solid-phase radioiodination reagent. Initially, a solution of 1 mg/mL Iodogen in chloroform was prepared. 10 µL of the Iodogen solution was transferred to a low-bind Eppendorf tube and dried with a low stream of air, creating a thin coating at the bottom of the tube. Subsequently, 6 µL Na^{125}I was added to the tube, allowing Iodogen to react with iodide ions for 2-3 minutes, resulting in oxidation and the formation of a reactive, mixed halogen species, iodine monochloride (ICl). Following this, 150 µL of 0.1 µg/µl

NGF in Phosphate Buffered Saline (PBS) pH 7.4 was added. The reaction ran for 12 minutes at RT with agitation. ICl can undergo a rapid reaction with either tyrosine or histidine side-chain groups within the NGF (Scheme 1). Tyrosine has been established as the primary site for iodine addition in large biomolecules. However, under conditions where the pH exceeds 8.5, a secondary site on the imidazole ring of histidine is favored for the reaction.[21] Following the completion of the reaction, the activity of crude was measured usinga dose calibrator (632 µCi). 2 µL from the crude reaction mixture was spotted on an instant thin layer chromatography (iTLC) plate to assess the radiochemical conversion (Fig. 16).

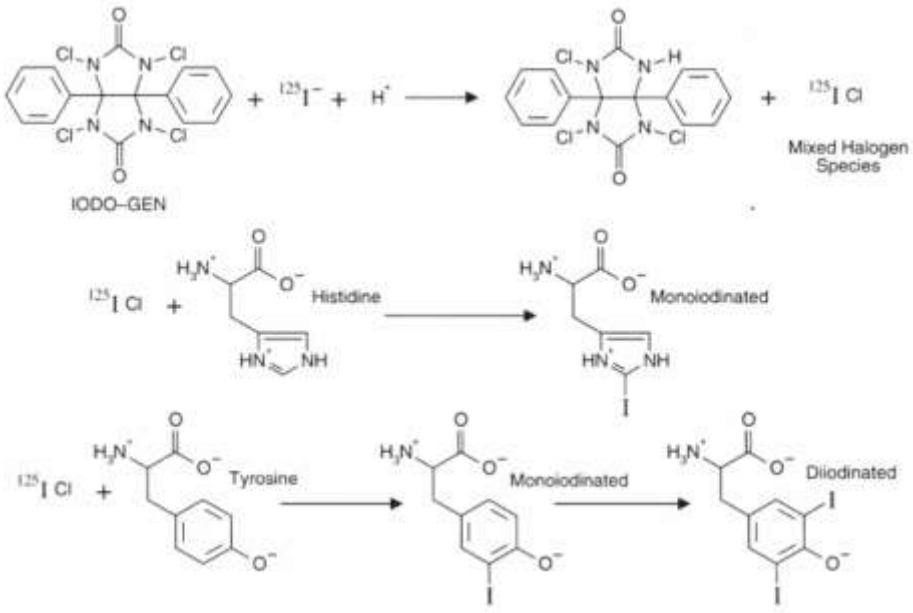

Scheme 1. Synthesis of the highly reactive mixed halogen species (ICl), using Iodogen and ^{125}I. This intermediate can add radioactive iodine atoms to tyrosine or histidine side chain rings.[18]

Previously established comparisons indicated that ultrafiltration through Centricon microconcentrators outperformed both Centriflo CF50A membrane and gel filtration with Bio-Gel P-60 in isolating highly pure ^{125}I-NGF. The use of centrifugal filtration not only streamlines the retrieval of ^{125}I-NGF but also reduces the amount of time that it is exposed to an unshielded

radioactive source during the handling of the iodination mixture.[40] Therefore, the contents of the tube were transferred to the Amicon Ultra-0.5 centrifugal filter with a 3 kDa cut-off. The empty reaction tube was washed with 200 µL PBS pH 7.4 and added to the filter. The contents were centrifuged for 4 cycles of 20 minutes at 4°C and 4000 rpm, with the addition of 300 µL PBS between each run (total PBS volume used: 1.1 mL). 2 µL was taken from the filter to assess the purity by iTLC (Fig. 16). Following this, the filter was inverted into a new Eppendorf tube and centrifuged for 15 seconds at 4000 rpm to collect the pure product in the tube (351 µCi). The specific activity estimated by tracking the activity at each purification step and calculated to be 42.814 ± 14.21 µCi/µg.

The implementation of this radioiodination method, by electrophilic substitution, and comprehensive assessment of purity using iTLC (Fig. 16) and HPLC (Fig. 18), indicated synthesis of ^{125}I-NGF with a radiochemical yield (RCY) of 91.08 ± 1.20% (n=8) and a high purity of 99.17 ± 0.18% (n=8). Additionally, stability evaluation of pure ^{125}I-NGF in PBS pH 7.4 after 24 hours, and in cell media after incubation at 37°C for 1 hour via iTLC, revealed that the compound remained stable in both conditions (Fig. 17).

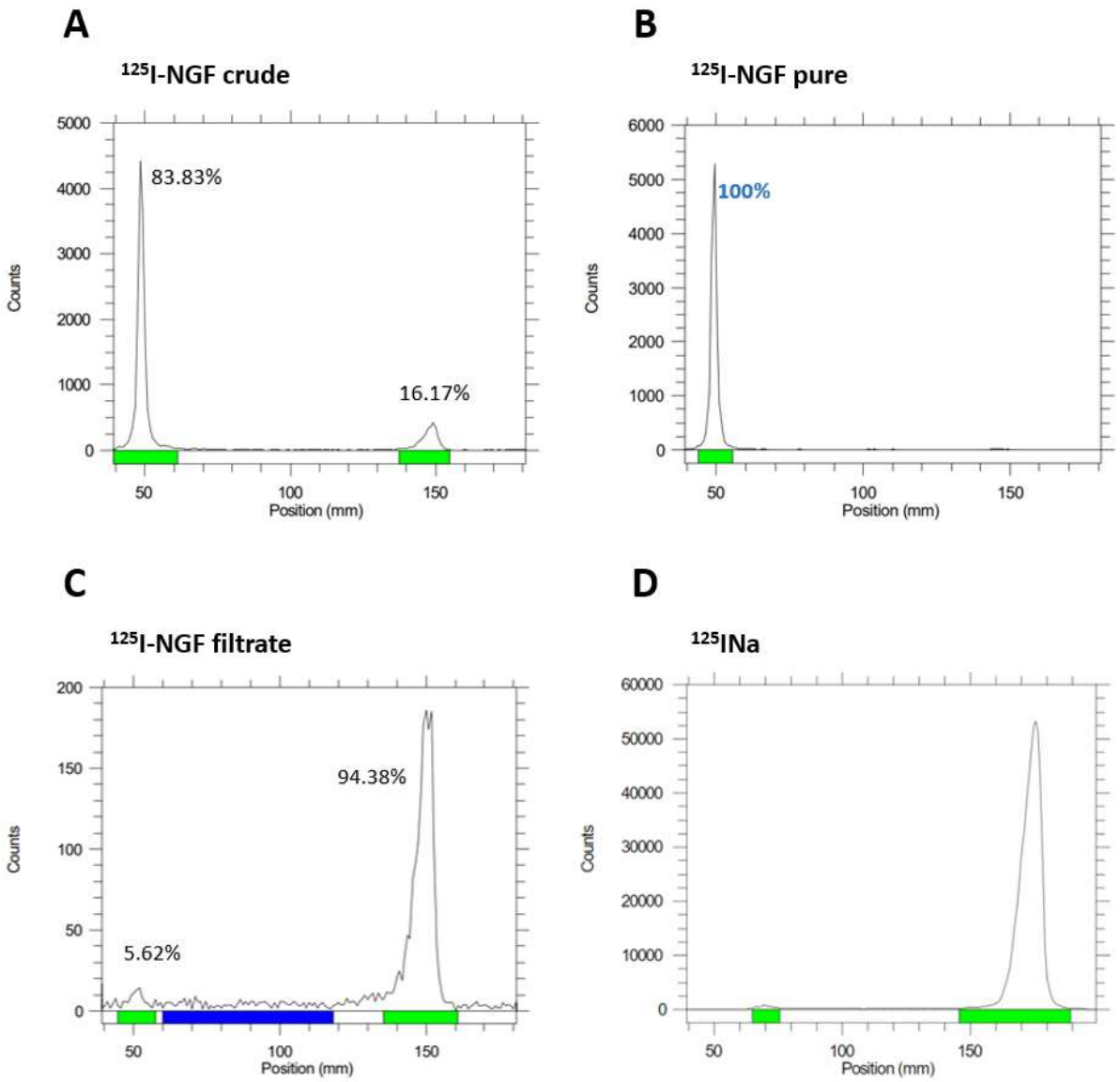

Figure 16. iTLC analyses illustrating the proportion of NGF labeled with ^{125}I relative to unlabeled ^{125}I. Radioiodinated NGF remained at the baseline, whereas free iodine migrated to the solvent front. A) iTLC showed a radiochemical yield of 83.83% before the crude underwent purification. B) iTLC demonstrated a 100% successful isolation of ^{125}I-NGF in the filter after the purification process. C) iTLC of the filtrates indicates the presence of free iodine. D) iTLC indicates the Na^{125}I migration with the solvent front.

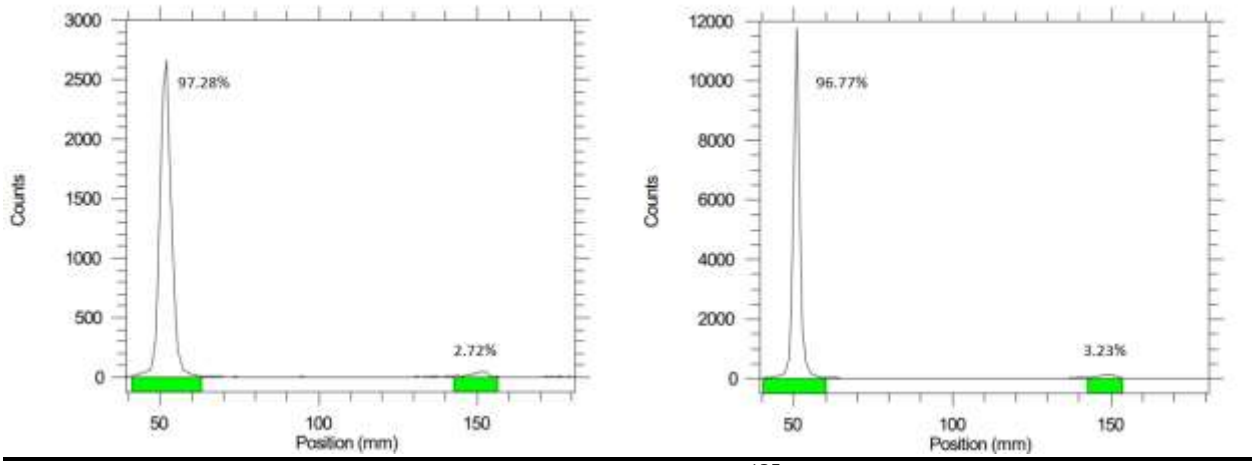

Figure 17. iTLC analyses demonstrating the stability of ^{125}I-NGF in cell media after 1 hour of incubation at 37°C (left), and in PBS pH 7.4 after 24 hours (right).

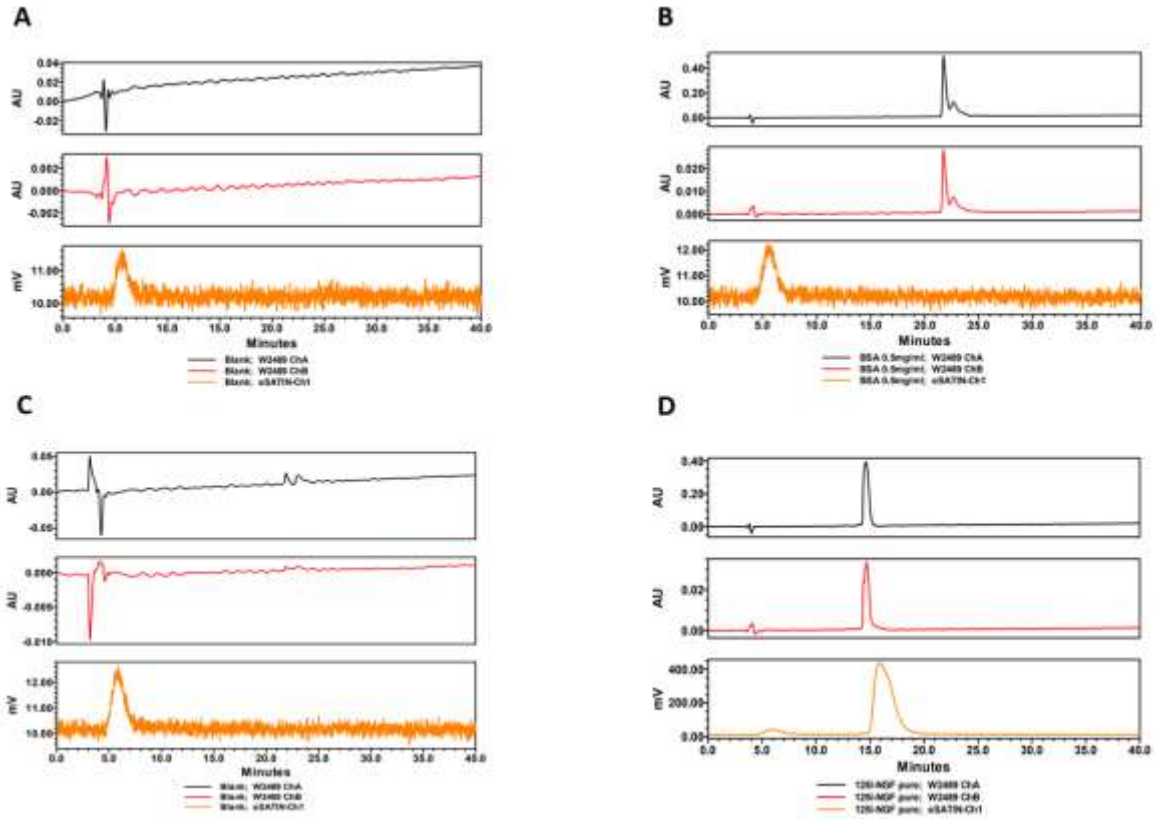

Figure 18. HPLC traces: (A) Blank PBS pH 7.4), (B) BSA 0.5 mg/mL dissolved in PBS pH 7.4, (C) Blank run following the BSA run. (D) Co-injection of 1 µL cold NGF (0.1 µg/ µL) + 10 µL^{125}I-NGF. In the traces, the BSA peak appears at 21.5 min, while the ^{125}I-NGF peak is observed at 14 min. The gamma trace exhibits a lag time attributed to the distance from the ultraviolet (UV) detector to the gamma detector. The low-intensity gamma peak, along with the eluent peak, represents the free ^{125}I remaining on the column from the previous injections. UV-HPLC trace at

280 nm (red), 240 nm (black), and gamma HPLC (orange). The gamma peak appears broader than the UV peak, possibly due to the shielding effect.

2.3.4 *In Vitro* Binding Assay

PC12 nnr5B5 and nnr5 cells, were cultured in complete media (RPMI 1640, 10% horse serum, 5% FBS, and 1% P/S).[38] On the day of the assay, cells were washed with PBS and resuspended in serum-free media for two hours. After the starvation period, cells were counted, and 250,000 cells were added to low-bind Eppendorf tubes. 250 µL of serial dilutions of ^{125}I-NGF from 0.01 to 33 nanomolar (nM) in serum-deprived media (each dilution was five times lower) were added to the tubes in triplicate. 33 nM ^{125}I-NGF were added in triplicate to tubes with 1650 nM unlabelled NGF (50-fold) to determine the non-specific binding. Finally, 33 nM ^{125}I-NGF were added in triplicate to tubes without cells to assess the extent of radiolabelled compound sticking to the tubes.

The samples were incubated for one hour at 37°C with mild agitation. The cells were then centrifuged (at 13 x g for 1 minute), washed 3 times with PBS, then lysed with 200 µL of 1% Triton X and 300 µL of 70% ethanol. The activity in the samples was quantified using an automated gamma counter (Fig. 19).

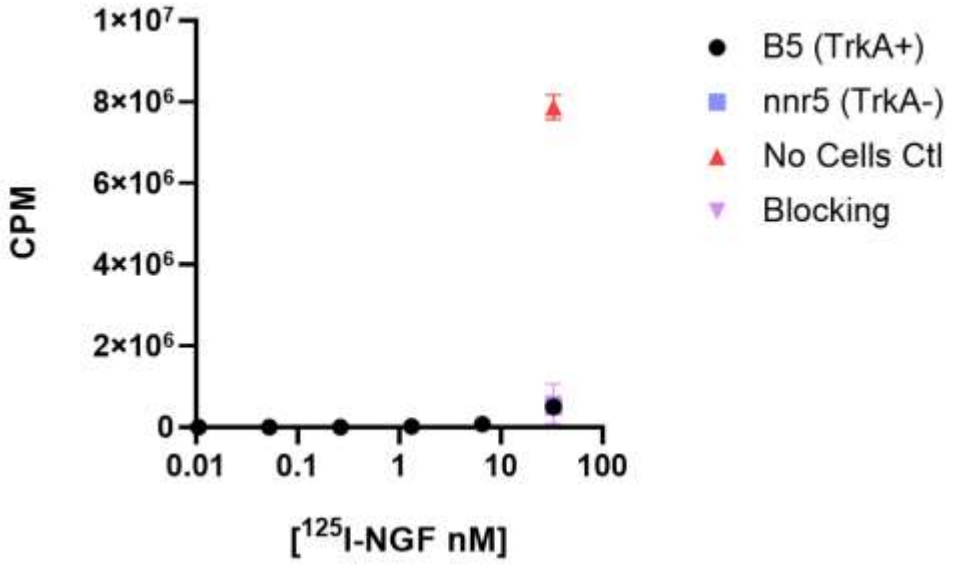

Figure 19. Binding and uptake of ^{125}I-NGF by PC12nnr5B5 and nnr5. The graph indicates the mean CPMs for each condition versus the concentration of ^{125}I-NGF.

The amount of activity in the no cell control was notably high, indicating that the radioligand binds the assay tube indiscriminately. Furthermore, there was no evidence of specific binding of ^{125}I-NGF to TrkA, as indicated by the overlapping counts in the nnr5B5, nnr5, and blocked control samples. The substantial non-specific interaction with the assay tube obscured the real specificity of ^{125}I-NGF binding to TrkA.

To optimize assay conditions and address the issue of non-specific binding, a series of tests were conducted. Eppendorf tubes were coated with 5% Bovine Serum Albumin (BSA), while others remained uncoated. The same procedure was repeated with low-bind Eppendorf tubes and a V-shaped 96-well plate. 3 µCi of ^{125}I-NGF was added to all the tubes and wells in the same volume used in the *in vitro* assay (250 µL). Additionally, 0.01% Tween 80 was added to some of the coated tubes and wells with BSA along with the radiolabeled compound stock solution. The tubes and plate were incubated at 37°C for one hour with agitation. The blank consisted of tubes and wells from each condition where no activity was added; instead, 250 µL of serum-free medium

was added to determine the background. Following the incubation period, the tubes and wells were washed with 1 mL and 300 µL PBS three times, respectively. The contents of each tube and well were then collected using 1% Triton and 70% ethanol and transferred to gamma tubes for gamma counting (Fig. 20).

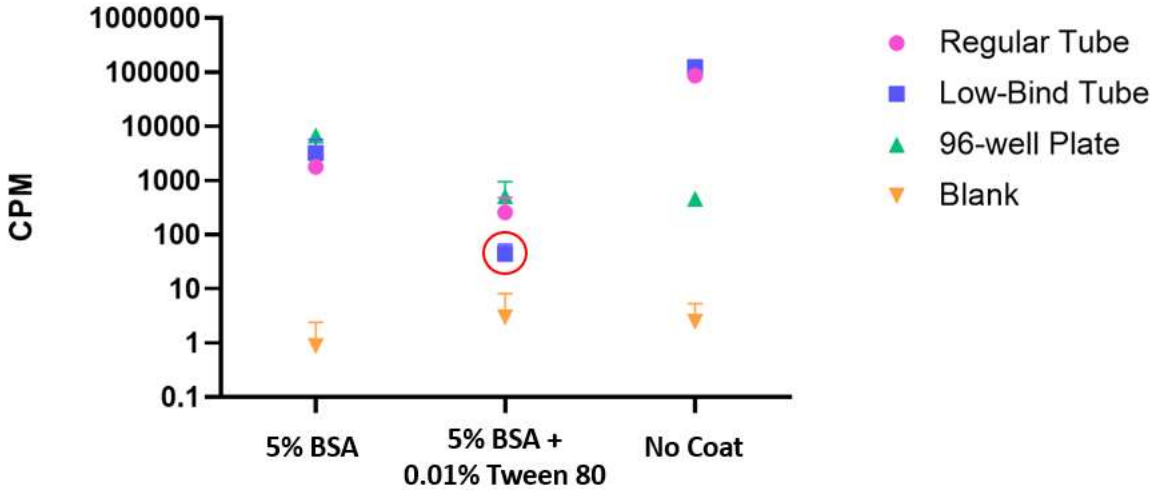

Figure 20. Evaluating 125I-NGF stickiness after BSA coating and Tween 80 addition.

Non-specific binding was reduced to almost background levels with the low-bind Eppendorf tubes coated with 5% BSA and the addition of 0.01% Tween 80 to the stock of radioactivity. Similarly, non-specific binding was very low for V-shape 96-well plates, whether coated with 5% BSA and 0.01% Tween 80, or left uncoated. This finding helps explain the low non-specific binding observed in the saturation binding assay initially performed with pPC12 and nnr5 cells in the 96-well plate (mentioned in the Appendix for chapter 2), where non-specific binding was measured to be approximately 1.4%. Therefore, using low-bind Eppendorf tubes or 96-well plates treated with the aforementioned conditions, or uncoated 96-well plates, would be ideal for conducting assays involving sticky proteins such as NGF, thereby reducing non-specific binding.

2.3.5 Optimized *In Vitro* Binding Assay: Minimizing Non-Specific Binding

The *in vitro* saturation binding assay was repeated with modifications, including the use of low bind Eppendorf tubes coated with 5% BSA and a slight adjustment in the concentration range of ^{125}I-NGF from 0.009 to 28 nM in serum-deprived media, based on the isolated pure ^{125}I-NGF obtained through the purification procedure. Additionally, 0.01% Tween-80 was added to the stock of each dilution. 28 nM ^{125}I-NGF were added in triplicate to tubes without cells to assess the extent of radiolabelled compound sticking to the tubes. Due to limited NGF availability, the blocked control was omitted here.

After cells were starved for two hours, 250 µL of each dilution of ^{125}I-NGF was added to the corresponding tubes in triplicate. Following incubation for one hour at 37°C with mild agitation, tubes were centrifuged at 400 g for one minute, the cell pellets were washed with PBS three times and subsequently, the contents of all tubes were collected using PBS and transferred to gamma tubes to quantify the iodine-125 in each sample using a gamma counter (Fig. 21).

The Scatchard analysis was also performed for the receptor binding assay described. The plot represents the relationship between CPM readings (log10 axis) from nnr5B5 cells incubated with 28 nM, 5.6 nM, 1.12 nM, 0.224 nM, 0.045 nM and 0.009 nM ^{125}I-NGF, which represent the amount of ligand bound to or taken up by the cells, and the ratio of bound ligand to free ligand concentration (Fig. 22).

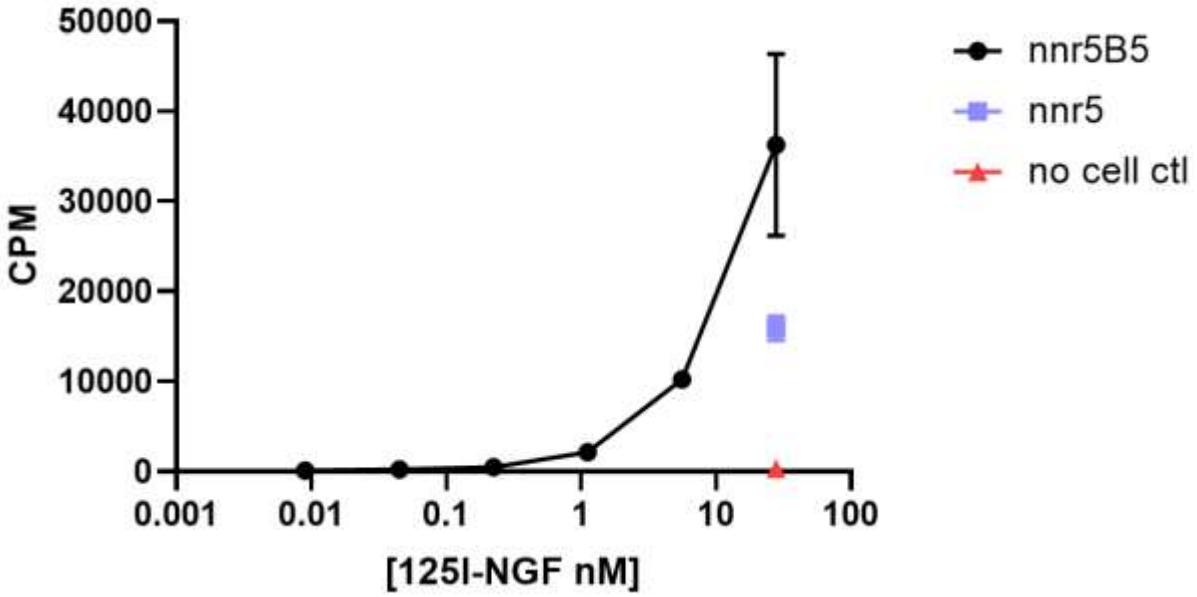

Figure 21. Binding and uptake of ^{125}I-NGF by PC12nnr5B5 and nnr5 under optimized assay conditions.

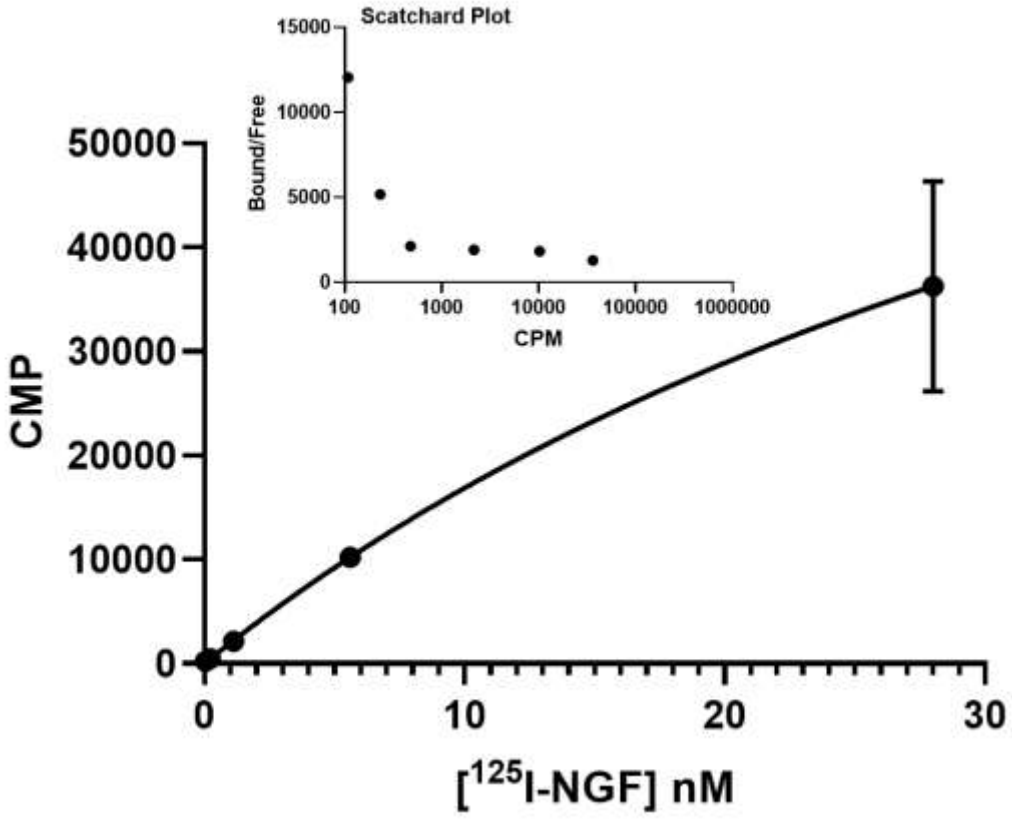

Figure 22. Non-linear regression and Scatchard analysis of ^{125}I-NGF binding to TrkA in nnr5B5 cells. Scatchard plot x-axis is counts per minute (CPM) and plotted on a logarithmic scale base 10. n = 3, mean ± SEM.

As shown, the Scatchard plot exhibits a biphasic curve, consistent with the presence of two binding sites for ^{125}I-NGF, TrkA and p75^{NTR}. The first phase (steep phase) represents the high affinity binding between ^{125}I-NGF and TrkA, whereas the second phase (shallow phase) represents weak affinity binding between ^{125}I-NGF and p75^{NTR} (Fig. 22). However, due to low CPM at anticipated Kd values (9.5 pM for TrkA and 1.1 nM for p75 ^{NTR}) [42], we were unable to accurately measure Kd and Bmax.

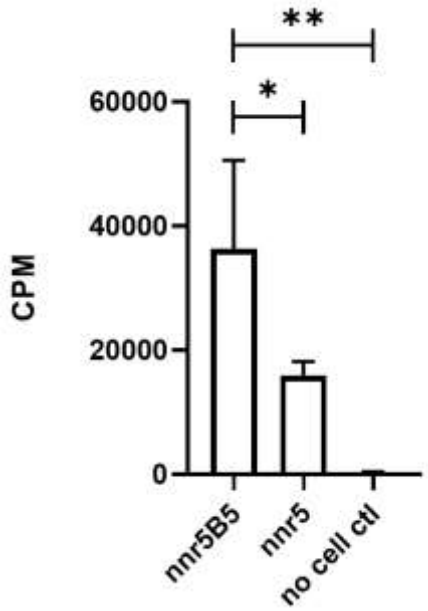

Figure 23. Binding and uptake of 28 nM ^{125}I-NGF by nnr5B5 and nnr5 cells. One-way analysis of variance was performed using GraphPad Prism. * $p < 0.05$; ** $p < 0.01$.

Additionally, CPM readings from TrkA-expressing (nnr5B5), TrkA-knockout (nnr5) PC12 cells, and no cell control for 28 nM were analyzed by one-way analysis of variance which revealed significant binding and uptake of ^{125}I-NGF by nnr5B5 cells compared to nnr5 and no cell control (Fig. 23). The limited binding observed in nnr5 cells at 28 nM could be attributed to the binding of ^{125}I-NGF to p75^{NTR}, the low-affinity receptor of NGF, as these cells are solely deficient in TrkA. Despite observing significantly increased binding and uptake in nnr5B5 cells, the dose/response curve did not reach a plateau (Fig. 22), which would indicate the saturation of all binding sites

under the test conditions. Furthermore, the percent binding did not exceed 1%. This limited binding may be attributed to assay conditions that were not optimized to maximize specific binding, but to minimize non-specific binding. To achieve high specific binding in saturation binding assays, several factors must be considered, including incubation time, radioligand concentration, receptor concentration, cell binding assay buffer system, and assay temperature.[41] The incubation time should be sufficient to reach equilibrium, or at least a steady state. Preferably, the radioligand concentration should approximate the concentration near the ligand's Kd. Enhanced binding is achievable with higher receptor expression. In most studies, maintaining room temperature is desirable, as 37°C may increase the dissociation rate, while ensuring that the pH falls within the physiological range is crucial. Cultured cells are typically maintained in a medium buffered with bicarbonate, in equilibrium with CO2 in the incubator atmosphere. However, upon removal from the incubator, the gradual evaporation of dissolved CO2 can lead to changes in pH. All these factors could potentially impact cellular defense mechanisms and alter biological priorities, prioritizing viability maintenance over facilitating uptake or binding of the radioligand.

2.4 Conclusion

The labeling of NGF with ^{125}I and its characterization were successfully achieved following established protocol. Binding affinity was studied with TrkA overexpressing nnr5B5 and nnr5 knockout cell lines where TrkA expression was validated using western blot. Despite encountering initial challenges in demonstrating the specificity and selectivity of ^{125}I-NGF towards TrkA (as mentioned in the Appendix for chapter 2), specificity was successfully demonstrated through *in vitro* binding assays using TrkA overexpressing cells PC12 nnr5B5s. Significant difference in

CPM from TrkA-overexpressing nnr5B5 cells compared to TrkA-nonexpressing cells (nnr5 cells) indicates increased binding and uptake of ^{125}I-NGF by nnr5B5 cells compared to nnr5 cells. These results indicate that ^{125}I-NGF retains its ability to specifically bind to TrkA *in vitro.* However, the calculated percentage of binding was very low (<1%), indicating a low affinity of ^{125}I-NGF to TrkA under our assay conditions. In a previous study investigating the Kd value for nnr5B5 cells, biphasic Scatchard binding curves were observed with ^{125}I-NGF. The reported Kd values for high and low affinity receptors were determined to be 9.5 pM and 1.1 nM, respectively.[42] Upon comparison with the values obtained in our studies, discrepancies were noted, suggesting potential inconsistencies.To address these issues, additional work is required to evaluate the effects of each parameter discussed above on low cell binding and optimize experimental conditions.

Furthermore, this experimental method demonstrated that the direct labeling of NGF with ^{125}I using Iodogen maintained its affinity for TrkA. While this *in vitro* study indicated the binding of ^{125}I-NGF to TrkA at the cellular level, other techniques such as autoradiography and *in vivo* evaluation will allow for the examination of TrkA binding at the level of intact organs or whole animals. These techniques will provide insights into the visualization and localization of radiolabeled molecules within biological samples with high spatial resolution and the role of the TrkA receptor in normal physiological processes and various disease states.

Chapter 3- Preliminary *In Vivo* Tracking of ^{125}I-NGF Following Intrahippocampal Injection

3.1 Abstract

It has been demonstrated that ^{125}I-NGF, when injected into the cortex or hippocampus of adult rats, is transported to the basal forebrain. In this study, we adapted the method for mice, enabling the IC delivery of ^{125}I-NGF into the hippocampus in a murine model. This adaptation allows for the examination of ^{125}I-NGF transport in transgenic models of AD and memory loss, and facilitates comparisons among young, aged, or diseased mouse models.

One aim of the study was to evaluate accuracy and consistency when injecting ^{125}I-NGF intracranially in a mouse brain. Moreover, the study aimed to monitor the transport of ^{125}I-NGF to the basal forebrain following intrahippocampal injection. To assess consistency, the radioligand was injected into the hippocampus of euthanized mice and distribution was evaluated immediately post injection. Additional time points post-injection were explored to evaluate the influence of time on the distribution and transport of ^{125}I-NGF to the basal forebrain.

This chapter details the stereotactic injections for convection-enhanced intracranial delivery of ^{125}I-NGF into the hippocampus of the young C57BL/6 mice. 1 µL (1.675 ± 0.4527 µCi, 47.23 ± 2.4147 ng) of solution of radiolabelled molecule in PBS pH 7.4 was injected into the brain over a span of five minutes (rate: 0.2 nL/min). With this method, we assessed the reproducibility of accurate injections by conducting multiple experiments under similar conditions and analyzing the consistency of the outcomes. Based on the statistical power analysis conducted on the data, we determined that the injection accuracy targeting the hippocampus in pre-euthanized mice achieved a reproducibility rate exceeding 75%, with minimal to no backflow. Injection coordinates for delivery into the hippocampal DG were optimized through pilot studies with Trypan blue. Following the injection of ^{125}I-NGF, mice in the other group of studies were euthanized at two

hours and six hours post-injection (four per time point per group). Tissues, including the basal forebrain, hippocampus, and other regions of the brain, were harvested for quantifying the amount of radioactivity in each brain region using an automated gamma counter. Autoradiography analysis was also conducted using one mouse per group for each time point.

3.2 Introduction

Previous research using ^{125}I-NGF has demonstrated that a subset of BFCNs projecting to the visual cortex of rats and hippocampus actively transports NGF, designating these neurons as potential targets for NGF-mediated effects.[43,44] Administration of ^{125}I-NGF into the visual cortex of rats at various postnatal stages led to the labeling of cells near the injection site. Gradually, during postnatal development, the number of NGF-positive cells in the basal forebrain and Diagonal Band of Broca increased and maintained elevated levels into adulthood.[42] The distribution assessment of 24 hours post injection into the hippocampus indicated a substantial amount of ^{125}I-NGF labeled neurons, particularly in the medial septal nucleus and the nucleus of the diagonal band (areas of basal forebrain).[45]

Therefore, the uptake and transport of radioiodinated NGF by cholinergic neurons to the basal forebrain, following the injections into the cortex and hippocampus, [41-44] was successfully observed in rats (Fig. 24).

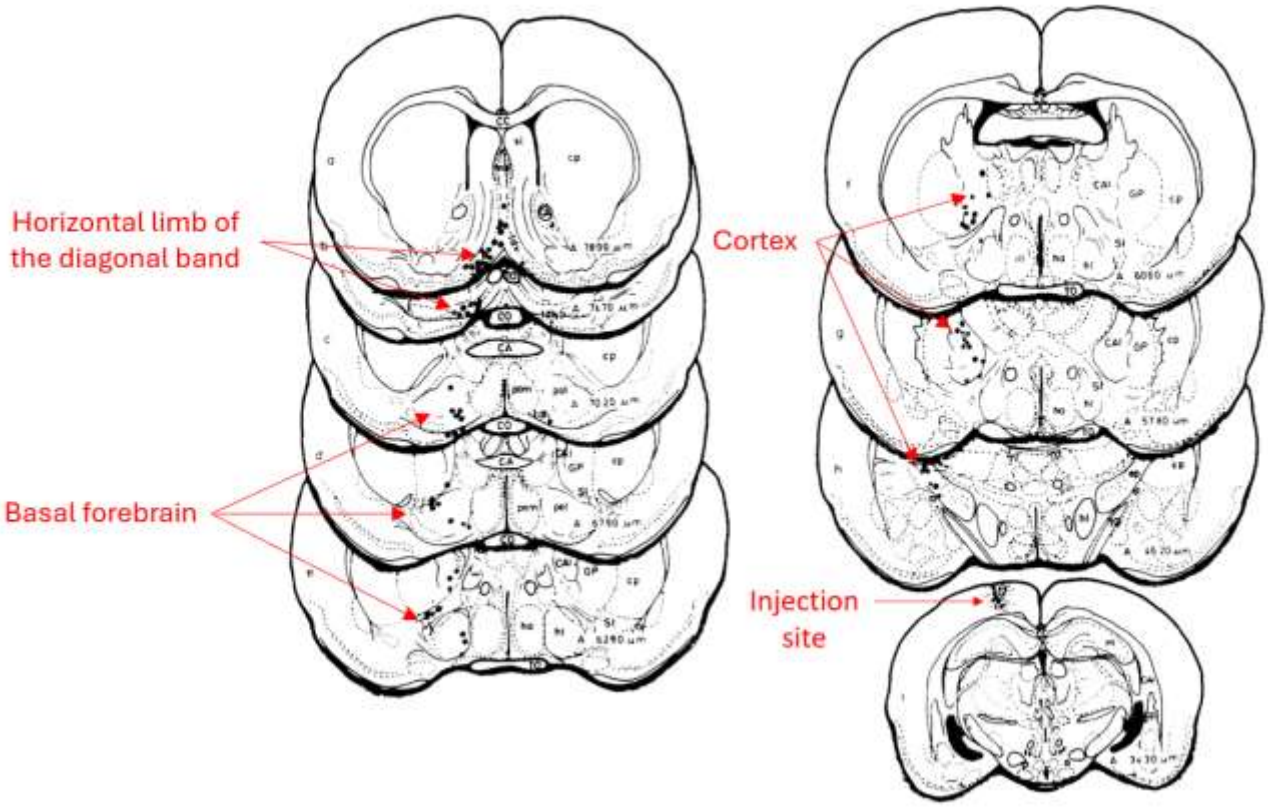

Figure 24. Topography of the injection site (cortex) and retrograde transport of ^{125}I-NGF to regions where BFCNs have projections, observed 24 hours post-injection.[45] • = heavily labeled cells; ○ = moderately labeled cells.

3.3 Experimental

3.3.1 Materials and Instruments

Procedures for animal use of aseptic cranial surgery and intracranial injections were approved by the Animal Research Ethics Board – McMaster University. For our experimental procedures, we utilized a range of specialized materials and instruments including Rat Stereotaxic Frame sourced from Stoelting, Microsyringe Pump Controller Model UMC4 (UMP3) from Micro 4, Hamilton Gastight Syringes (25 μL, 26 gauge) variant from Millipore Sigma, PeaNut Clipper, 5/4-0 ETHICON Suture, Swann-Morton Scalpel Blades (size 15), and Dremel Rotary Tool with a 0.6mm ball size, acquired from Stoelting.

3.3.2 Animal Studies General

All animal studies were approved by the Animal Research Ethics Board at McMaster University. Mice were maintained under clean conditions with 12 h light/dark cycles and given food and water ad libitum. Experimental mice were monitored post-surgery for clinical abnormalities and for ethical endpoints which include a decrease in weight, change in appearance (skin tent and posture), attitude, general body condition, head tilt and swelling, circling, and neurological disorder signs.

3.3.3 *In-vivo* Study of ^{125}I-NGF Transport in C57BL/6 Mice

We examined the distribution of ^{125}I-NGF into the brain following IC injections of the radioligand into the hippocampal DG of C57BL/6 mice. Due to NGF's limited ability to penetrate the blood-brain barrier, the utilization of ^{125}I-NGF *in vivo* relies on invasive neurosurgical procedures.[46] The study aimed to investigate the difference in ^{125}I-NGF transport from the hippocampus to the basal forebrain in C57BL/6 mice at different time points. Gamma measurements were conducted to quantitively assess the radioactivity in each brain region at these specified time points. Additionally, autoradiography analysis was performed to visualize the spatial distribution of radioligands within brain coronal slices, providing insights into the localization of ^{125}I-NGF in brain sections. This is achieved by exposing the specimen to a medium capable of capturing energy, phosphor-imagers.[48] The reproducibility in targeting and injecting the area of interest with ^{125}I-NGF was refined through preliminary practices using trypan blue on euthanized mice to optimize the injection coordinates according to the atlas of Paxinos and Franklin (Fig. 25 & 26).[49] With the optimal coordinates, we observed the accumulation and diffusion of trypan blue in the right hippocampus, the target site.

The study with ^{125}I-NGF was initially conducted on pre-euthanized mice, with data collected at time points 2 and 6 hours, as described below:

- **Pre-euthanized**: Two groups of four female C57BL/6 mice (6-8 weeks old) were euthanized by cervical dislocation while under isoflurane anesthesia. The mouse was positioned on the stereotaxic frame, the skin was incised, and bregma was identified. Coordinates for the Dentate Gyrus were determined relative to bregma (Anteroposterior (AP): -2 mm, Mediolateral (ML): 1.3 mm, Dorsoventral (DV): -1.9 mm). A hole was drilled using a dremel, and 1 µL ^{125}I-NGF (1.25±0.75 µCi, 52 ng) was injected through a 26-gauge Hamilton syringe into the right hemisphere at a flow rate of 200 nL/min. The injection volume and rate were controlled with a microsyringe pump controller. After completion of the injection, a 5-minute interval was observed, and then the needle was slowly removed from the brain. The mouse was decapitated; the brain was extracted and cut into two hemispheres. Each hemisphere was further micro dissected into five sections: hippocampus, basal forebrain and olfactory bulb, cortex, midbrain, and whole cerebellum. Each brain region was placed in corresponding gamma counter tubes to quantify the activity in each sample.

The brain from the 4th mouse in both groups was used for autoradiography; the brain was removed, fixed in Optimal Cutting Temperature (O.C.T) compound, snap-frozen using liquid nitrogen, and stored at -20°C. The next day, frozen brain slices were cut at 100 µm thickness in a coronal plane using the Leica cryostat machine with specimen temperature (OT) and chamber temperature (CT) set at -17°C. Slices were mounted on microscopic glass slides and dried by exposure to the room air. The brain slices were then exposed to a phosphor plate for one week at RT, and the autoradiograms were imaged using a Typhoon imager.

- **Time points-2 hours:** Four female C57BL/6 mice (8 weeks old) were anesthetized with isoflurane (5%) and 1% oxygen, and placed into the stereotaxic apparatus. For the maintenance of the animal in anesthesia, isoflurane was decreased to 2% and oxygen increased to 2%. Prior to the surgical procedure, 0.1 mg/kg Buprenorphine (0.03 mg/mL) and 1 mL of saline were administered subcutaneously, and 0.4 µL/g Lidocaine 2% was injected under the scalp. The head fur was shaved using a clipper, and the area was sterilized with 10% iodine solution scrub, 70% isopropanol, and 7.5% iodine solution detergent, respectively. Mice were injected following the incision and determiation of coordinates, with the injection formulation, volume, rate, and duration consistent with those used for pre-euthanized mice. Following the interval of 5 minutes, the needle was removed, and the incision was sutured with 5/4-0 Monocryl suture. After 2 hours, mice were euthanized by cervical dislocation under isoflurane anesthesia, and the brain was collected, and micro dissected as described above. Mouse four was used for autoradiography analysis.
- **Time point-6 hours**: The mice (4 female C57BL/6-8 weeks old) were gavaged with 0.1 mg/kg 0.1% potassium iodide (KI) to saturate the thyroid one hour prior to surgery. The surgical procedure was repeated on mice as mentioned from time point 2, except with a recovery period of 6 hours. Their organs including liver, kidney, thyroid, blood, adipose tissue, and skeletal muscle were dissected and harvested for quantitative analysis using the gamma counter. Due to the loss of one mouse under anesthesia before injection, autoradiography was not performed for 6 hours post-injection.

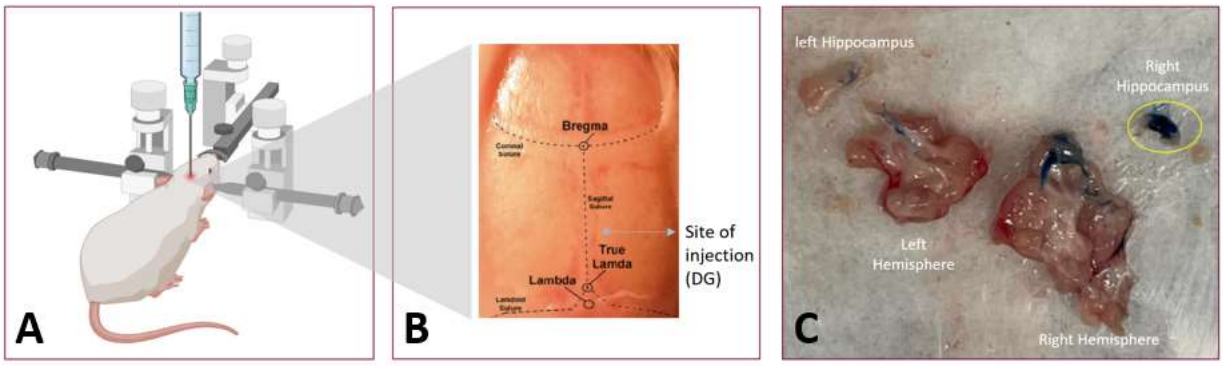

Figure 25. Pilot injection practice is used to optimize the coordinates for the injection site. A: illustrating the injection setup (mouse placement in the stereotaxic equipment) for IC injection. B: Determining coordinates relative to bregma, which is the common reference point in stereotaxic brain surgery. C: Indicating the localization of the Trypan blue in the right hippocampus, the site of injection.

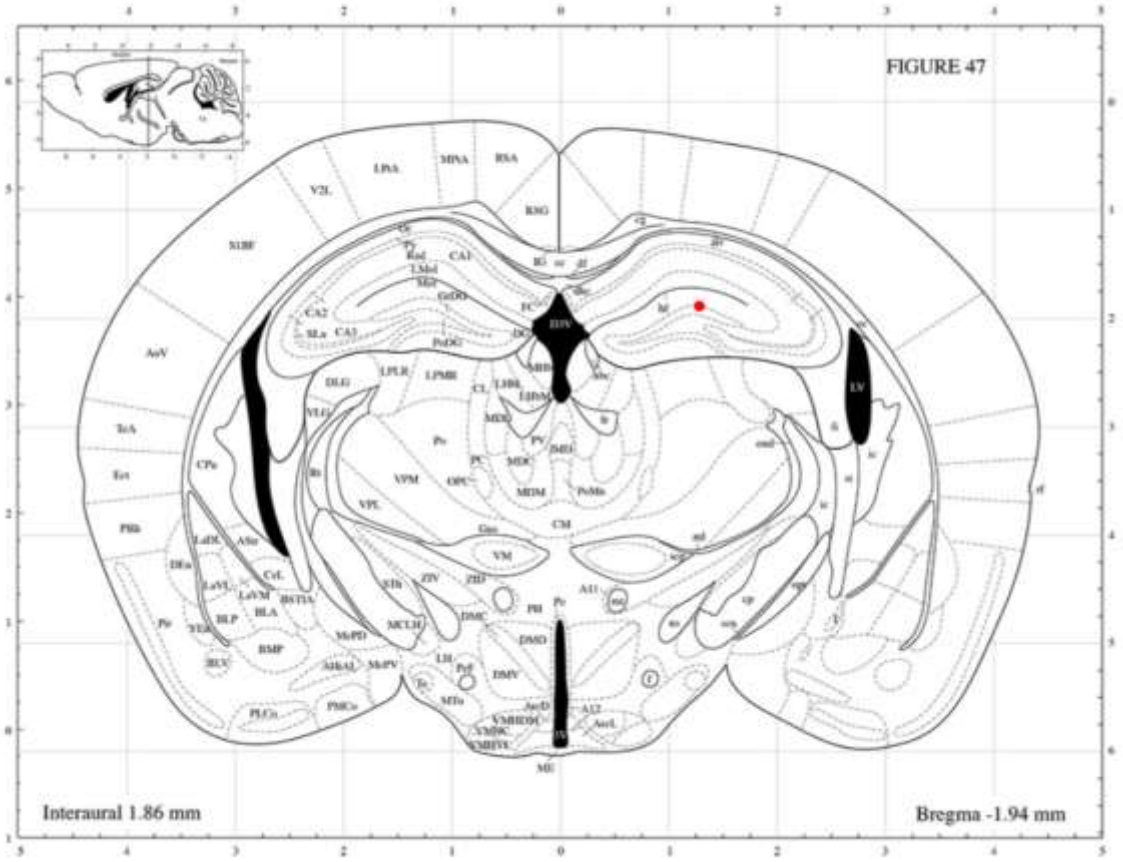

Figure 26. Coronal brain slice (1.94 mm anterior to the bregma) indicating the target coordinates (ML: -1.3 mm, AP: -2 mm, DV: -1.9 mm) highlighted by the red dot.[49]

3.4 Results and Discussion

3.4.1 *In vivo* Distribution Results

The percentage injected dose per gram (%ID/g) was calculated by determining the percentage of activity contained in each brain section relative to the total activity injected into each mouse brain (sum of the activity contained in all the brain sections), divided by the weight of each brain section. Bar graphs with the means and standard error of the mean (SEM) for each condition were created using GraphPad Prism version 8.0.2 (Fig. 27 & 28).

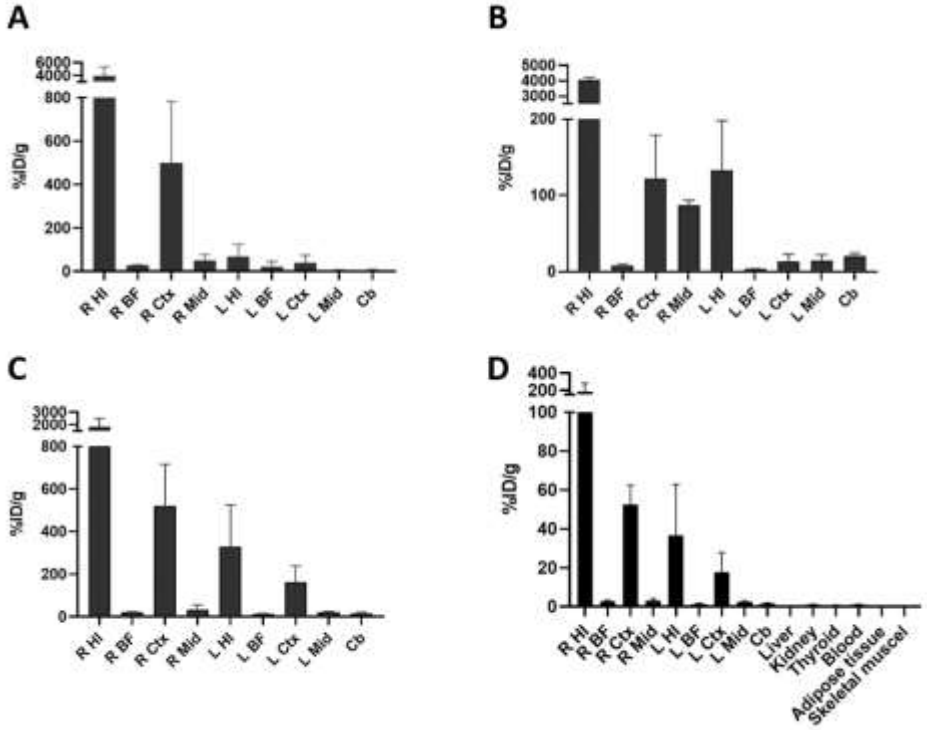

Figure 27. Bar graphs depicting the distribution of ^{125}I-NGF across distinct brain regions: A) pre-euthanized, B) 2 hours, and C) 6 hours post-injection. D) Biodistribution of ^{125}I-NGF in brain regions and other organs 6 hours post-injection (%ID/g was calculated by assessing the percentage of activity in each organ relative to the total activity injected into each mouse (sum of the activity taken up by each brain section and organ, divided by the weight of each brain section or organ)).

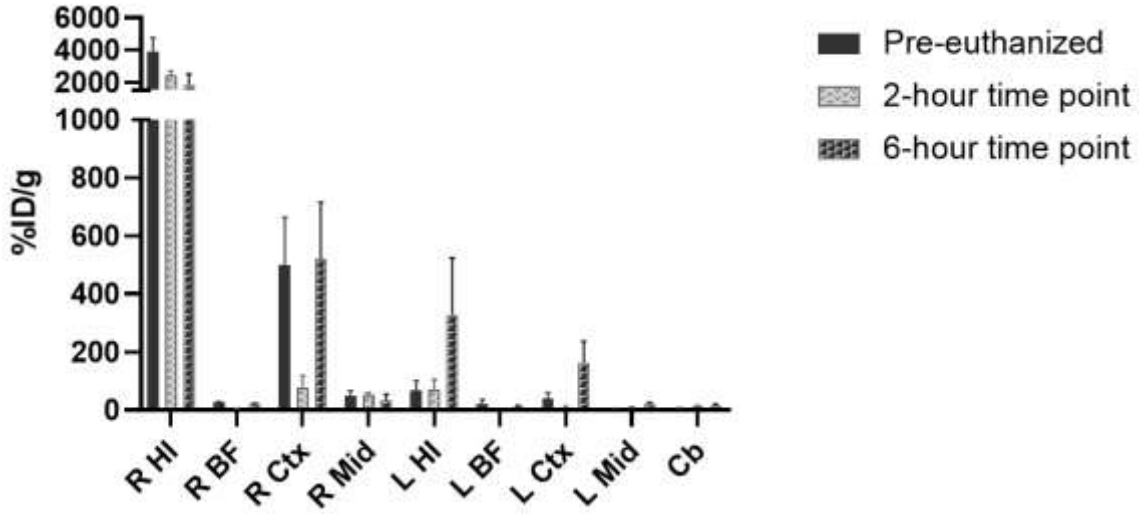

Figure 28. Comparison between uptake and distribution of ^{125}I-NGF: pre-euthanized, 2-, and 6-hours post-injection in various brain sections.

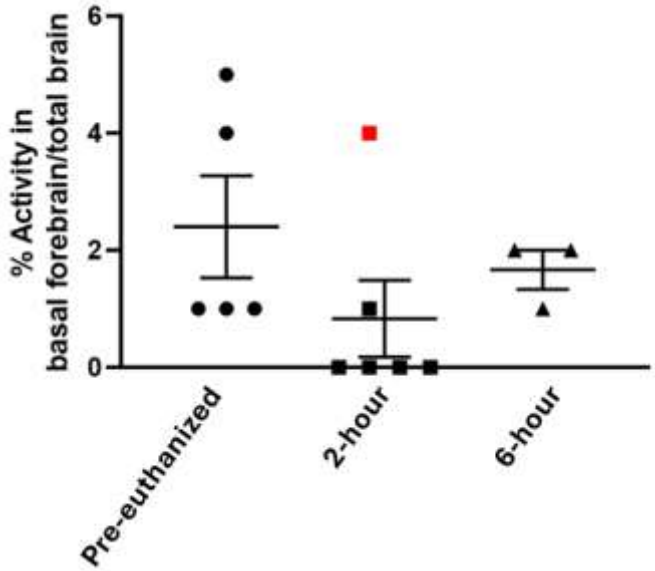

Figure 29. Percent ratio of ^{125}I activity in basal forebrain to activity detected in total brain. Mice were either euthanized prior to surgery (pre-euthanized, circle), 2 hours (square), or 6 hours (triangle) post-surgery. The data point shown in red is an outlier. Each symbol on the plot represents one mouse. $N_{pre\text{-}euthanized} = 5$, $n_{2\text{-}hour} = 6$, $n_{6\text{-}hour} = 3$. mean ± SEM.

The highest amount of activity in the brain was concentrated in the right hippocampus, aligning with the targeted injection site. This was observed with pre-euthanized mice where significant activity was accumulated in the right hippocampus as compared to right cortex. Two

hours post-injection, there was a slight decrease in the amount of ^{125}I-NGF in the right hippocampus, and some activity migrated to the left hemisphere. However, the amount of activity in the basal forebrain was low (3.190 ± 0.884 %ID/g). Six hours post-injection, ^{125}I-NGF had spread into the right cortex and further into the left hemisphere, particularly into the left cortex and hippocampus. The amount of activity in the basal forebrain remained low (16.80 ± 2.683 %ID/g). The activity was thoroughly analyzed and plotted on an interleaved scatter plot, representing the percent CPM detected in the basal forebrain divided by the sum of CPM from the entire brain of each mouse using one-way ANOVA (Fig. 29). The analysis indicated that there were no significant differences between groups. One outlier was identified in the 2-hour time point group (Fig. 29, point highlighted in red), however, removal of this outlier from the dataset did not yield significance between groups. While the mean for 6 hours post-injection was slightly higher than at 2 hours post-injection, suggesting ongoing transport, these data imply that 6 hours of *in vivo* incubation is still insufficient for complete ^{125}I-NGF transport from the hippocampus to the basal forebrain. This suggests that C57BL/6 mice may not be a suitable animal model for this study, or an extended interval of 24 hours needs to be investigated, as it has previously shown notable transport in rats.[44]

Despite the lack of retrograde transport, a robust technique was developed to target the hippocampus as the region of interest (ROI) by effectively administering trypan blue. Injecting into the brains of pre-euthanized mice, the majority of the activity was delivered into the right hippocampus. However, the low diffusion into the cortex, consistent with the pattern observed during the practice phase with trypan blue, suggests that it might be beneficial to decrease the volume of injection to minimize diffusion.

3.4.2 Autoradiography Analysis

After being exposed to the phosphor plate for 7 days, the fixed tissue slides were carefully removed from the film. Subsequently, the film was scanned using a Typhoon scanner configured for phosphor imaging at a resolution of 25 µm. Images of brain coronal sections from both pre-euthanized and mice at 2 hours post-injection are displayed (Fig. 30). However, the autoradiography results did not meet our expectations of visualizing distinct signals in different brain regions due to a lack of spatial resolution. While testing the resolution of 25 µm, a controlled volume of ^{125}I-NGF with varying activity was exposed for seven days to assess spatial resolution and pixel saturation. The presence of fine details and clear signals suggests adequate resolution for the intended purposes. However, the resulting signals from 1 µL of activity after the 7-day exposure lacked clarity in the autoradiograph (Fig. 31). Moreover, activities above 0.008 µCi saturated the pixels, while pixel saturation was not observed in the brain autoradiogram. This suggests that the activity amounts in brain regions are less than 0.008 µCi. In practice, expectations for spatial resolution and pixel saturation in autoradiography should consider the specific experimental setup and goal to optimize other parameters such as injected activity, exposure time, tissue processing techniques, and the scanned resolution accordingly. This would help to achieve the highest level of detail possible while maintaining sensitivity and accuracy in the results. In our study, the lack of spatial resolution may be attributed to the small size of the brain, which hindered the observation of distinct signals.

Nonetheless, the main intensity accumulation was observed in the hippocampus and cortex areas at both time points. While there were some signals observed in the cerebellum, there was no accumulation of labeled NGF found in the basal forebrain and olfactory bulb. However, even if there is transport of a low amount of activity to the basal forebrain, it may not be detectable by the

scanner due to its limited sensitivity. This sensitivity limitation can arise due to factors such as the type of radioactive isotope used, the exposure time during imaging, the resolution of the imaging system, and the background noise present in the autoradiograph.[50] Therefore, insufficient sensitivity may result in the inability to detect low levels of radioactivity, leading to a reduced ability to visualize and quantify ^{125}I-NGF in the brain tissue.

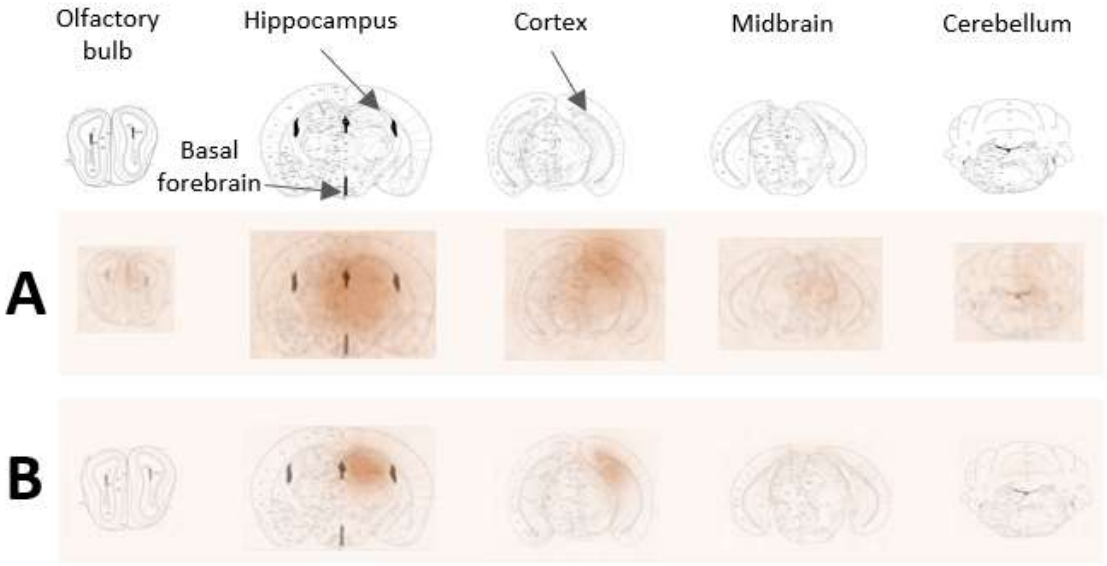

Figure 30. Autoradiography of brain slices: Strongest signal was observed in the hippocampus area, the site of injection, in pre-euthanized mice (A). At 2-hours post-injection, the strongest signal was detected in the hippocampus, followed by the cortex, with minimal signal in the cerebellum (B). Brain slices were obtained from the Paxinos and Franklin mouse brain atlas, and superimposed onto the autoradiograph.[49]

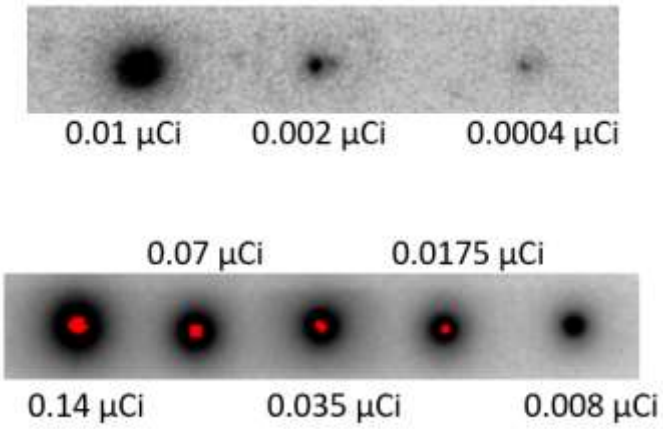

Figure 31. Assessment of Pixel Saturation and Resolution following 7 days of exposure. A controlled volume of ^{125}I-NGF with varying activity was exposed for seven days to evaluate pixel saturation at a resolution of 25 µm. Red dots indicate saturated pixels >0.008 µCi.

3.5 Conclusion

In conclusion, the optimization of targeting coordinates and refinement of the technique for delivering ^{125}I-NGF to the hippocampus in mouse brains was successfully achieved. Regarding the study's aim to assess ^{125}I-NGF transport, the mean count obtained for the basal forebrain at 6 hours post-injection was slightly higher than those at 2 hours post-injection, as analyzed by gamma quantitative analysis. However, these counts remained consistently low across both time points, approximating background levels. These results raise questions about the suitability of the C57Bl/6 mice for this study, primarily due to challenges in maintaining consistent injections in their small brains. Furthermore, autoradiography results failed to exhibit the expected spatial resolution in distinguishing signals within different regions, particularly in discerning the hippocampus at the top of the brain slice and the basal forebrain at the bottom when the brain is being sliced coronally. Considering these issues (small brain size and coronal slicing), adopting a horizontal slicing may be beneficial due to a minimal gap (~1 mm) [49] between the hippocampus and basal forebrain in a half-profile view of the brain (Fig. 32). This could enable extending exposure periods for the slices comprising the basal forebrain to enhance detection sensitivity, facilitating the detection of even the lowest signals. Further future studies are recommended to examine the retrograde transport of ^{125}I-NGF over an extended time point of 24 hours, and to utilize horizontal sectioning for autoradiography.

Injecting into the brains of euthanized mice resulted in the diffusion of ^{125}I-NGF into surrounding regions due to altered tissue permeability, as observed in both gamma counting analysis and autoradiography in this study. To determine the biodistribution of ^{125}I-NGF

immediately post-injection, further studies would require euthanizing mice immediately after completing the injection rather than prior to injection.

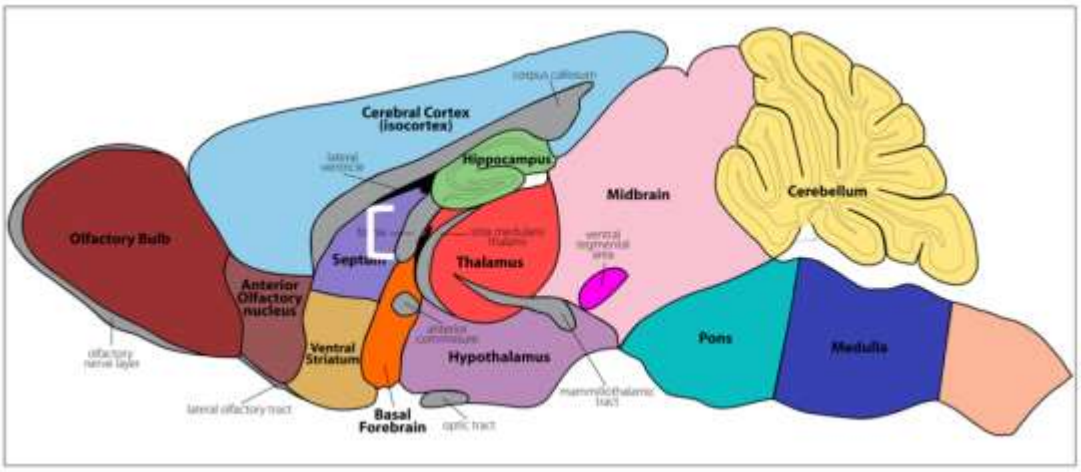

Figure 32. Mouse brain half-profile view: the white bracket indicates the minimal distance between the hippocampus and basal forebrain.[49]

Chapter 4 – Conclusion and Future Work

4.1 Summary

This research aimed to synthesize and demonstrate the retrograde transport of ^{125}I-NGF by BFCNs in adult mice following intrahippocampal injection. In the study's first phase, ^{125}I-NGF was successfully synthesized, purified, and characterized. Additionally, the specificity and selectivity of the radioligand to TrkA was demonstrated through *in vitro* studies using PC12nnr5B5 cells.

Due to potential deficits in uptake and retrograde transport of NGF by BFCN axons in aging and AD, the goal was to initially assess the efficacy of ^{125}I-NGF transport in young adult mice and to optimize the injections in healthy mice before proceeding to diseased mouse models. The coordinates for the injection site and conditions for IC injection were optimized using stereotaxic equipment and a syringe pump prior to *in vivo* tracking of ^{125}I-NGF (Chapter 3). Following the injection of 1 µL ^{125}I-NGF (>98% purity) into 6–8-week-old C57BL/6 mice at an injection rate of 200 nL/min, gamma counting analysis of each brain region revealed significant retention of ^{125}I-NGF in the hippocampus for all examined time points. There was very little distribution to the contralateral site of injection and minimal transport to the basal forebrain at the 6-hour time point compared to 2 hours. Due to limited spatial resolution, we were unable to resolve specific brain regions with autoradiography. However, qualitative observation of the images suggested that the compound primarily localized in the hippocampus, with little dispersion to the cortex and cerebellum at the 2-hour time point. These findings corresponded with the quantitative gamma counting results. Therefore, the distribution studies indicated that there was no efficient transport of ^{125}I-NGF at the various time intervals studied and highlighted the need for further assessment

and evaluation of extended time points post-injection, and utilizing animal models such as rats, which possess larger brains.

4.2 Future Directions

4.2.1 *In Vitro* Binding Assay Improvement

As discussed in Chapter 2, we have shown that ^{125}I-NGF retains its binding activity to TrkA. PC12nnr5B5 cells overexpress TrkA receptors, while PC12nnr5 cells do not express TrkA, but still express $p75^{NTR}$.[38,39] Significant CPM readings from nnr5B5 cells compared to nnr5 cells, following their incubation with ^{125}I-NGF, indicates greater binding activity between ^{125}I-NGF and nnr5B5 compared to nnr5 cells due to the presence of high affinity TrkA receptors on nnr5B5 cells. Scatchard analysis of ^{125}I-NGF binding to nnr5B5 cells confirmed the presence of two binding sites on these cells. Based on the dissociation constants (Kd) described in chapter 2, in order to occupy half of the available TrkA binding sites in nnr5B5 cells, approximately 50 nM of ^{125}I-NGF must be added to 2.5×10^5 nnr5B5 cells. Further investigation is still necessary to elucidate the underlying reasons for the observed disparity in Kd values between our study and previous research.

Although the specificity of ^{125}I-NGF towards TrkA has been demonstrated, the average percentage of binding to nnr5B5s through *in vitro* saturation binding assay was < 1%. This low binding percentage may be attributed to factors associated with the assay conditions, which were elaborated in detail in Chapter 2. Hence, further optimization is necessary to enhance specific binding, which can be done by testing various factors independently to discern their impact on the binding percentage. For instance, the impact of incubation conditions on the cell's viability could be examined through cell viability methods such as staining with trypan blue or flow cytometry.

Due to radioactive contamination, these studies necessitate conducting cell viability assessments within radioactive laboratories. Performing a blocking binding assay with unlabeled NGF and ^{125}I-NGF can be another useful method of assessing the specificity of binding, as it allows for competition with the radiolabeled ligand for receptor binding sites.

To evaluate the efficacy of radiolabeling with Iodogen and verify its impact on NGF's biological activity, various studies can be conducted. This includes exposing PC12 cells to ^{125}I-NGF and assessing neurite outgrowth, as well as detecting downstream protein signaling pathways using Western blotting. Another approach, although not optimal, is to examine the retrograde transport of ^{125}I-NGF via TrkA using BFCNs cultured in microfluidic chambers. The study can be conducted similarly to the previous investigation involving QD-proNGF.[15] The microfluidic chamber is a specialized device designed to study neuronal cell culture and axonal transport *in vitro*. It consists of two compartments separated by microgrooves, allowing for the isolation and manipulation of axonal and cell body compartments.[51] To study the transport of ^{125}I-NGF using the microfluidic chamber, the radiolabeled NGF can be added to the axonal compartment and incubated for a specific period. Autoradiography can be utilized to track the transport of ^{125}I-NGF, or, the contents from the axon and neuronal cell body compartments can be pipetted and quantitatively analyzed using gamma counting. Challenges may arise when optimizing the assay conditions to ensure accurate and reliable results. Factors such as incubation time, concentration of ^{125}I-NGF, cell culture conditions, and microfluidic chamber setup need to be carefully controlled and adjusted to achieve optimal experimental conditions and meaningful data interpretation.

4.2.2 Retrograde Transport of ^{125}I-NGF in Adult Mice

In vivo studies with an IC injection of ^{125}I-NGF into the healthy adult mouse brain, demonstrated that extending the time to six hours may be insufficient for the retrograde transport of ^{125}I-NGF. As stated in chapter 3, there was no significant difference in the ratio of activity in the basal forebrain (right and left hemispheres) to the sum of activity from the entire brain between the timepoint groups. Previous research involving intrahippocampal and intracortical injections of ^{125}I-NGF has demonstrated the presence of ^{125}I-NGF in the basal forebrain and septum, 24-hour post injection.[43,44] Considering the modestly elevated accumulation of ^{125}I-NGF in the basal forebrain at 6 hours post-injection compared to 2 hours, it is prudent to explore a 24-hour interval for the present investigation. However, if the interval shows ineffective transport, a shift to rat models is warranted. The larger brain size will facilitate injection precision and better spatial resolution in autoradiography. The McGill-Thy-APP rat model, characterized by Alzheimer's plaques, basal forebrain degeneration, and memory loss,[51] can be employed for further investigation into disease pathology.

4.2.3 Assessing TrkA Levels and NGF Transport in Rodent Models of Aging and Disease with a PET Tracer

With respect to targeting TrkA in the mouse brain, multiple MI modalities satisfy spatial resolution and dynamic scanning requirements, including photoacoustic imaging (PAI) and optical imaging (OI). However, these methods are flawed for limited sensitivity, ability for quantification, and depth penetration, which are especially problematic given the optical impedance provided by a mouse's skull. On the other hand, radionuclide-based MI (PET and SPECT) provides excellent spatial resolution, dynamic scanning, quantification, unlimited depth penetration, and improved sensitivity.[21]

Radiolabelled probes used to image the Trk family have garnered significant prospective applications in the clinical imaging of dementia, cancer detection and patient monitoring. Bernard-Gauthier et al. reported the development of radiolabeled Trk-targeted quinazoline-based small molecules. The lead compound, [^{18}F] TRACK, exhibited a Ki (inhibition constant) of 2.65, 0.32, and 0.14 for TrkA, TrkB, and TrkC, respectively, with their works culminating in clinical imaging studies.[51] However, the PET tracers (^{18}F-small molecules) demonstrated limited specificity for imaging individual Trk family members [53-55], precluding their utility in preclinical investigations of neurological disorders and AD pathophysiology. While the probes demonstrated feasibility of radionuclide-based MI from the Trk family, the *in vivo* study of NGF retrograde transport awaits probes with selectivity towards each member of the Trk family, particularly TrkA. It is essential to have probes for each Trk family receptor to accurately study their individual roles and functions in various cellular processes. Therefore, the availability of selective probes for TrkA enables the investigation and validation of its distinct contribution to the process of retrograde transport.

Given the harsh conditions and low radiochemical yields associated with the traditional method of nucleophilic radiofluorination, radiolabeling with $\{Al^{18}F\}^{2+}$ is a future alternative approach to the radiolabeling method. This method, which enables the radiofluorination of biomolecules in aqueous solutions, creates an in vivo stable ^{18}F compound while avoiding the time-consuming processes required for other methods of fluorine-18 labeling of biomolecules.[56] While F-18 radiolabeling offers a commendable spatial resolution of <2mm, a drawback lies in its short half-life of approximately 2 hours.[19] Another radiolabeling approach could substitute ^{125}I with ^{124}I, a PET radioisotope. The direct iodination method for labeling with ^{125}I has been optimized, ensuring high radiochemical yield and purity without perturbing the biological activity of NGF. This PET tracer can then be used to quantify the amount of NGF

transported to the basal forebrain. Ultimately, this method can serve as a measure of TrkA expression by BFCNs.

4.2.4 Therapeutic Approaches for Reversing Aging and Neurodegenerative Disorders

A previous study investigated the retrograde transport of proNGF via TrkA in an antioxidant-poor medium, to determine the impact of induced oxidative stress on the transport process.[16,56] This study addressed the long-standing hypothesis that oxidative stress contributes to aging and AD, impacting the mechanisms associated with the retrograde transport of proNGF. The findings revealed that heightened intracellular oxidative stress resulting from antioxidant deprivation significantly decreased TrkA immunoreactivity and retrograde transport of proNGF in rat BFCNs that were cultured in microfluidic chambers.[57]

Upon ligand binding, TrkA receptors in nerve terminals undergo activation, leading to phosphorylation and subsequent internalization for retrograde trafficking. NGF-TrkA signalling endosomes move towards neuronal cell bodies, where they regulate pathways crucial for neuron survival, growth, and synaptic connectivity.[14,57] Upon reaching the cell body, TrkA receptors, intended for transcytosis, undergo dephosphorylation facilitated by the ER-resident tyrosine phosphatase, protein tyrosine phosphatase 1B (PTP1B). PTP1B activity in the cell body is pivotal in axonal targeting, ensuring that inactive receptors are anterogradely transported to engage with NGF at axon terminals.

Studies utilizing a PTB1B inhibitor demonstrated its ability to suppress PTP1B, hindering its capacity to dephosphorylate TrkA receptors.[14] Additionally, selective inhibition of PTP1B in cell bodies resulted in the abolishment of ligand-induced anterograde transcytosis of TrkA receptors. Thus, without PTP1B activity, TrkA receptors in cell bodies are redirected to lysosomes

for degradation.[14] Shekari et al. indicated that Thioredoxin-1 treatment, recognized for reactivating oxidized PTP1B, increased TrkA levels in BFCNs following antioxidant deprivation.[56] Therefore, PTP1B-dependent mechanisms could contribute to reduced TrkA levels and proNGF transport during aging and in AD.

These investigations highlight a potential strategy for reversing cognitive decline associated with aging. This underscores the necessity for developing *in vivo* techniques to quantify TrkA levels and assess NGF transport. The capability to measure TrkA levels *in vivo* and monitor NGF transport from axon terminals to cell bodies with the developed TrkA-PET tracer could serve as a diagnostic tool for identifying synaptic and axonal loss preceding cognitive decline. Subsequently, this method would facilitate *in vivo* testing and monitoring of potential therapeutics to address memory loss, including antioxidant treatments or PTP1B targeting pharmaceuticals.

Appendix I

Chapter 2 – Supplementary Information

A-1 Materials and Methods

LC-ESI-MS analysis was conducted utilizing a Jupiter analytical RP C4 column. The solvent system was comprised of the following gradients: 0-2 minutes (80% H2O: 20% ACN), 18-20 minutes (10% H2O: 90% ACN), and 20-26 minutes (80% H2O: 20% ACN), at a flow rate of 1 mL/min. Protein concentration for *in vitro* studies was measured with a Bicinchoninic Acid (BCA) assay from Thermo Scientific (Cat. 23225) performed per the manufacturer's instruction.

PC12 cells were purchased from ATCC (CRL-1721). 6-well plate (Cat. 83.3920), 24-well plate (Cat. 83.3922), and scrapers (83.3950) were acquired from SARSTEDT. NGF was a gift from Dr. Micheal Coughlin. Poly L-Lysine (PLL) (Cat. P4707-50mL) was purchased from Sigma-Aldrich. Primary Abs used were as follows: TrkA Rabbit Ab (1:500, Cell Signalling, Cat. 25055), p-TrkA (Tyr409) Rabbit Ab (1:500, Cell Signalling, Cat. 9141S), P42/44 MAPK (Erk1/2) Rabbit Ab (1:1000, Cell Signalling, Cat. 9102S), p-P42/44 MAPK (T202/Y204) (E10) Mouse mAb (1:1000, Cell Signalling, Cat. 9106S), AKT Rabbit Ab (1:1000, Cell Signalling, Cat. 9272S), p-AKT Mouse mAb (1:1000, Cell Signalling, Cat. 4051S). Secondary Antibodies used were: IRDye 680 Goat Anti Rabbit (1:15,000 in BB/PBS-T, Licor BioSciences 926-32221), IRDye 800CW Goat-Anti-Mouse (1:15,000 in BB/PBS-T, Licor BioSciences 926-32210). Fluorescent western blot stripping buffer was purchased from Thermo Scientific (Cat. 62299).

A-2 PC12 Cells Priming and Neurite Outgrowth

The study initially encountered challenges culturing PC12 nnr5B5 and nnr5 cells. As a workaround, the research commenced by priming PC12 cells to induce overexpression of the surface binding site for TrkA. Therefore, PC12 cells were cultured in a T75 flask until they reached confluence. Then cells were counted, and 500,000 PC12 cells were seeded into each well (2 mL) of a pre-coated 6-well plate with Poly L Lysine (PLL) in complete medium (RPMI 1640, 10% horse serum, 5% FBS, and 1% P/S). Subsequently, the cells were treated with 100 ng/mL (200 ng/well) of NGF, generously gifted by Dr. Michael Coughlin, for a duration of five days (half of the cell media was replenished with fresh media and 100 ng NGF every other day).[58,59] Cells were observed for morphological changes in neurite outgrowth on day 0, 2, 4 and 5 (Fig. S2-1).

For plate coating with PLL, 1 mL of PLL was added to each well of the 6-well plate, and the plate was incubated for 24 hours at 37 °C and 5% CO2. After 24-hour incubation, the wells were washed with 1 mL of PBS. After removing the PBS, 2 mL of complete media was added to each well, and the plate was placed back in the incubator for another hour. The media was then removed, and the plate was prepared for cells in culture.

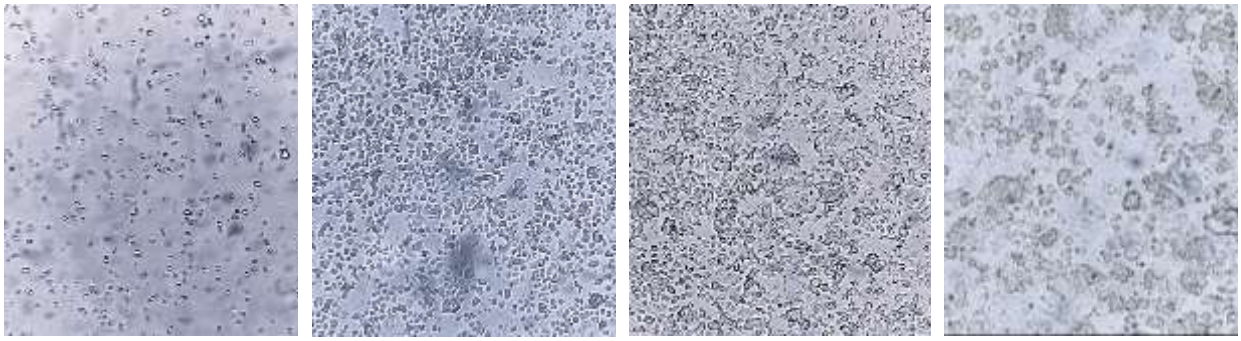

A. Day 0 B. Day 2 C. Day 4 D. Day 5

Figure S2-1. Microscopy images capturing the progression of cell growth and neurite outgrowth over five days treatment period with NGF. A) Initial plating of PC12 in a pre-coated 6-well plate. B) Cells on the 2nd day, exhibiting a spindle shape. C) Cells after 4 days in culture with NGF, displaying the initiation of neurite outgrowth. D) Cells on the day of harvest for further

investigation showcasing extended axons. The images were captured using a magnification of 170x.

A-3 Western Blot Analysis of PC12 and nnr5 Cells

On the fifth day, one well of pPC12 cells was counted to estimate the number of cells in each well. PC12 and nnr5 cells were then counted, and the same number as primed PC12 cells were plated in a pre-coated 6-well plate. All cells were starved with serum-free media for 24 hours. One well of each group of cells was stimulated with 4 nM NGF for five minutes. Cells were then lysed using RIPA lysis buffer and scraped off the wells into Eppendorf tubes. The concentration of each sample of the pPC12, PC12 and nnr5 was assessed with the DC protein assay. Subsequently, the samples were loaded onto a 10% polyacrylamide gel for western blot, following the volumes and µg protein values outlined in the table below (Table S2-1).

	Sample	Concentration	Amount [µg]	Sample volume [µL]	Assay Buffer [µL]	4xLB [µL]	Total [µL]
L1	BLUeye Prestained Protein Ladder			14.0			
L2	nnr5B5 (+ control)	0.9	8.0	8.5	21.5	10.0	40.0
L3	SHSY5Y cells + BDNF (+ control)	1.2	8.0	7.0	23.0	10.0	40.0
L4	s1 - pPC12-S	5.9	30.0	5.1	24.9	10.0	40.0
L5	s2 - PC12-S	1.4	30.0	21.0	9.0	10.0	40.0
L6	s3 - nnr5-S	0.3	9.9	30.0	0.0	10.0	40.0
L7	s4 - pPC12-NS	5.7	30.0	5.3	24.7	10.0	40.0
L8	s5 - PC12-NS	0.9	30.0	32.1	0.0	10.5	42.1
L9	s6 - nnr5-NS	0.2	8.0	33.3	0.0	10.8	43.3
L10	nnr5-Aishwaria (- control)	6.0	10.0	1.7	28.3	10.0	40.0

Table S2-1. Concentration of samples obtained from DC protein assay and the corresponding amount of protein loaded per lane in a 10 well SDS PAGE. Lane 1 was loaded with the standard protein ladder to determine protein MW, followed by membrane scanning. Lane 2 was loaded with nnr5B5 cells' lysates as a positive control for TrkA overexpression. Lane 3 was loaded with SHSY5Y cells' lysates stimulated with BDNF as a positive control for phospho-protein (activated form of the proteins following stimulation), and lane 10 was loaded with nnr5 cells' lysates as a negative control for either no TrkA expression or no phospho-proteins existence.

*Note: The inconsistency in the amount of protein load is due to insufficient amount of cell lysates to load for the nnr5 cells.

The proteins were then transferred to PVDF membrane at 4°C for 1.5 hours. After washing the membrane with TBS without Tween-20, it was incubated with a mixture of 2.5 mL blocking buffer and 2.5 mL TBS without Tween-20 for one hour at RT. Following the removal of the buffer, the membrane was incubated with a solution containing 5 mL TBS/blocking buffer, 12 µL 20% Tween-20 and primary antibodies. Their designated MW are shown in table S2-2: TrkA-Phosphorylated, Erk1/2-Total, Erk1/2-Phophorylated, AKT-Total, and AKT-Phosphorylated overnight at 4°C. The primary antibodies were then removed and after Tris-Buffered Saline and 0.1% Tween-20 (TBS-T) wash, the membrane was incubated with secondary antibodies (IRDye 680 goat anti-rabbit and IRDye 800CW goat anti-mouse) in 5 mL of blocking buffer/TBS-T (0.05% Tween-20) for one hour at RT. Membrane was then scanned with an Odyssey Infrared Imager with an 84 µm resolution (Fig. S2-2).

Rabbit- Channel 700	**Mouse- Channel 800**
Phospho-TrkA (140 kDa)	Phospho-Erk (42/44 kDa)
Total-Erk (42/44 kDa)	Phospho-Akt (57 kDa)
Total-Akt (57 kDa)	GAPDH (36 kDa)
Total-TrkA (140 kDa)	

Table S2-2. The table indicates the expected MW and the channel for observing the protein bands for each protein.

A1 A2

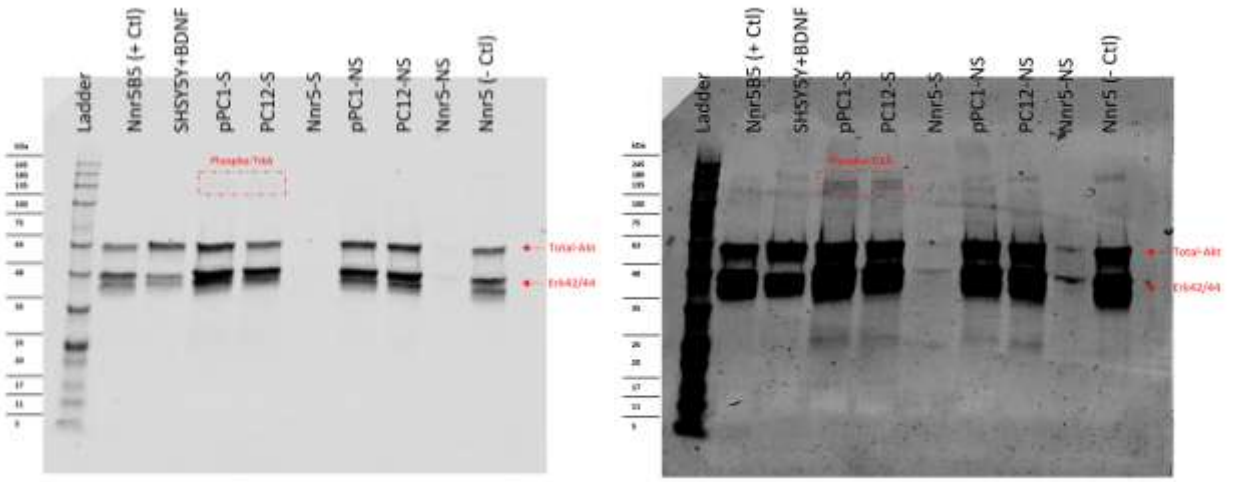

B1 B2

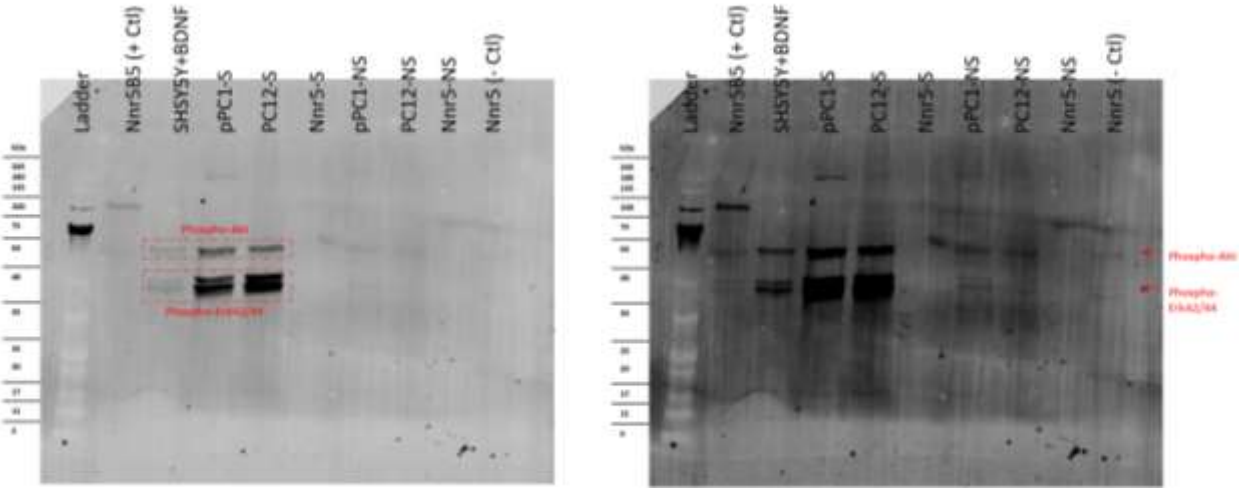

Figure S2-2. Scanned membrane depicting the order of samples loaded in each lane. Lane 1: protein standard ladder, lane 2: PC12 nnr5B5 (overexpressed TrkA) lysates, lane 3: SHSY5Y cells stimulated with BDNF (positive control for phospho-proteins), lane 4: pPC12 cells stimulated with NGF before lysis, lane 5: PC12 cells stimulated with NGF, lane 6: nnr5 stimulated with NGF, lane 7: pPC12 (not stimulated), lane 8: PC12 (not stimulated), lane 9: nnr5 (not stimulated), lane 10: nnr5 lysates (TrkA knock out) lysates. A1 and A2) Low-contrast and high-contrast images of the membrane in the channel 700 respectively. B1 and B2) Low-contrast and high contrast images of the membrane in the channel 800 respectively.

Thereafter, as both phospho and total TrkA antibodies were sourced from rabbit, we proceeded to strip the membrane to enable normalization of the phospho-proteins to either their

total counterparts or to the housekeeping gene, Glyceraldehyde-3-Phosphate Dehydrogenase (GAPDH), using a series of stripping buffers: first with a 1:4 (5 mL) buffer for 20 minutes, followed by two rounds of 1:2 (6 mL) buffer for 10 and 45 minutes on a tube rotator, and finally with a 5X (neat 5 mL) buffer for 30 minutes on a shaking incubator with Fluorescent western blot stripping buffer (5X). The membrane was re-incubated with GAPDH antibody and total-TrkA antibody for one hour at room temperature. The membrane was incubated with secondary antibody following the same procedure as described above, and then scanned (Fig. S2-3).

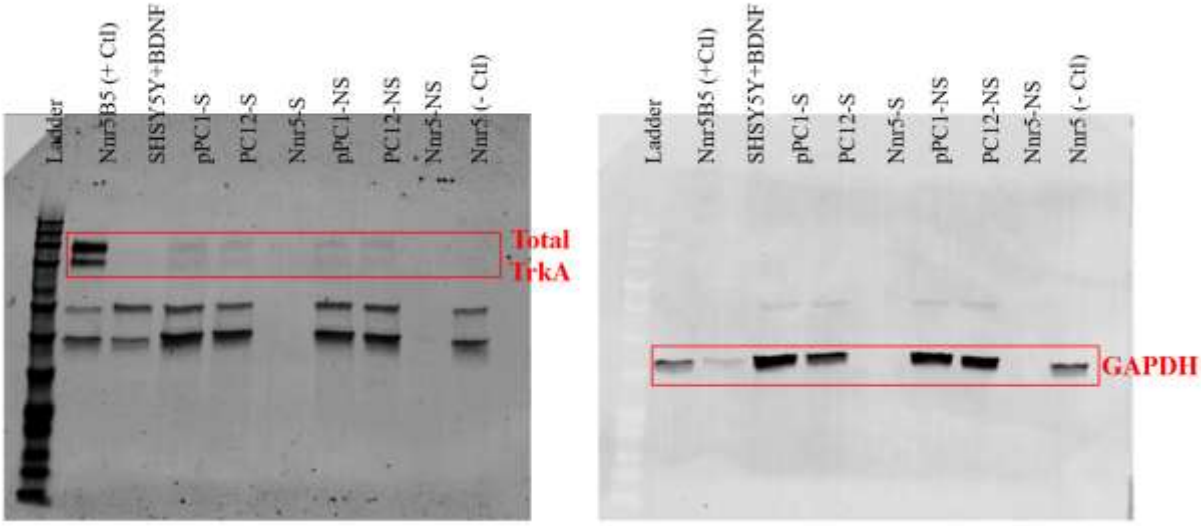

Figure S2-3. Scanned membrane after stripping and reintubation with GAPDH and total-TrkA antibodies. On the left (channel 700), total-TrkA was probed; on the right (channel 800), GAPDH was probed. The images were scanned at a resolution of 84µm using an Odyssey infrared imager.

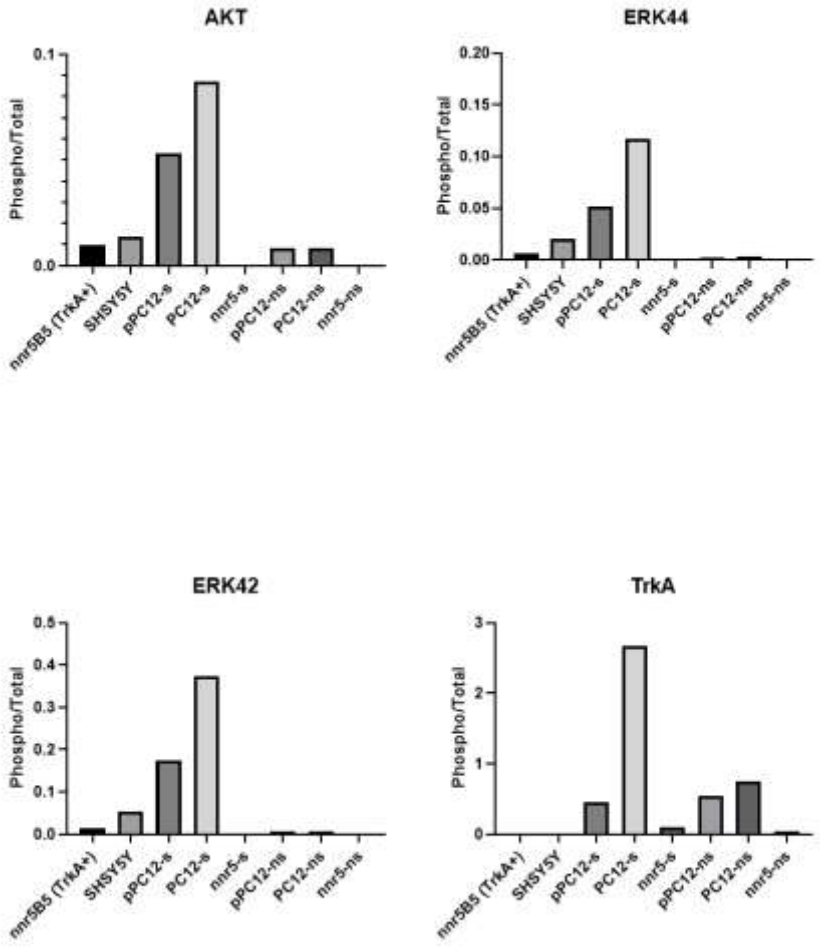

Figure S2-4. Western blot analysis comparing levels of downstream proteins, AKT, ERK44 and 42, and TrkA among pPC12, PC12, and nnr5.

The quantitative western blot analysis revealed higher levels of AKT, ERK44/42, and TrkA (0.087, 0.117/0.174, 2.674) for PC12 cells stimulated with NGF compared to pPC12 cells stimulated with NGF (0.053, 0.051/0.373, 0.455). This pattern was consistent in PC12 and pPC12 cells that were not stimulated with NGF.

For the positive controls, nnr5B5 and SHSY5Y cells, low signal was observed in the bar graph above for any downstream proteins or TrkA since the cell lysates were not stimulated to induce phosphorylation. Additionally, samples from nnr5 (TrkA -) cells, whether stimulated or

not, experienced cell viability issues, leading to lower protein loading in the gel compared to other lanes. Consequently, there was insufficient protein on the membrane for visualization. However, it should be noted that undetectable signals in nnr5s samples could be due to uneven amounts of protein that were loaded initially for these samples. While the objective of priming PC12 cells aimed to enhance surface binding density for an improved *in vitro* model, repeated western blot experiments with pPC12 cells treated with NGF for varying durations also revealed no significant differences in TrkA expression and downstream proteins compared to PC12 cells. This suggests that TrkA expression levels remain consistent between PC12 and pPC12 cells, indicating that the priming protocol may be inefficient or may not be accurately assessed by western blot.

A-4 ^{125}I-NGF Characterization

Size exclusion HPLC is commonly used for protein characterization and analysis, providing information about protein size, purity, aggregation, and stability. The radio-HPLC, while being a lower-throughput method for characterizing radiochemical purity vs radio-iTLC, makes use of compound-specific retention times and UV-Vis absorptivity to provide additional information on the identity of radiolabeled compounds in a mixture. As stated in Chapter 2, the radioiodination of NGF was performed through electrophilic substitution using direct method of labeling with Iodogen. To characterize and confirm the radio-iTLC measurements of radiochemical purity, HPLC was performed on a Yarra 3µm SEC-3000 column loop size of 20 µl, using phosphate buffer pH 6.7 as the eluent and 1mL/min flow rate.

Upon performing HPLC with unlabeled NGF and ^{125}I-NGF, broad peaks with low intensity were observed in the traces. The suspicion arose regarding the possibility of aggregation, given

that protein aggregation poses a threat to product quality, stability, and efficacy. Therefore, a test was designed to determine whether aggregation is the cause, and to conduct quality control on the NGF being used.

Several samples were prepared according to Scheme S2-1: unlabeled NGF in PBS before and after passing the sample through 0.22 µm filter, and ^{125}I-NGF before and after 0.22 µm filtration. Purification of ^{125}I-NGF in this specific test was conducted using gravity gel filtration through a PD-10 column (Sephadex G-25) due to concerns that centrifugal forces generated during centrifugal filtration may induce protein aggregation under harsh conditions such as high speeds or prolonged centrifugation times. From the gel filtration, fraction 2, which contained the highest amount of activity and presumably the highest concentration of ^{125}I-NGF, was selected for further assessment (Fig. S2-5).

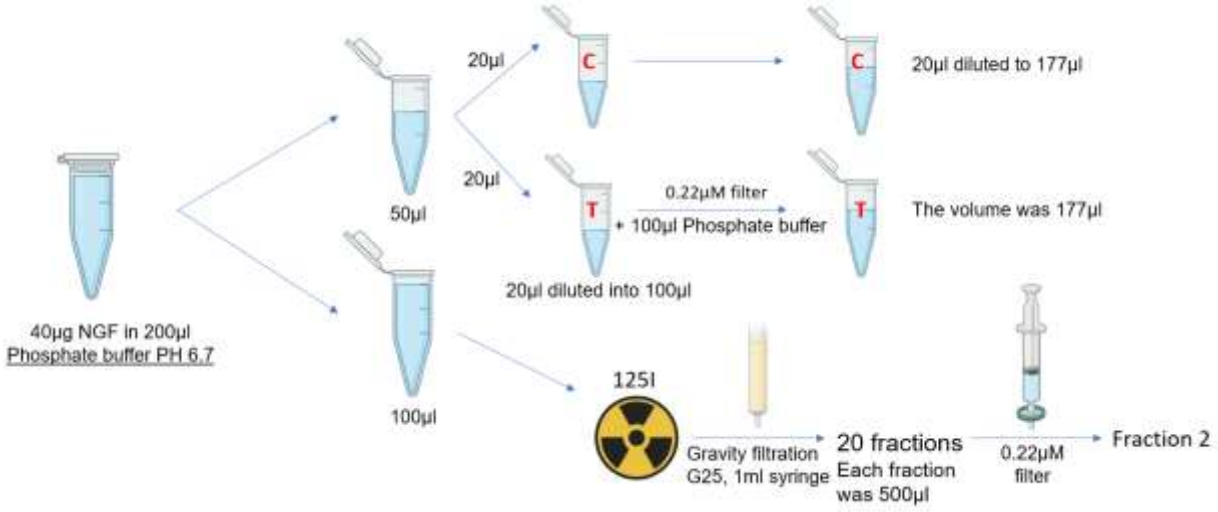

Scheme S2-1. Sample preparation for characterization analysis of unlabelled NGF and ^{125}I-NGF.

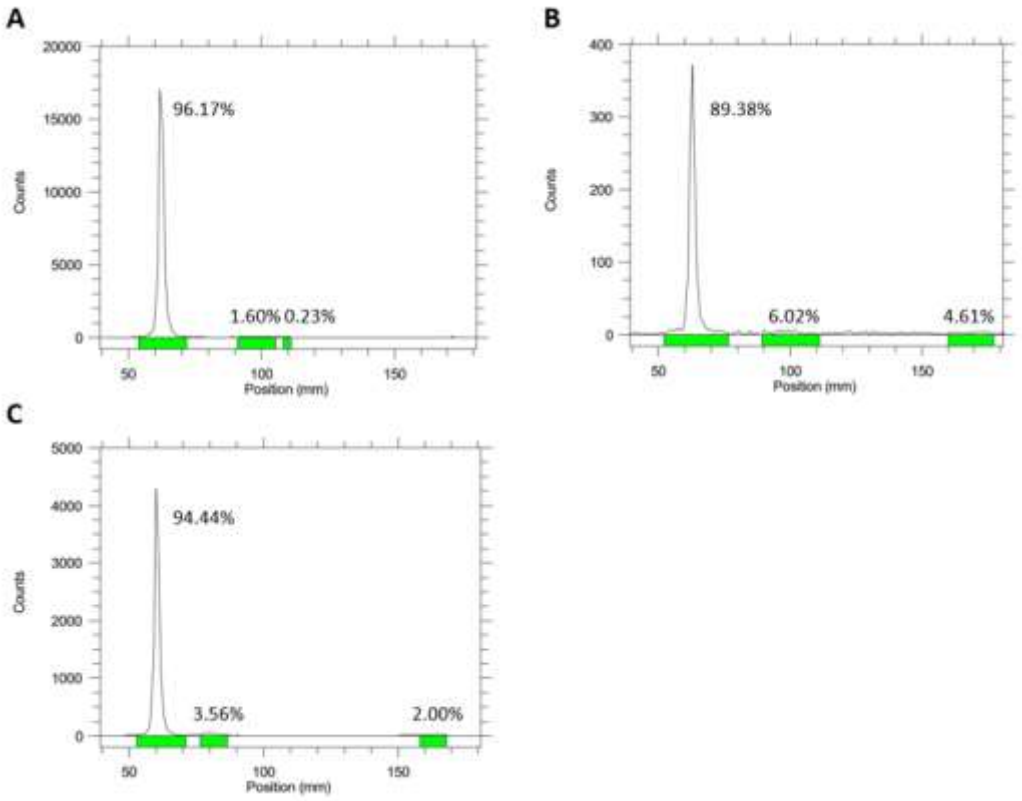

Figure S2-5. Radio-iTLC of crude ^{125}I-NGF (A), fraction 1 (B), fraction 2 (C).

Given that NGF exhibits high molecular absorptivity at both 245 nm (Fig. S2-6) and 280 nm (the latter of which arises specifically from the absorbance of aromatic amino acids), the HPLC UV traces were recorded at both wavelengths. Unlabeled NGF (4 µg) and labeled NGF (4 µCi) are shown in Figure S2-7 and S2-8, respectively.

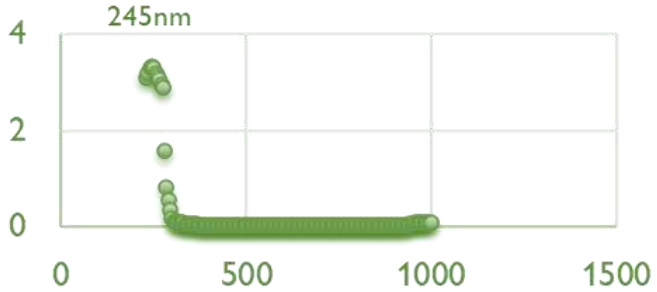

Figure S2-6. Maximum UV wavelength absorbance of NGF, measured using the TECAN microplate reader.

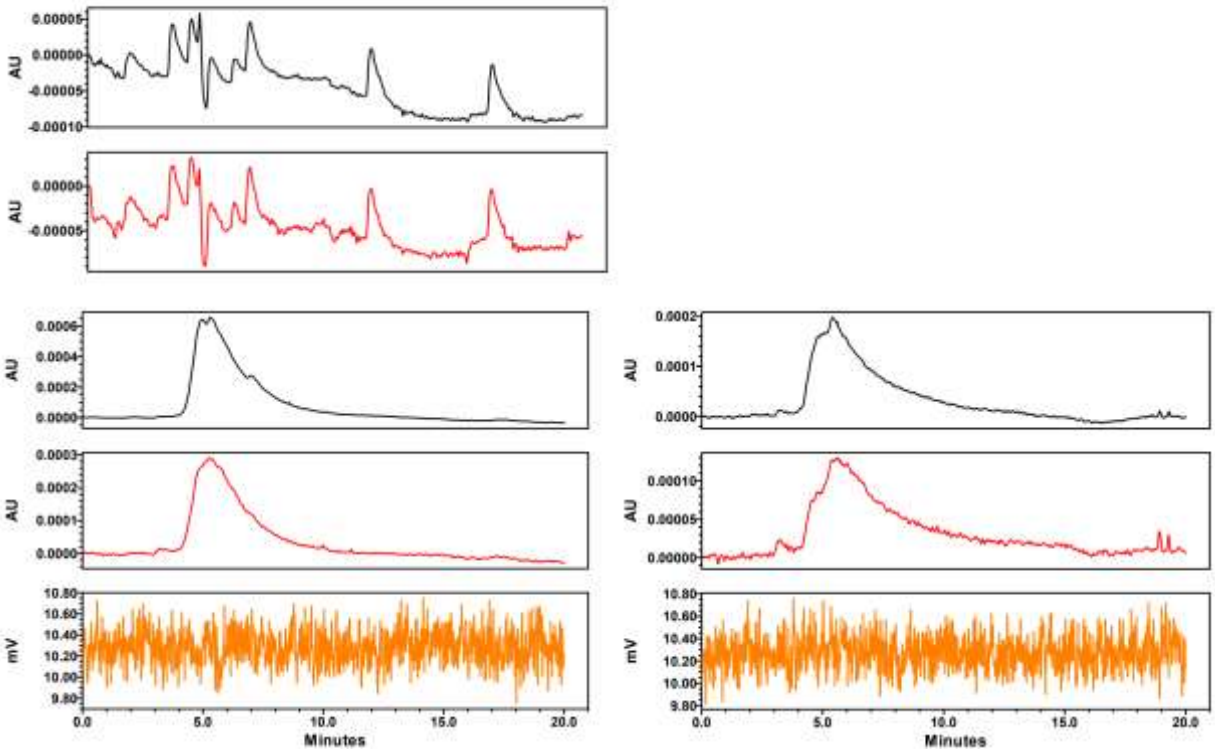

Figure S2-7. HPLC trace for blank (top), "test" tube (bottom, left) and "control" tube (bottom, right) at 245nm (black) and 280nm (red), and gamma trace (orange).

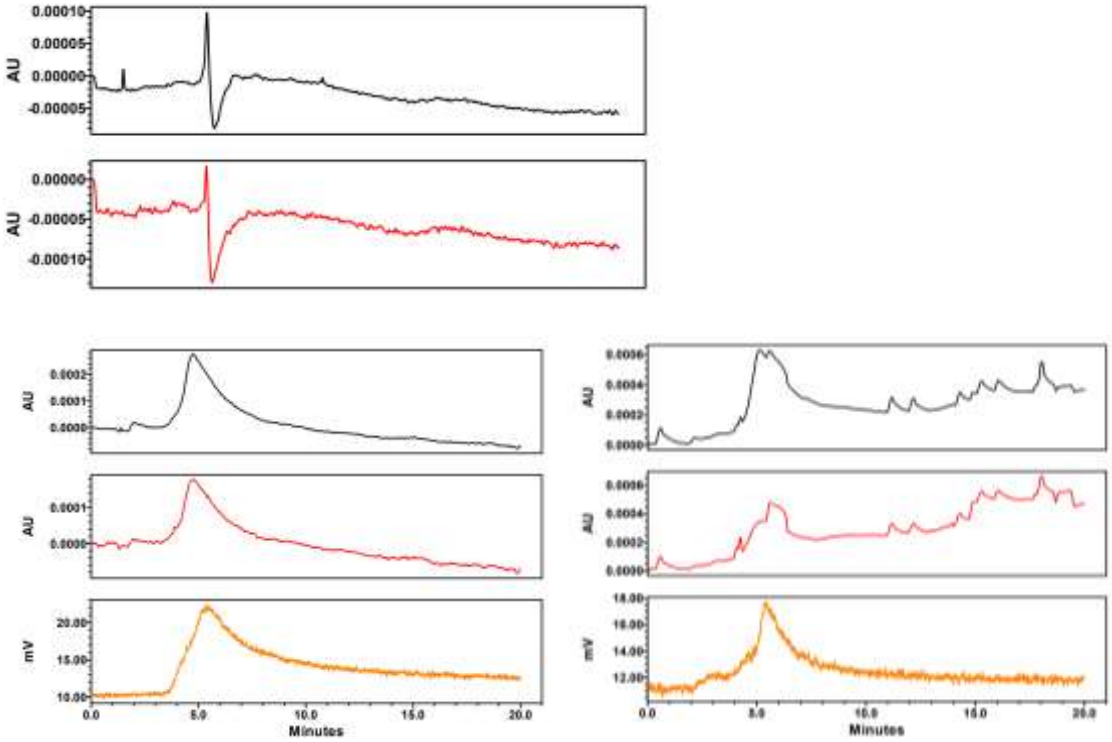

Figure S2-8. HPLC trace for blank (top), fraction 2 non-filtered (bottom, left) and fraction 2 filtered through 0.22µm filter (bottom, right) at 245nm (black), 280nm (red) and gamma trace (orange).

SEC-HPLC results from Figure S2-6 show that NGF elutes from the column from minutes 4-8. In Figure S2-6, colocalization of the gamma trace and UV-Vis trace at approximately the same elution time as unlabeled NGF, without secondary peaks eluting at a different retention time, reinforce that ^{125}I-NGF was isolated in high radiochemical purity. Control studies injecting free ^{125}I showed that the radionuclide elutes off the column at a much later time (around 11 minutes) in comparison to ^{125}I-NGF. Therefore, from a resolution perspective, the radio-HPLC results should be able adequately measure the free ^{125}I. However, NGF fragments, possibly generated by radioiodination, would elute with a similar time to ^{125}I-NGF, and would likely evade resolution by radio-iTLC due to it having a similar hydrophilicity as the unfragmented protein. However, the wide peak breadth obtained for ^{125}I-NGF and unlabeled NGF precludes analysis of fragmentation.

A-5 Gel Electrophoresis

Samples from Scheme S2-1, unlabelled NGF in PBS before and after 0.22 μm filtration exposed to Iodogen under typical radioiodination conditions, two different concentrations of BSA as controls, and a standard protein ladder, were then loaded for gel electrophoresis (Table S2-3).

In addition to stickiness/non-specific binding, it was considered that NGF could be forming large aggregates at some points during the radioiodination process. SDS-PAGE using non-reducing conditions was performed, and samples were not heated prior to loading. It was suggested that if aggregates were forming, they might be detectable in the SDS-PAGE results as large bands in high molecular weight regions of the gel, so some samples were 0.22 μm filtered to observe the effects on the migration.

The SDS-PAGE was run for 2 hours at 120 V. The gel was carefully removed and then stained with QC Colloidal Coomassie stain for one hour, and destained with water for another one hour (Fig. S2-9). To image radioactivity, the gel was exposed on a phosphor plate for approximately 48 hours, and the plate was scanned with a Typhoon imaging scanner (Fig. S2-10).

Well	Sample	Protein Loaded (µg)	Sample Volume (µL)	Activity (µCi)	Loading Buffer (µL)	Total (µL)
1	Ladder	-	5	-	15	20
2	NGF	2	10	-	10	20
3	NGF filtered	0.22	10	-	10	20
4	NGF-Iodogen	2	10	-	10	20
5	NGF filtered-Iodogen	0.22	10	-	10	20
6	^{125}I-NGF filtered	0.096	15	1.2	15	30
7	BSA	2	10	-	10	20
8	BSA	0.2	10	-	10	20
9	^{125}I-NGF	0.048	15	0.6	15	30
10	Ladder	-	5	-	15	20

Table S2-3. Gel electrophoresis loaded wells specifications.

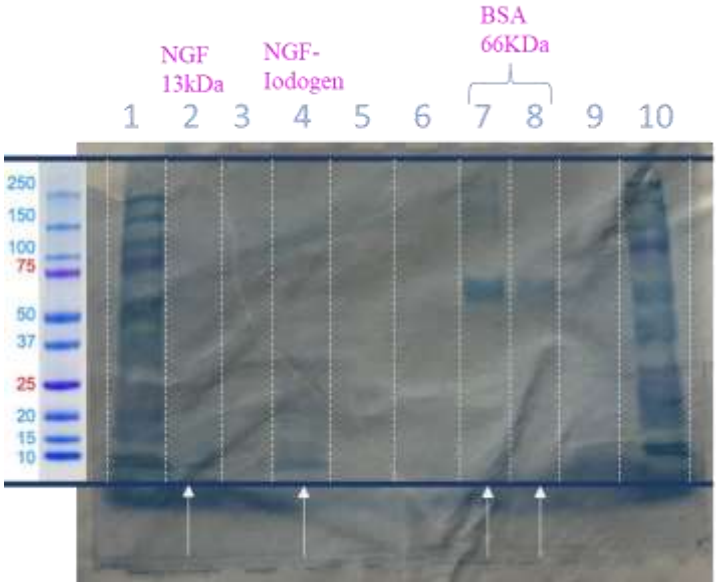

Figure S2-9. Gel electrophoresis result after staining with QC Colloidal Coomassie Blue and destaining with water.

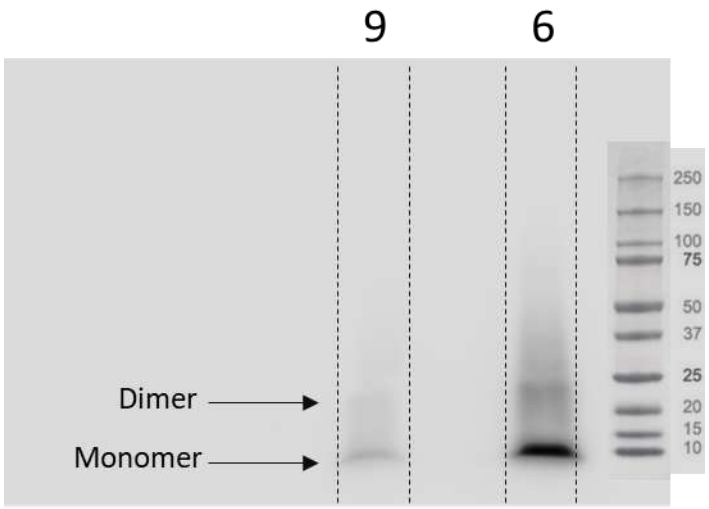

Figure S2-10. Autoradiography obtained by phosphor plate scanning with Amersham Typhoon imaging machine.

The results obtained from the gel electrophoresis revealed the presence of dimers in the labeled NGF samples, whereas only one single band for monomer was observed for non-labeled NGF. However, the sensitivity of Coomassie stain is limited, and the protein mass was too low to detect a signal for the possible dimer in non-labeled NGF. According to a previous study, a single band could be seen in ~13 kDa for purified NGF, as just monomer.[60] Interestingly, a trail of radioactivity above 25 kDa is observable in lane 6 (0.05 µg ^{125}I-NGF), which might suggest the presence of higher molecular weight oligomeric species. While these results indicated that the radioiodinated NGF eluted on SDS-PAGE in primarily monomeric form, future work will be required to determine whether the SDS containing the elution buffer had an influence on the monomer-dimer equilibrium, or on the possible formation of NGF aggregates.

After conducting the filtration test to assess NGF's stickiness or aggregation, we passed ^{125}I-NGF through a 0.22 µm filter twice and measured the compound's activity before and after each filtration. We expected any potential aggregation to be removed during the first pass, with

consistent activity remaining during the second pass. However, the results showed that during each pass through the filter, more than half of the activity remained trapped in the filter and was not eluted after PBS wash. These findings, along with the results from gel electrophoresis, suggest that NGF exhibits stickiness rather than aggregation, which corresponds to previous findings where a significant fraction of NGF adheres to surfaces, particularly at low concentrations.[61]

A-6 Liquid Chromatography Mass Spectroscopy

High resolution liquid chromatography electrospray ionization mass spectroscopy (LC-ESI-MS) was then utilized to ascertain the precise molecular weight of the NGF, providing data that suggests how to utilize it efficiently in a range of research endeavors. This rigorous qualification and characterization process would also evaluate the reliability and quality of the NGF for its intended purposes.

To find out the NGF stock molecular weight and possibility of dimer existing in addition to monomer, or vice versa, 1 µg/µL of protein sample was assessed for LC-ESI-MS. Two peaks with two different retention times (RT) could be seen through the reverse phase HPLC with Jupiter C4 column and gradient percentage of water and acetonitrile as eluents. The peaks were further assessed for the molecular weight. The spectral deconvolution of peaks revealed two protein isoforms at 12359.7 Da and 13982.9 Da, neither of which corresponded to the NGF dimer (Fig. S2-11).

A

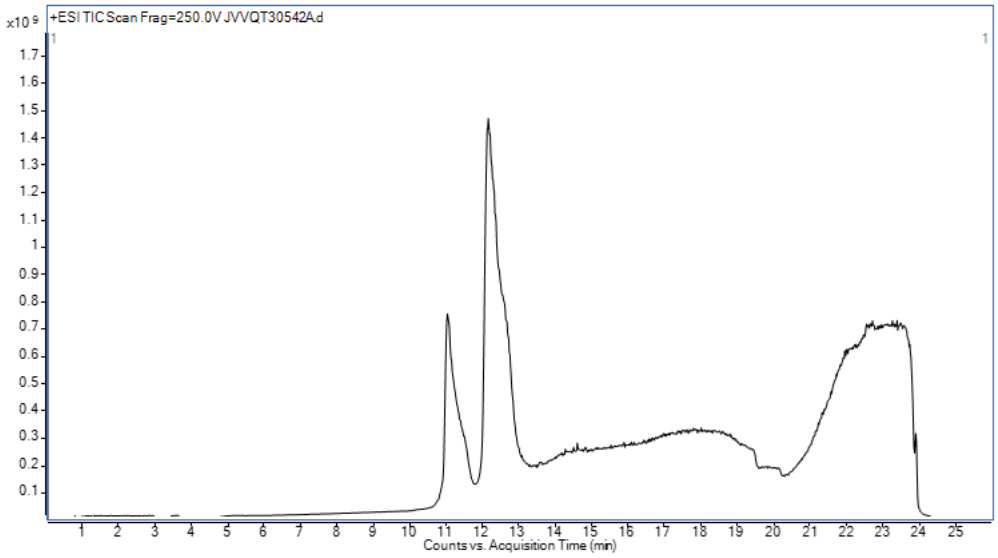
+ESI TIC Scan Frag=250.0V JVVQT30542A.d
x10 9
Counts vs. Acquisition Time (min)

B

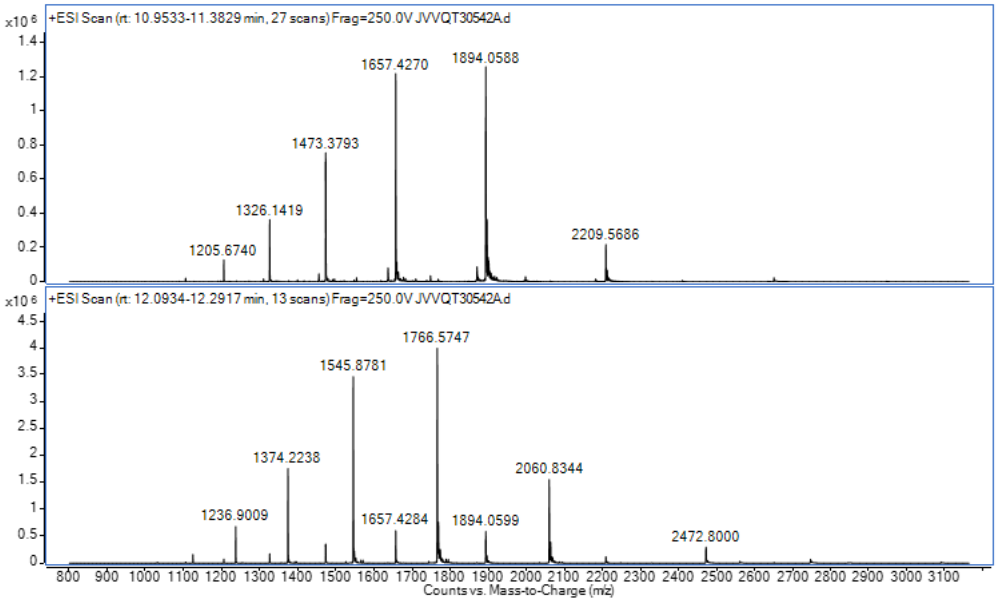
+ESI Scan (rt: 10.9533-11.3829 min, 27 scans) Frag=250.0V JVVQT30542A.d
x10 6
1657.4270
1894.0588
1473.3793
1326.1419
1205.6740
2209.5686
+ESI Scan (rt: 12.0934-12.2917 min, 13 scans) Frag=250.0V JVVQT30542A.d
x10 6
1766.5747
1545.8781
1374.2238
2060.8344
1236.9009
1657.4284
1894.0599
2472.8000
Counts vs. Mass-to-Charge (m/z)

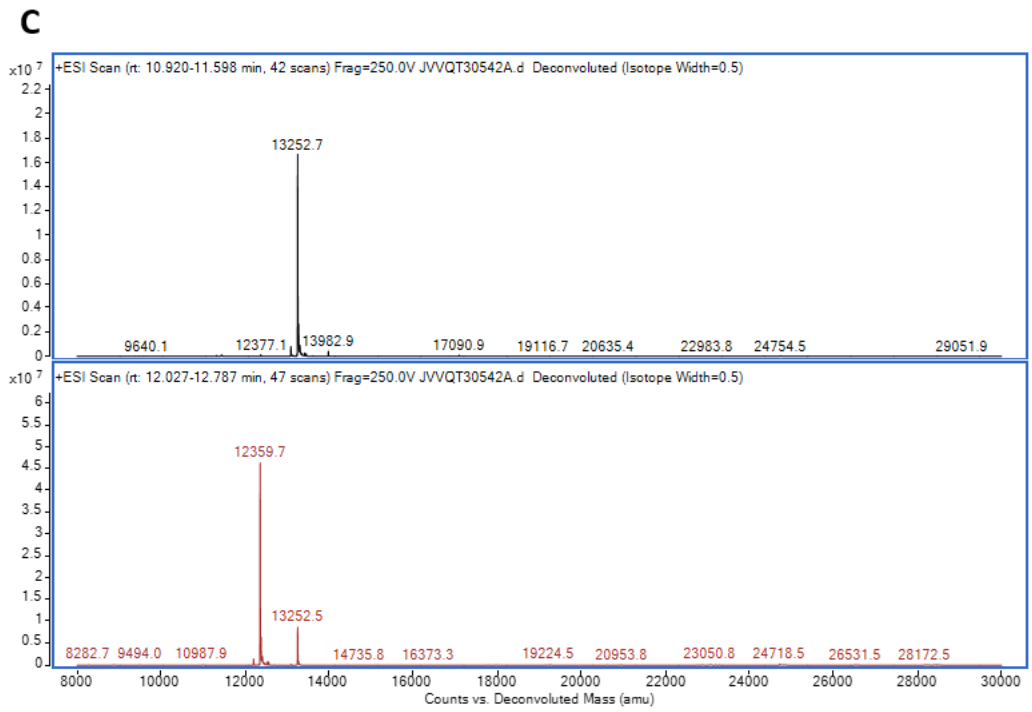

Figure S2-11. A: UV-HPLC chromatogram using a Jupiter analytical RP C4 column. B: LC-ESI-MS analysis- top: 11 mins and bottom: 12.2 mins. C: Deconvolution of LC-MS- top: 11 mins and bottom: 12.2 mins.

As previous studies indicated, the precursor of NGF is subjected to additional post translational processing to produce a 13.2 kDa mature protein.[11] Thus, it is highly probable that 13252.7 Da isoform refers to NGF, and 12359.7 Da could be truncated protein which coexists with NGF in stock. The lack of dimer form observed in LC-ESI-MS might be explained by: a) ESI-MS measurements conditions causing fragmentation, or b) the acetonitrile (ACN) containing mobile phase promoting the monomer form over the dimer of NGF. Constitution of NGF in ultrapure water, followed by infusion into to mass spectrometer rather elution by than LC MS, would reduce exposure to the organic containing mobile phase and dimer might be detectable. If monomers are formed by fragmentation, reducing the temperature and voltage of the spectrometer could reduce fragmentation, and the dimer might be observable.

Therefore, due to impurities found in the NGF stock, 99% pure 2.5S NGF was purchased from Alomone Labs. Characterization and research were carried out with this new pure batch of NGF as described in Chapter 2.

A-7 *In Vitro* Saturation Binding Study

To ensure the specificity of the radioligand toward its receptor *in vitro*, various types of assays including saturation and competition assays, were conducted under different conditions using PC12, primed PC12, and nnr5 cells.

Initially, a saturation binding assay was performed by maintaining a consistent number of cells in each tube while increasing the concentration of ^{125}I-NGF. Prior to the in-vitro study, PC12 cells were treated with 4 nM NGF for five days in pre-coated 6-well plate with PLL as described previously. On day five, the cell medium replaced complete medium with NGF-free medium to starve the cells for 24 hours. On the day of the assay, cells were mechanically scraped off the 6-well plate wells and collected in a 50 mL falcon tube. Primed PC12 and nnr5 cells were then counted using a hemocytometer. Subsequently, 500, 000 cells from both cell lines were put in each well of the 96 v-well plate, and serial dilutions of ^{125}I-NGF (0.12 nM-75 nM) were prepared in complete medium. Each dilution was added to the corresponding wells for each cell line in triplicates. Cells were then incubated with the radioligand for two hours at 37°C. Afterwards, the plate was centrifuged, and the supernatant was removed from each well. Each well was washed with PBS three times. The cells were lysed with Milli-Q water, and the contents of each well were collected into the related gamma tubes. The counts per tube were measured using the gamma counter for a 1-minute run method (Fig. S2-12).

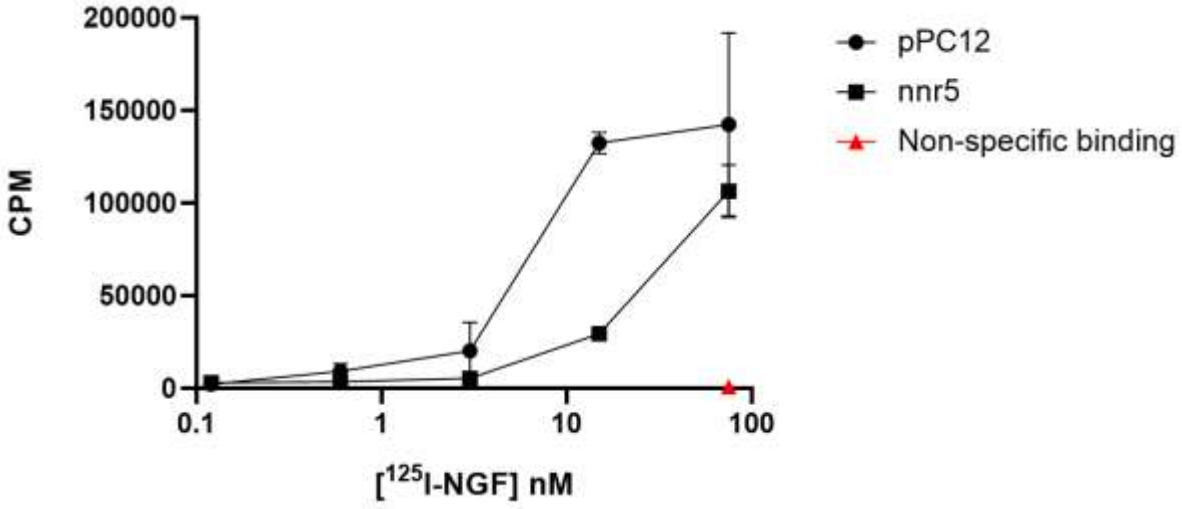

Figure S2-12. Saturation binding assay with pPC12 and nnr5 cells, indicating CPM versus concentration of ^{125}I-NGF.

Based on the saturation binding assay results, there appeared to be indications of specific binding in pPC12 cells. The higher CPMs recorded with a mean of 132,411 at a lower concentration (15 nM) suggest the potential presence and binding to the high-affinity receptor, TrkA. In contrast, nnr5 cells showed lower CPMs with a mean of 29,364 at 15 nM, indicating their lower expression of TrkA receptors. The observed increase in CPMs with nnr5 cells as the concentration increased could be attributed to their expression of the low-affinity receptor (p75 ^{NTR}), which exhibited higher binding at higher concentrations (75 nM) of ^{125}I-NGF. Moreover, the study revealed that the stickiness of ^{125}I-NGF to the plate was low, at 1.4%.

Morphological changes in nnR5 cells were assessed when exposed to NGF, and they began to grow neurites (Fig. S2-13). This observation could potentially explain the insignificant binding observed between treated PC12 cells and nnr5 cells. Genetic or epigenetic alterations in nnr5 cells may lead to changes in cellular behavior and responses to NGF. Typically, nnr5 cells do not exhibit neurite outgrowth when exposed to NGF because they lack the TrkA receptor. Therefore, due to

challenges associated with reviving the nnr5s, the decision was made to continue the study with primed PC12 and regular PC12 cells.

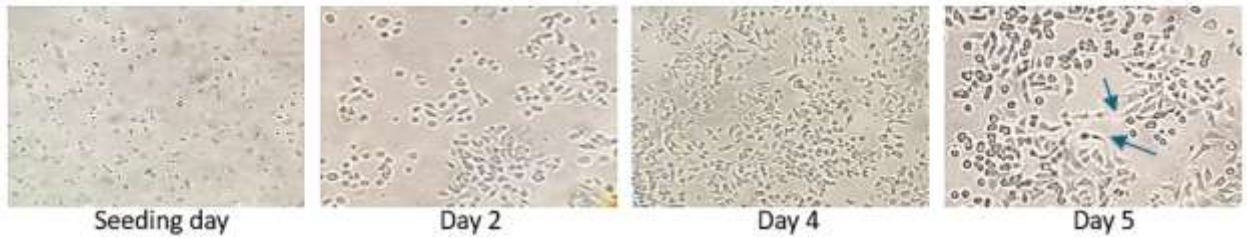

Figure S2-13. Morphological assessment of nnr5 cells exposed to 4 nM NGF for five days. By day five, cells exhibited neurite outgrowth and axons. The images were captured using a magnification of 170x.

For the next study, the experimental setup was modified from cells in suspension to cells in adherent form to enhance the likelihood of interaction between ^{125}I-NGF and the cells. Consequently, 60,000 PC12 cells were seeded in pre-coated 24-well plates. The cells were primed with 4 nM NGF for five days, and on the fifth day, the media was exchanged to NGF-free medium for two hours before incubation with ^{125}I-NGF. The decision to shorten the starvation time was influenced by the reversible nature of TrkA-induced overexpression [33], as a 24-hour starvation period could reverse the TrkA induction. Following starvation, dilutions of ^{125}I-NGF (0.12 nM-75 nM) were added to each well in triplicate (as depicted in Fig. 23). The cells were then incubated with the radioligand for 1 hour at 37°C. Subsequently, after three washes with PBS, cells in each well were lysed with RIPA lysis buffer. The cells were scraped off the wells using a scraper, and the contents were transferred to gamma tubes for counting using a gamma counter with a 1-minute run method. After gamma counter readings, a BCA protein assay was conducted to determine the total protein concentration in each well. The counts from each well were then normalized to the protein concentration of that well (Fig. S2-14).

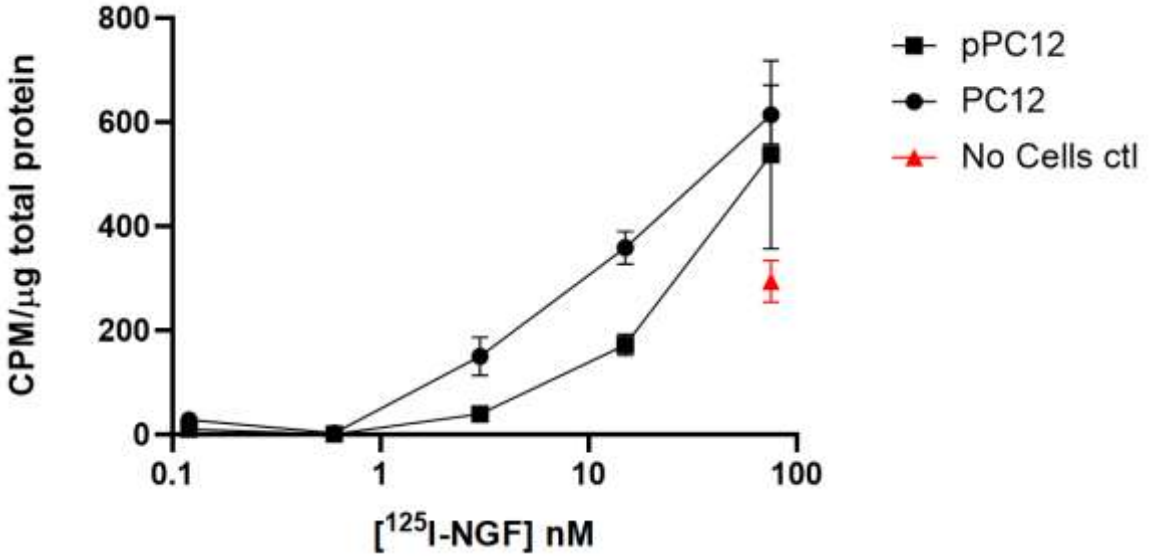

Figure S2-14. Saturation binding assay with pPC12 and PC12 cells, indicating CPM versus concentration of ^{125}I-NGF.

As illustrated in the graph above, pPC12 cells displayed slightly lower counts compared to regular PC12 cells at points with same concentration of ^{125}I-NGF. This suggest that the 2-hour starvation period may not have been sufficient for the NGF from priming to dissociate from the receptors, preventing ^{125}I-NGF form efficiently binding to TrkA. Despite the lower signals observed in pPC12 cells, no significant differences were found between the two cell lines, as the mean counts for pPC12 and PC12 at 75 nM were 537.739 and 614.628, respectively. Moreover, there was a considerable increase in non-specific binding (Approximately 50% of the counts obtained for pPC12 and nnr5 were observed at the highest concentration), particularly compared to when cells were in suspension. Despite repeating the study and introducing modification such as adding the radioligand to uncoated wells and incorporating 0.1% Tween 80 to reduce stickiness, these adjustments did not effectively mitigate non-specific binding. Therefore, the protocol was reverted to using cells in suspension because non-specific binding to the plate was obscuring specific binding, leading to inaccurate binding assessment. Moreover, competition assays with a

kinase inhibitor called K252a were conducted instead of proceeding with the saturation binding assay.

A-8 *In Vitro* Competition Binding Assay

PC12 cells were treated with NGF according to the priming protocol. On the fifth day, the medium replaced with NGF-free medium for 24 hours. Subsequently, the media was replaced with serum-fee medium for an additional two hours. The short duration of serum-free medium starvation is attributed to the compromised cell viability associated with its incubation. After two hours, cells were scraped off the wells, collected in a 50 mL Falcon tube, and counted. One million cells in 50 µL were placed in each low-bind Eppendorf tube. For each tube, 0.04 nM ^{125}I-NGF and dilutions of K252a in serum-deprived media respectively, were added in triplicate, and cells were incubated for one hour at 37°C. Subsequently, cells were washed with PBS three times, lysed with 200 µL 1x Triton X-100 and 300 µL methanol, and the lysates were transferred to gamma tubes for counting. The study performed with PC12 cells had the same conditions as pPC12, except the cells were not treated with NGF, and the concentration of ^{125}I-NGF added was 0.4 nM (Fig. S2-15).

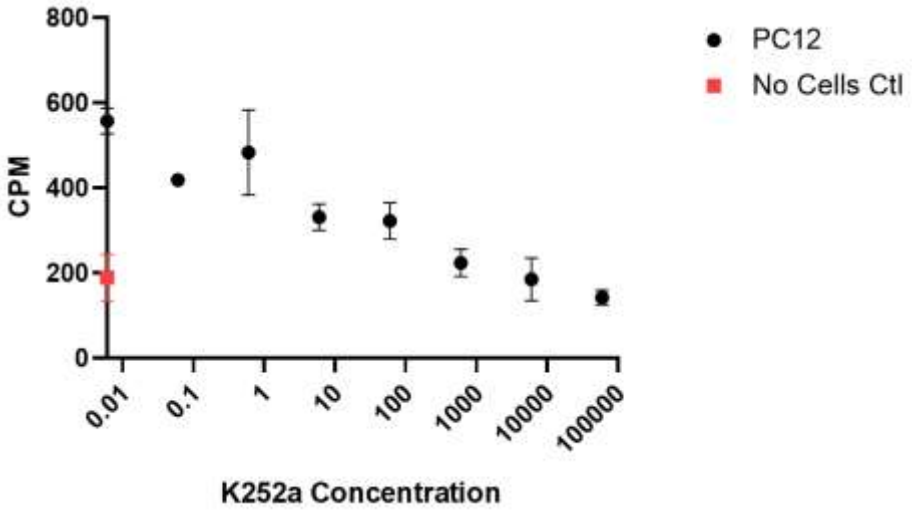

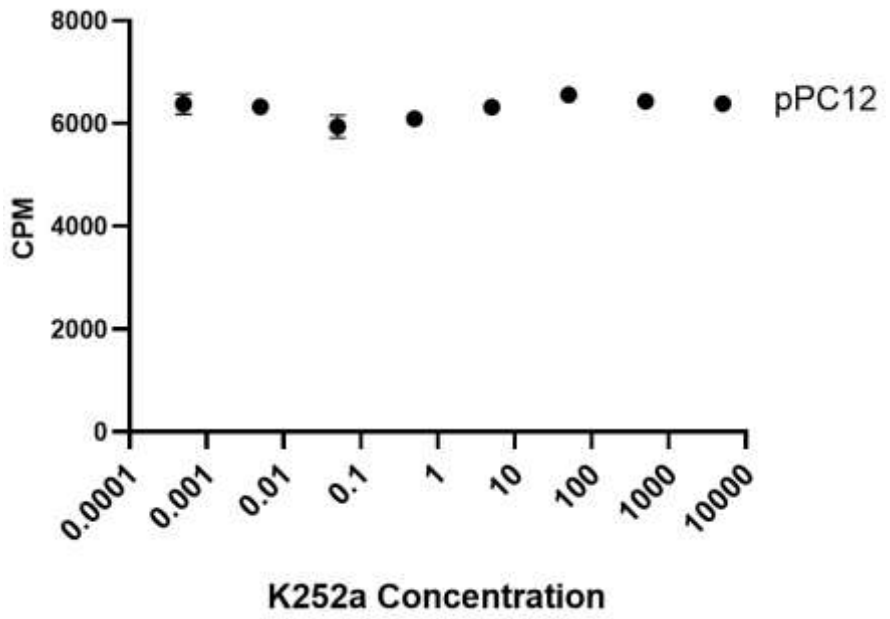

Figure S2-15. Competition assay performed with PC12 (top) and pPC12 (bottom), illustrating CPM versus concentrations of K252a.

Upon repeating this study with regular PC12 and pPC12s, no inhibitory properties from K252a were observed. This is because K252a binds specifically to the adenosine triphosphate (ATP)-binding site within the intracellular kinase domain of the TrkA. This binding event effectively suppresses the kinase activity of TrkA and blocks the stimulation of neurite outgrowth with NGF upon its addition to PC12 cells. In contrast, NGF interacts with the extracellular domain of TrkA. Thus, K252a and NGF act on different domains of the TrkA receptor, resulting in distinct mechanisms of action.[62,63]

Despite K252a not being a suitable inhibitor for the competition assay, pPC12 cells exhibited higher binding of ^{125}I-NGF compared to regular PC12 cells even with a 10-fold lower concentration of ^{125}I-NGF. This suggests the effectiveness of the priming protocol, which may not be reflected in western blot analysis.

Consequently, we reverted to our protocol of performing saturation binding assays with modifications, including conducting the assay with suspension cells in low-bind Eppendorf tubes

to reduce non-specific binding. In addition to the modifications made to optimize the conditions for performing the assay, PC12 nnr5B5 and nnr5 cells were successfully cultured. The decision was made to proceed with the study using these superior cell lines, as discussed in Chapter 2.

References

1. Knopman, D. S., Amieva, H., Petersen, R. C., Chételat, G., Holtzman, D. M., Hyman, B. T., Nixon, R. A., & Jones, D. T. (2021). Alzheimer disease. *Nature Reviews Disease Primers*, *7*(1), 33.
2. Moncaster, J. A., Moir, R. D., Burton, M. A., Chadwick, O., Minaeva, O., Alvarez, V. E., Ericsson, M., Clark, J. I., McKee, A. C., Tanzi, R. E., & Goldstein, L. E. (2022). Alzheimer's disease amyloid-β pathology in the lens of the eye. *Experimental Eye Research*, *221*, 108974.
3. Cuello, A. C., Pentz, R., & Hall, H. (2019). The Brain NGF Metabolic Pathway in Health and in Alzheimer's Pathology. *Frontiers in Neuroscience*, *13*, 62.
4. Schmitz TW, Nathan Spreng R, et al. Basal forebrain degeneration precedes and predicts the cortical spread of Alzheimer's pathology. 2016; Nat. Commun. 7:13249.
5. Fahnestock M, Shekari A. ProNGF and Neurodegeneration in Alzheimer's Disease. Front Neurosci. 2019; 13: 129.
6. Rydén, M., Hempstead, B., & Ibáñez, C. F. (1997). Differential Modulation of Neuron Survival during Development by Nerve Growth Factor Binding to the p75 Neurotrophin Receptor. *Journal of Biological Chemistry*, *272*(26), 16322–16328.
7. Mufson EJ, Lavine N, Jaffar S, Kordower JH, Quirion R, Saragovi HU. Reduction in p140-TrkA receptor protein within the nucleus basalis and cortex in Alzheimer's disease. Exp. Neurol. 1997; 146: 91–103.
8. Boskovic, Z., Meier, S., Wang, Y., Milne, M. R., Onraet, T., Tedoldi, A., & Coulson, E. J. (2019). Regulation of cholinergic basal forebrain development, connectivity, and function by neurotrophin receptors. *Neuronal Signaling*, *3*(1), NS20180066.
9. Mufson EJ, Ma SY, Cochran EJ, Bennett DA, Beckett LA, Jaffar S, Saragovi HU, Kordower JH. Loss of nucleus basalis neurons containing trkA immunoreactivity in individuals with mild cognitive impairment and early Alzheimer's disease. J Comp Neurol. 2000 Nov 6;427(1):19-30.
10. Bamji, S. X., Majdan, M., Pozniak, C. D., Belliveau, D. J., Aloyz, R., Kohn, J., Causing, C. G., & Miller, F. D. (1998). The p75 Neurotrophin Receptor Mediates Neuronal Apoptosis and Is Essential for Naturally Occurring Sympathetic Neuron Death. *The Journal of Cell Biology*, *140*(4), 911–923.
11. Counts SE, Nadeem M, Wuu J, et al. Reduction of cortical TrkA but not p75(NTR) protein in early-stage Alzheimer's disease. Annals of Neurology. 2004 Oct;56(4):520-531.
12. Cooper, J. D., Salehi, A., Delcroix, J.-D., Howe, C. L., Belichenko, P. V., Chua-Couzens, J., Kilbridge, J. F., Carlson, E. J., Epstein, C. J., & Mobley, W. C. (2001). Failed retrograde transport of NGF in a mouse model of Down's syndrome: Reversal of cholinergic neurodegenerative phenotypes following NGF infusion. *Proceedings of the National Academy of Sciences*, *98*(18), 10439–10444.
13. Fahnestock, M., Michalski, B., Xu, B., & Coughlin, M. D. (2001). The Precursor Pro-Nerve Growth Factor Is the Predominant Form of Nerve Growth Factor in Brain and Is Increased in Alzheimer's Disease. *Molecular and Cellular Neuroscience*, *18*(2), 210–220.
14. Yamashita, N., Joshi, R., Zhang, S., Zhang, Z.Y., Kuruvilla, R., 2017. Phospho-Regulation of Soma-to-Axon Transcytosis of Neurotrophin Receptors. Dev. Cell 42, 626-639.e5.

15. Shekari, A., & Fahnestock, M. (2019). Retrograde axonal transport of BDNF and proNGF diminishes with age in basal forebrain cholinergic neurons. Neurobiology of Aging, 84, 131–140.
16. Kropf E, Fahnestock M. Effects of Reactive Oxygen and Nitrogen Species on TrkA Expression and Signalling: Implications for proNGF in Aging and Alzheimer's Disease. *Cells*. 2021; 10(8):1983.
17. Chul Paeng, J.; Soo Lee, D. Multimodal Molecular Imaging In Vivo. Open Nucl. Med. J. 2010, 2, 145–152.
18. Kim, S. J., & Lee, H.-Y. (2022). In vivo molecular imaging in preclinical research. *Laboratory Animal Research*, *38*(1), 31.
19. Lewis, J. S., Windhorst, A. D., & Zeglis, B. M. (Eds.). (2019). *Radiopharmaceutical Chemistry*. Springer International Publishing.
20. Blankenberg, F. G., & Strauss, H. W. (2002). Nuclear medicine applications in molecular imaging. *Journal of Magnetic Resonance Imaging*, *16*(4), 352–361.
21. Wernick, M. N., & Aarsvold, J. N. (2004). Emission Tomography: The fundamental of PET and SPECT. Academic press.
22. Dijkgraaf, I., M. Agten, S., Bauwens, M., & M. Hackeng, T. (2022). Strategies for Site-Specific Radiolabeling of Peptides and Proteins. IntechOpen.
23. Tolmachev, V., & Stone-Elander, S. (2010). Radiolabelled proteins for positron emission tomography: Pros and cons of labelling methods. *Biochimica et Biophysica Acta (BBA) - General Subjects*, *1800*(5), 487–510.
24. Zhang, X., Zhang, Y., & Malhotra, A. (2015). Radiolabeling in Biology. *Cell Biochemistry and Biophysics*, *72*(1), 1–10.
25. James ML, Gambhir SS. A molecular imaging primer: modalities, imaging agents, and applications. Physiol Rev. 2012 Apr;92(2):897-965. doi: 10.1152/physrev.00049.2010. PMID: 22535898.
26. Bruno, M. A., & Cuello, A. C. (2006). Activity-dependent release of precursor nerve growth factor, conversion to mature nerve growth factor, and its degradation by a protease cascade. *Proceedings of the National Academy of Sciences*, *103*(17), 6735–6740.
27. Osterwalder, T., Cinelli, P., Baici, A., Pennella, A., Krueger, S. R., Schrimpf, S. P., … Sonderegger, P. (1998). The axonally secreted serine proteinase inhibitor, neuroserpin, inhibits plasminogen activators and plasmin but not thrombin. Journal of Biological Chemistry, 273(4), 2312–2321.
28. Iulita Florencia M. and Cuello Claudio A., The NGF Metabolic Pathway in the CNS and its Dysregulation in Down Syndrome and Alzheimer's Disease, Current Alzheimer Research 2016; 13(1).
29. Cuello, A. C., Pentz, R., & Hall, H. (2019). The Brain NGF Metabolic Pathway in Health and in Alzheimer's Pathology. *Frontiers in Neuroscience*, *13*, 62.
30. Decristoforo, C., & Pfister, J. (2022). In vitro studies with radiopharmaceuticals. In *Nuclear Medicine and Molecular Imaging* (pp. 631–639). Elsevier.
31. Holtzman, D., Kilbridge, J., Li, Y., Cunningham, E., Lenn, N., Clary, D., Reichardt, L., & Mobley, W. (1995). TrkA expression in the CNS: Evidence for the existence of several novel NGF-responsive CNS neurons. *The Journal of Neuroscience*, *15*(2), 1567–1576.
32. Fahnestock, M. (1991). Structure and Biosynthesis of Nerve Growth Factor. In M. Bothwell (Ed.), *Neuronal Growth Factors* (Vol. 165, pp. 1–26). Springer Berlin Heidelberg.

33. Greene, L. (1978). Nerve growth factor prevents the death and stimulates the neuronal differentiation of clonal PC12 pheochromocytoma cells in serum-free medium. Journal of Cell Biology, 78(3), 747–755. 33.
34. Badisa, R. B., Batton, C. S., Mazzio, E., Grant, S. C., & Goodman, C. B. (2018). Identification of biochemical and cytotoxic markers in cocaine treated PC12 cells. *Scientific Reports*, *8*(1), 2710.
35. Bernd, P., & Greene, L. A. (1984). Association of 125I-nerve growth factor with PC12 pheochromocytoma cells. Evidence for internalization via high-affinity receptors only and for long-term regulation by nerve growth factor of both high- and low-affinity receptors. *Journal of Biological Chemistry*, *259*(24), 15509–15516.
36. Eggert, A., Ikegaki, N., Liu, X., Chou, T. T., Lee, V. M., Trojanowski, J. Q., & Brodeur, G. M. (n.d.). Molecular dissection of TrkA signal transduction pathways mediating differentiation in human neuroblastoma cells. 9.
37. Zhou, J., Valletta, J. S., Grimes, M. L., & Mobley, W. C. (1995). Multiple Levels for Regulation of TrkA in PC12 Cells by Nerve Growth Factor. *Journal of Neurochemistry*, *65*(3), 1146–1156.
38. Ioannou, M., & Fahnestock, M. (2017). ProNGF, but Not NGF, Switches from Neurotrophic to Apoptotic Activity in Response to Reductions in TrkA Receptor Levels. *International Journal of Molecular Sciences*, *18*(3), 599.
39. Green, S. H., Rydel, R. E., Connolly, J. L., & Greene, L. A. (1986). PC12 cell mutants that possess low- but not high-affinity nerve growth factor receptors neither respond to nor internalize nerve growth factor. *The Journal of Cell Biology*, *102*(3), 830–843.
40. Ennulat, D. J., & Stach, R. W. (1985). Improved procedure for the purification of an iodinated protein: Beta nerve growth factor. *Neurochemical Research*, *10*(7), 1009–1014.
41. Bylund, D. B., & Toews, M. L. (1993). Radioligand binding methods: practical guide and tips. *American Journal of Physiology. Lung Cellular and Molecular Physiology*, *265*(5), 421-L429.
42. MacDonald, J. I. S., & Meakin, S. O. (1996). Deletions in the Extracellular Domain of Rat TrkA Lead to an Altered Differentiative Phenotype in Neurotrophin Responsive Cells. *Molecular and Cellular Neuroscience*, *7*(5), 371–390.
43. Domenici L, Fontanesi G, Cattaneo A, Bagnoli P, Maffei L. Nerve growth factor (NGF) uptake and transport following injection in the developing rat visual cortex. Vis Neurosci. 1994 Nov-Dec;11(6):1093-102.
44. DiStefano PS, Friedman B, Radziejewski C, Alexander C, Boland P, Schick CM, Lindsay RM, Wiegand SJ. The neurotrophins BDNF, NT-3, and NGF display distinct patterns of retrograde axonal transport in peripheral and central neurons. Neuron. 1992 May;8(5):983-93.
45. Seiler M, Schwab ME. Specific retrograde transport of nerve growth factor (NGF) from neocortex to nucleus basalis in the rat. Brain Res. 1984 May 21;300(1):33-9.
46. Lapchak PA, Araujo DM, Carswell S, Hefti F. Distribution of [125I] nerve growth factor in the rat brain following a single intraventricular injection: correlation with the topographical distribution of trkA messenger RNA-expressing cells. Neuroscience. 1993; 54: 445–460.

47. Friden PM, Walus LR, Watson P, Doctrow SR, Kozarich JW, Bäckman C, Bergman H, Hoffer B, Bloom F, Granholm AC. Blood-brain barrier penetration and in vivo activity of an NGF conjugate. Science. 1993 Jan 15;259(5093):373-7.
48. Fabian Kiessling, Bernd J. Pichler, and Peter Hauff. *Small Animal Imaging: Basics and Practical Guide.* Springer International Publishing AG. docID=4864827.
49. Paxinos , G., & Franklin, K. B. J. (2004). The Mouse Brain in Stereotaxic Coordinates (2nd ed.). Academic Press.
50. Peng, L., Nadia, B., Wen, J., Simons, B. W., Hanwen, Z., Hobbs, R. F., David, U., Baumann, B. C., Pachynski, R. K., Jha, A. K., & Thorek, D. L. J. (2022). Blind Image Restoration Enhances Digital Autoradiographic Imaging of Radiopharmaceutical Tissue Distribution. *Journal of Nuclear Medicine*, *63*(4), 591–597.
51. Habibey, R., Rojo Arias, J. E., Striebel, J., & Busskamp, V. (2022). Microfluidics for Neuronal Cell and Circuit Engineering. *Chemical Reviews*, *122*(18), 14842–14880.
52. Petrasek T, Vojtechova I, Lobellova V, Popelikova A, Janikova M, Brozka H, Houdek P, Sladek M, Sumova A, Kristofikova Z, Vales K, Stuchlík A. The McGill Transgenic Rat Model of Alzheimer's Disease Displays Cognitive and Motor Impairments, Changes in Anxiety and Social Behavior, and Altered Circadian Activity. Front Aging Neurosci. 2018 Aug 28;10:250.
53. Bernard-Gauthier V, Mossine AV, Mahringer A, Aliaga A, Bailey JJ, Shao X, Stauff J, Arteaga J, Sherman P, Grand'Maison M, Rochon PL, Wängler B, Wängler C, Bartenstein P, Kostikov A, Kaplan DR, Fricker G, Rosa-Neto P, Scott PJH, Schirrmacher R. Identification of [(18)F]TRACK, a Fluorine-18-Labeled Tropomyosin Receptor Kinase (Trk) Inhibitor for PET Imaging. J Med Chem. 2018 Feb 22;61(4):1737-1743.
54. Schirrmacher R, Bailey JJ, Mossine AV, Scott PJH, Kaiser L, Bartenstein P, Lindner S, Kaplan DR, Kostikov A, Fricker G, Mahringer A, Rosa-Neto P, Schirrmacher E, Wängler C, Wängler B, Thiel A, Soucy JP, Bernard-Gauthier V. Radioligands for Tropomyosin Receptor Kinase (Trk) Positron Emission Tomography Imaging. Pharmaceuticals (Basel). 2019 Jan 3;12(1):7.
55. Bailey JJ, Kaiser L, Lindner S, Wüst M, Thiel A, Soucy JP, Rosa-Neto P, Scott PJH, Unterrainer M, Kaplan DR, Wängler C, Wängler B, Bartenstein P, Bernard-Gauthier V, Schirrmacher R. First-in-Human Brain Imaging of [(18)F]TRACK, a PET tracer for Tropomyosin Receptor Kinases. ACS Chem Neurosci. 2019 Jun 19;10(6):2697-2702.
56. Krishnan HS, Ma L, Vasdev N, Liang SH. ^{18}F-labeling of sensitive biomolecules for positron emission tomography. *Chem A Eur J*. 2017; **23**(62): 15553-15577.
57. Shekari A, Wu C, Fahnestock M. Oxidative Stress Triggers Basal Forebrain Neurodegeneration by Impairing proNGF Axonal Transport. Submitted.
58. Masoudi, R., Ioannou, M. S., Coughlin, M. D., Pagadala, P., Neet, K. E., Clewes, O., Allen, S. J., Dawbarn, D., & Fahnestock, M. (2009). Biological Activity of Nerve Growth Factor Precursor Is Dependent upon Relative Levels of Its Receptors. *Journal of Biological Chemistry*, *284*(27), 18424–18433.
59. Fahnestock M, Yu G, Michalski B, Mathew S, Colquhoun A, Ross GM, Coughlin MD. The nerve growth factor precursor proNGF exhibits neurotrophic activity but is less active than mature nerve growth factor. J Neurochem. 2004 May;89(3):581-92.

60. Kawaja, M. D., Smithson, L. J., Elliott, J., Trinh, G., Crotty, A.-M., Michalski, B., & Fahnestock, M. (2011). Nerve growth factor promoter activity revealed in mice expressing enhanced green fluorescent protein. The Journal of Comparative Neurology, 519(13), 2522–2545.
61. Bothwell, M. A., & Shooter, E. M. (1977). Dissociation equilibrium constant of beta nerve growth factor. *Journal of Biological Chemistry*, *252*(23), 8532–8536.
62. Ohmichi, M., Decker, S. J., Pang, L., & Saltiel, A. R. (1992). Inhibition of the cellular actions of nerve growth factor by staurosporine and K252A results from the attenuation of the activity of the trk tyrosine kinase. *Biochemistry*, *31*(16), 4034–4039.
63. Berg, M. M., Sternberg, D. W., Parada, L. F., & Chao, M. V. (1992). K-252a inhibits nerve growth factor-induced trk proto-oncogene tyrosine phosphorylation and kinase activity. *Journal of Biological Chemistry*, *267*(1), 13–16.